GROUND-WATER HYDROLOGY AND HYDROCHEMISTRY OF EAGLE FLAT AND SURROUNDING AREA

by

Bruce K. Darling
Barry J. Hibbs
Alan R. Dutton

Jay Raney, Principal Investigator

Final Report

Prepared for

Texas Low-Level Radioactive Waste Disposal Authority
under Interagency Contract No. (92-93)-0910

Bureau of Economic Geology
Noel Tyler, Director
The University of Texas at Austin
Austin, Texas 78713-8924

Revised November 1994

CONTENTS

Plate

Tables

Figures

EXECUTIVE SUMMARY

This report presents the results of the Bureau of Economic Geology's investigation of the saturated-zone hydrology and hydrochemistry of Eagle Flat, Red Light Draw, and surrounding areas of southern Hudspeth County, Texas. Boundaries of the study area are the Rio Grande and Quitman Mountains to the south and west, the Van Horn and Carrizo Mountains to the east, and the Diablo Plateau to the north. Total land area is about 1,200 mi^2 (3,110 km^2).

The Bureau of Economic Geology initiated this study in July 1991 at the request of the Texas Low-Level Radioactive Waste Disposal Authority (TLLRWDA). The objective of the investigation was to ascertain whether northwest Eagle Flat may be considered a suitable location for disposal of low-level radioactive waste.

Methods of investigation included standard hydrological and hydrochemical techniques, including installation of observation wells, water quality sampling, aquifer testing, stream gauging, and measurement of water levels. The study relied upon well-established hydrochemical and isotopic methods to trace local, intermediate, and regional flowpaths, to describe the distribution of ground-water facies, and to account for ground-water origins. Basic physical and chemical hydrologic data were used to develop a conceptual model of ground-water flow in the study region. A numerical model was developed to test hypotheses regarding flow and to estimate flowpaths, residence times, and ground-water velocities. Study results are as follows:

(1) The study area is sparsely populated. Sierra Blanca, the largest community in the study area, had a population of 700 in 1990. Sierra Blanca formerly depended upon local wells to satisfy municipal water needs but currently has most of its water piped in from Van Horn. Van Horn derives its water supplies from basin fill at Wild Horse Flat, a bolson aquifer east of the study area. In rural areas, water use is mainly limited to domestic and livestock consumption. A small number of low-capacity wells satisfy the needs of the local population and livestock industry.

(2) The study area is divided into three basins based on watersheds and ground-water drainage divides. The area within the Eagle Flat Draw watershed is referred to as

southeast Eagle Flat. The area within the Blanca Draw watershed is northwest Eagle Flat. Red Light Draw includes everything within the Red Light Draw watershed, including Indian Hot Springs. The three basins differ in ground-water chemistry.

(3) Ground water occurs in unconfined, leaky confined, and confined aquifers in the study area. In mountainous areas, ground water is typically unconfined. One flowing artesian well (50-24-SHT) in southern Red Light Draw was one of several shot holes drilled as part of a geophysical survey of southern Hudspeth County in the late 1970's. Further evidence that the aquifer is confined in that area is that when well 50-16-703 was deepened, water levels rose 150 ft and well yield increased. Aquifer pump tests and associated hydrogeologic investigations indicate leaky confined aquifers in northwest Eagle Flat and unconfined to leaky confined aquifers in southeast Eagle Flat.

(4) Recharge is limited to areas having exposures of bedrock or where bedrock is covered by thin basin fill. Recently recharged waters have low total dissolved solids, ^{14}C signatures between 60 to 100 percent modern carbon (pmc), and tritium ranging from 1.5 to 8.0 TU (tritium units). The Streeruwitz, Bean, and Millican Hills, which lie south of the Diablo Plateau, constitute the most significant recharge zone. The Eagle Mountains constitute the second major recharge area, but within short distances of the mountain front, low carbon-14 values and tritium levels that are indistinguishable from background suggest very slow rates of ground-water drainage. There is no evidence of recharge through the basin floors.

(5) Depths to water typically vary between 667 and 920 ft (203.5 and 280.5 m) in northwest Eagle Flat (between 667 and 751 ft [203.5 and 229 m] at Faskin Ranch) and between 160 and 700 ft (49 and 213.5 m) in southeast Eagle Flat. Depths to water in Red Light Draw vary from only a few feet in the Rio Grande alluvium to over 450 ft (137 m) in the northwestern part of the draw. Depths to water in the mountains typically are variable, as little as 15 to 20 ft (4.5 to 6 m) on the Eagle Mountains and

Streeruwitz Hills and as great as 1,130 ft (344.5 m) on the flanks of Sierra Blanca Mountain.

(6) Local flow systems originate in mountains and along mountain fronts and replenish the aquifers in the low-lying draws and flats. Regional ground-water flow paths are oriented along a ground-water trough, northwest-southeast from the Diablo Plateau, across northwest Eagle Flat and Red Light Draw where ground-water probably discharges in very small amounts to low-lying areas along the Rio Grande. Waters to the east of the Eagle Flat ground-water divide probably move via interbasin flow through Scott's Crossing to Lobo Valley.

(7) Hydraulic gradients vary between 0.066 in the mountains and 0.0005 in the flats and draws. The Rio Grande is the apparent aquifer discharge area for waters in northwest Eagle Flat and Red Light Draw. A low-relief ground-water divide separates northwest and southeast Eagle Flat into two separate aquifers. Very small to moderate fluctuations in head (for example, 1 to 10 ft [0.3 to 3 m]) over a 30-yr period with no consistent patterns are shown in aquifer hydrographs that compare historical with recent water-level data.

(8) Aquifer test results from five well tests in northwest Eagle Flat indicate leaky confined aquifers of very low to moderately low yield. Transmissivity values in northwest Eagle Flat vary from 2.4 to 68 ft^2/day (0.2 to 6.5 m^2/day; using Hantush-Jacob [1955] type curve matches). Approximate hydraulic conductivity values vary from 0.007 to 0.3 ft/day (0.002 to 0.09 m/day). Within the footprint of Faskin Ranch, transmissivities and approximate hydraulic conductivities vary from 2.4 to 10.2 ft^2/day (0.2 to 0.95 m^2/day) and from 0.007 to 0.12 ft/day (0.002 to 0.035 m/day), respectively. In southeast Eagle Flat, a pump test provided a transmissivity estimate of about 270 ft^2/day (25 m^2/day) using the modified Theis (1935) equation for unconfined aquifers (modification discussed in Kruseman and De Ridder, 1979). The approximate hydraulic conductivity estimated from the pump test in southeast Eagle Flat was

5.2 ft/day (1.6 m/day). Calibrated transmissivity estimates from nine specific capacity tests in wells completed in bedrock aquifers varied from 0.40 to 20,499 ft^2/day (0.04 to 1,904 m^2/day). Approximate hydraulic conductivity values estimated from transmissivity calculations varied from 0.00094 to 539 ft/day (0.00029 to 164 m/day). The median transmissivity value for the nine specific capacity tests was 891.27 ft^2/day (82.80 m^2/day).

(9) The hydrochemical composition of ground water in southern Hudspeth County varies significantly from one basin to another. In southeast Eagle Flat, ground water is mixed-HCO_3 in composition, with total dissolved solids less than 500 mg/L. In northwest Eagle Flat, most wells produce water that is Na-Cl to Na-SO_4-Cl, with total dissolved solids between 1,500 and 4,000 mg/L. The more dilute waters from this area range from Ca-HCO_3 to Na-SO_4-HCO_3 in composition. Ground water in the northeastern part of Red Light Draw is mixed-HCO_3 with total dissolved solids less than 500 mg/L. The southwestern part of the draw is dominated by Na-HCO_3-SO_4 to Na-SO_4-HCO_3 ground water, with total dissolved solids between 600 to 1,200 mg/L. A zone of high-TDS Na-Cl ground water is found along the Rio Grande in the area between Indian Hot Springs and the southeastern corner of Red Light Draw. Cl/Br ratios, stable isotopes, and unstable isotopes indicate that upwelling of high-TDS water is the primary source of salinity in lower Red Light Draw and at Indian Hot Springs. This water mixes with the low-TDS water draining from Red Light Draw. The chemistry of the mixture is dominated by the high-TDS water.

(10) The ^{14}C values range from 109 to less than 1.5 pmc, with most falling within the 0 to 20 pmc range. The highest ^{14}C values are associated with recently recharged waters of southeast Eagle Flat, where ^{14}C is typically between 109 and 45 pmc. In northwest Eagle Flat and Red Light Draw, ^{14}C is generally much lower, indicating very slow rates of ground-water drainage. At the Faskin Ranch in northwest Eagle Flat, ^{14}C values in

northwest Eagle Flat are less than 8 pmc and as low as 1.5 pmc. Tritium values are zero, indicating no recent recharge through the basin floor.

(11) The δD versus $\delta^{18}O$ compositions all lie along the global meteoric water line but vary in amount of depletion of the heavy isotopes (fig. 24). The most depleted values of deuterium and oxygen-18 are associated with the lowest pmc levels. This association, interpreted to indicate paleoclimatic labeling of stable isotopes, is supported by comparison of ground-water δ-values with the range of $\delta^{18}O$ from nearly 500 samples of precipitation from West Texas and southeast New Mexico. With few exceptions, $\delta^{18}O$ of ground water with less than 20 pmc is more depleted in oxygen-18, compared with average values of recent rainfall. Lambert and Harvey (1987) reached similar conclusions in their study of ground water in the confined aquifers of southeastern New Mexico. This hypothesis is supported by the $\delta^{18}O$ map, which shows the most isotopically depleted waters lying along the central parts of basins and draws (fig. 26).

(12) A two-dimensional, cross-sectional (profile) ground-water flow model was developed to estimate and predict flowpaths, residence times, and ground-water velocities between the Diablo Plateau and the Rio Grande (53.98-mi profile). In four model simulations, the simulated hydraulic gradient was matched with the measured hydraulic gradient by varying rock hydraulic conductivities and recharge rates within limits provided by field measurements and published literature values. In the first three model scenarios, the average recharge rate to the Diablo Plateau was specified as 0.0966 inch/yr (0.24 cm/yr or 0.8 percent of mean annual precipitation). This rate is consistent with the estimated recharge rate of 0.5 to 3 percent of the available precipitation falling on mountain drainage areas (Kelly and Hearne, 1976; Orr and Risser, 1992). Horizontal hydraulic conductivity values included: Precambrian rocks, 0.006 ft/day (0.002 m/day); basin fill, 0.25 ft/day (0.076 m/day); Permian and Cretaceous carbonate and siliciclastic rocks, 0.0091 to 3.2 ft/day (0.0028 to 1.0 m/day). These hydraulic conductivity values were selected from aquifer tests, specific capacity tests, and published literature values

(for example, Bedinger and others, 1986). Combinations of isotropy, anisotropy, and heterogeneity were simulated. Ground-water travel times between the Diablo Plateau and the Rio Grande were 60,178; 97,789; and 101,820 yr in the three model scenarios. Travel times between Faskin Ranch and the Rio Grande varied from 19,134 to 43,619 yr.

(13) In the fourth model scenario, horizontal and vertical hydraulic conductivities were increased by one order of magnitude to test the sensitivity of the model to higher hydraulic conductivity values. Travel time between the Diablo Plateau and the Rio Grande was 8,054 yr in the model (2,995 yr from Faskin Ranch to the Rio Grande). Recharge rates in the Diablo Plateau had to be increased to 1.23 inches/yr (3.12 cm/yr or 10.3 percent of mean annual precipitation) to match the simulated hydraulic gradient with the measured hydraulic gradient. The shorter residence times in the final model scenario were inconsistent with ground-water ages determined by ground-water isotopes. The recharge rate of 10.3 percent of mean annual precipitation on mountain drainage areas was much higher than the accepted 0.5 to 3 percent for recharge areas in Trans-Pecos aquifers (Kelly and Hearne, 1976; Orr and Risser, 1992). Model simulations in model scenario 4 implied that hydraulic conductivity values are closer to values specified in model scenarios 1 through 3.

(14) Circuitous, three-dimensional flow components; fracture and double porosity flow; hydrochemically distinct "pockets" of water formed by successions of permeable and low-permeability rock and poorly consolidated strata; and areal transitions between unconfined, confined, and leaky confined aquifers mark some of the complexities of the regional ground-water flow system. Hydrochemical and isotopic data provide many insights on the ground-water flow system and allow testing of hypotheses regarding ground-water flow.

INTRODUCTION

Study Objectives

At the request of the Texas Low-Level Radioactive Waste Disposal Authority (TLLRWDA), the Bureau of Economic Geology undertook this regional and site-specific study to characterize the ground-water hydrology and hydrochemistry of southern Hudspeth County and to provide a framework for interpreting site-specific hydrologic conditions at the Faskin Ranch Site (fig. 1). The information is to be used to ascertain whether the Faskin Ranch Site might be a suitable location for disposal of low-level radioactive waste. The study uses well-established hydrological, hydrochemical, and isotopic methods to delineate the boundaries of the ground-water flow system; trace local, intermediate, and regional flowpaths; describe the distribution of ground-water facies; and infer the age and source of the ground water.

Location, Physiography, and Surface Water

The area encompassed by this study lies between north latitudes 30° 37′ 30″ and 31° 15′ 22" and west longitudes 104° 52′ 30" and 105° 30′ 00" in southern Hudspeth County, Texas (fig. 1). The village of Sierra Blanca lies in the northwestern part of the study area, approximately 90 mi (144 km) east of El Paso and 33 mi (53 km) west of the city of Van Horn, along Interstate Highway 10.

The study area lies in the physiographic Basin and Range Province with its typical sharp differences in relief. Major topographic features are valley floors (flats), such as Eagle Flat, Red Light Draw, and Green River Valley, and mountains (ranges), such as Sierra Blanca and Eagle Mountains; Diablo Plateau; Streeruwitz, Bean, and Millican Hills; and the Carrizo, Van Horn, and Quitman Mountains (fig. 2). In addition, Devil Ridge, Love Hogback, and the Indio Mountains cross the area (fig. 2).

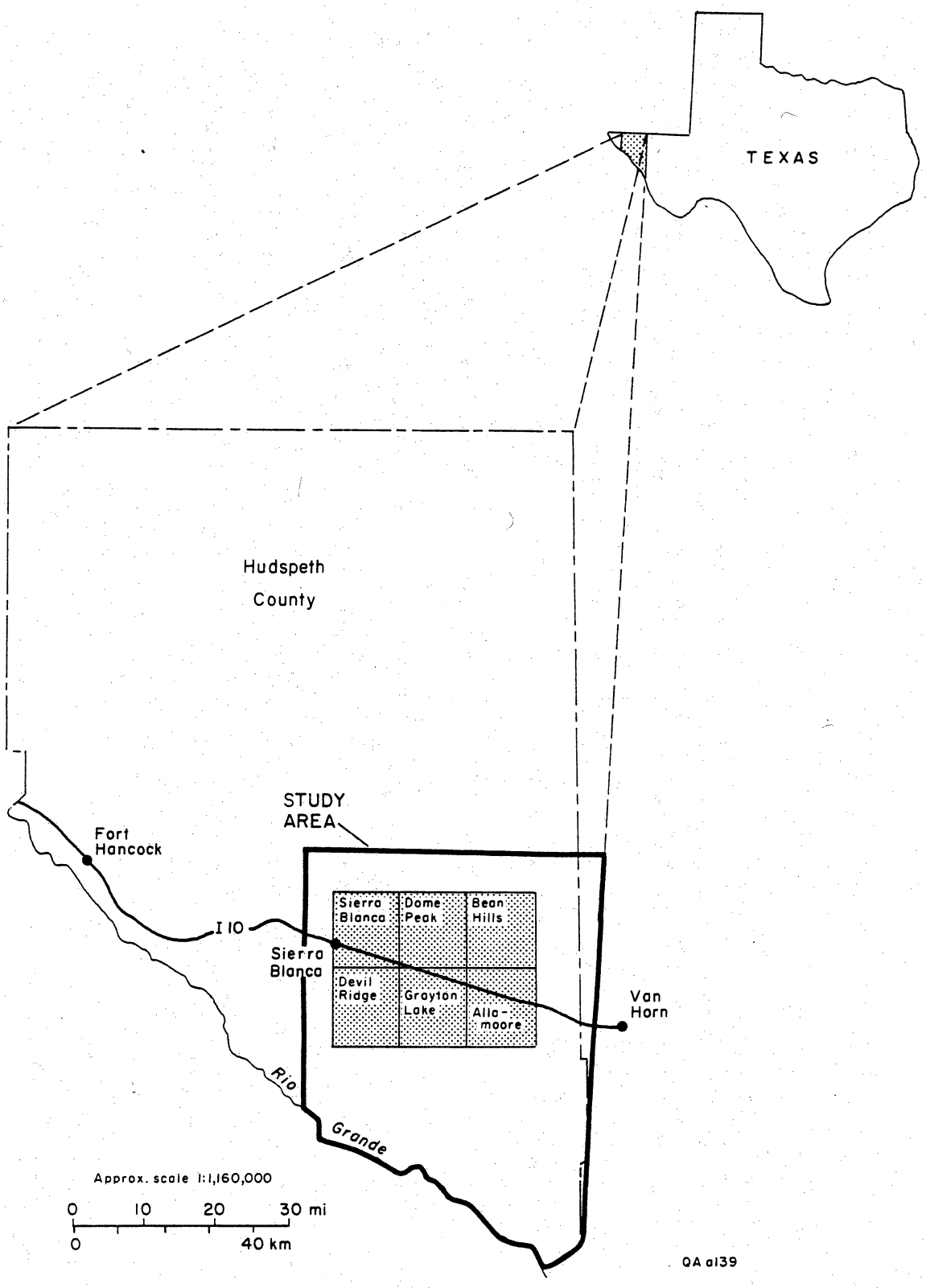

Figure 1. Location of the study area.

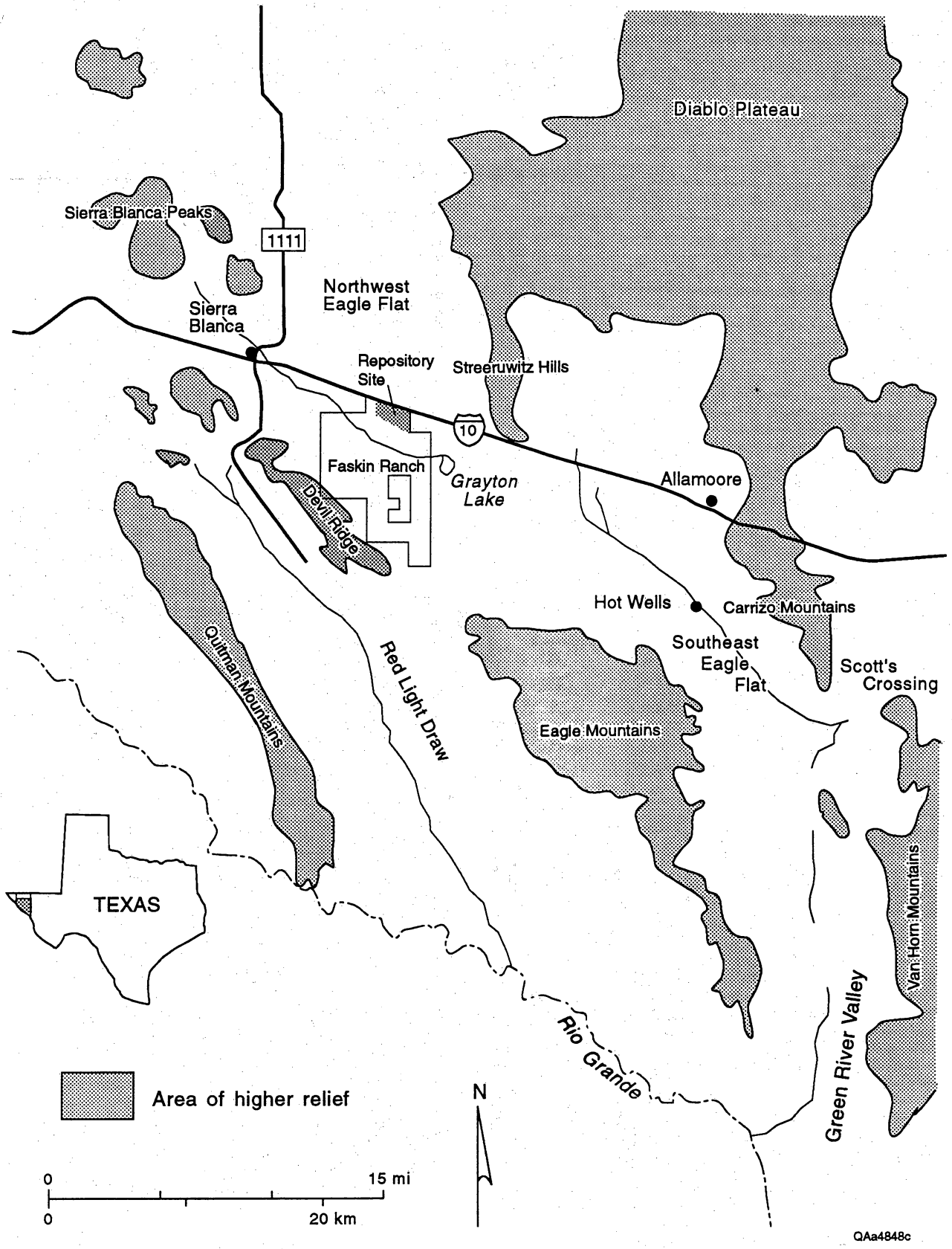

Figure 2. Prominent physiographic features in study area.

The highest point is in the Eagle Mountains at 7,510 ft (2,290 m). At opposite ends of Eagle Flat are Sierra Blanca and Allamoore, both at 4,500 ft (1,372 m). Grayton Lake lies in the center of Eagle Flat at 4,270 ft (1,300 m). The Carrizo and Van Horn Mountains rise to more than 5,200 ft (1,585 m), and the Quitman Mountains are at least 6,200 ft (1,890 m). Along its southeasterly course, the elevation of the Rio Grande decreases from 3,300 ft (1,006 m) near Indian Hot Springs to less than 3,200 ft (975 m) at the southeastern corner of Green River Valley.

The Rio Grande forms the southern boundary of the study area. It is the only perennial stream in the study area. All other water courses flow only after heavy rainfall (Underwood, 1962). Surface flow in Red Light Draw and southern Green River Valley is toward the Rio Grande. Eagle Flat Draw flows eastward toward Scott's Crossing. Northwestern Eagle Flat is an area of internal drainage. Runoff from this watershed collects in Grayton Lake, which is a desert playa (Motts, 1965). Grayton Lake is a topographic low with 45 ft (14 m) of closure. It is dry for extended periods of time (Underwood, 1962), and water accumulates in the playa only after exceptionally heavy rainfalls. The northwestern and southeastern sections of Eagle Flat are separated by a surface-water divide about 6 mi (9.5 km) east of Grayton Lake. The divide extends southward from the Streeruwitz Hills to the Eagle Mountains. Another surface-water divide separates Green River Valley from southeastern Eagle Flat to the north.

This report divides the study area into three subsurface basins based on surficial watersheds and ground-water drainage divides. The area within the Blanca Draw watershed, including Grayton Lake and the Faskin Ranch Site, is referred to as the Northwest Eagle Flat Watershed. Southeast Eagle Flat Watershed is defined by the surface-water divide bounding Eagle Flat Draw. Red Light Draw Watershed includes Red Light Draw, its source areas, and parts of the aquifer in Rio Grande Alluvium at the lowermost reaches of the watershed. Indian Hot Springs and Red Bull Spring lie within the Hueco Bolson but are included in Red Light Draw Watershed for ease of discussion.

Structural Geology

The tectonic history of southern Hudspeth County includes two episodes of thrust faulting in the late Precambrian and one in the early Tertiary, followed by igneous activity and extensional faulting. The extensional faulting formed the local basin and range setting, a series of northwest-trending fault blocks and intermontane basins superposed on the previously deformed strata (King and Flawn, 1953; Underwood, 1962; Albritton and Smith, 1965; Henry and others, 1983; Raney and Collins, 1993).

Extensive outcrops of Precambrian metasedimentary rocks are found in the Streeruwitz, Bean, and Millican Hills and in the Carrizo Mountains. The metasedimentary rocks include greenschist to amphibolite facies of the Carrizo Mountain Group and low-grade greenschist facies of the Allamoore Formation (Raney and Collins, 1993). Cretaceous rocks are exposed in thrust-faulted blocks and folds with repeated sections at Devil Ridge, Love Hogback, the Eagle Mountains, the Indio Mountains, and the Quitman Mountains (Underwood, 1962; Albritton and Smith, 1965; Raney and Collins, 1993). The Cretaceous section ranges in age from late Aptian to late Turonian and averages 7,000 ft (2,135 m) in thickness. The marine sediments were deposited on a platform margin and in adjoining areas of the Chihuahua trough; carbonate and siliciclastic rocks are interbedded throughout the section (Underwood, 1962). The Cretaceous rocks were deformed by regional compression in Late Cretaceous–Early Tertiary time (Underwood, 1962; Albritton and Smith, 1965).

Basin Fill

The basins are filled with Miocene, Pliocene, and early Pleistocene deposits of alluvial fan, fluvial, and playa depositional facies and Quaternary wind-blown sediments (King and Flawn, 1953; Underwood, 1962; Albritton and Smith, 1965; Groat, 1972; Gustavson, 1991; Langford, 1993; Jackson and others, 1993). The thickness of the fill varies greatly among and within the basins (fig. 2 in Collins and Raney, 1993) (Albritton and Smith, 1965; Gates and White, 1976; Gates and

others, 1980), as indicated by resistivity profiles, cores, well logs, and driller's logs. Monitor wells, core holes, and geophysical surveys in northwest Eagle Flat, 5 to 7 mi (8 to 11.2 km) east of Sierra Blanca, show that the basin fill increases from less than 100 ft (30.5 m) to more than 700 ft (214 m) over a distance of 3 mi (4.8 km). Along the axis of southeast Eagle Flat, the fill increases from nearly 700 ft (214 m) at well 48-63-601 to more than 2,000 ft (613 m) at the U.S. Geological Survey (USGS) test hole 51-01-504 near Scott's Crossing (Gates and others, 1980), over a distance of 13 mi (21 km). Well 48-64-BTH was completed in fine-grained basin fill at a depth of 1,050 ft (320 m). Based on the original basin-fill isopach map of Gates and others (1980), bedrock was expected to be encountered between 700 and 800 ft (213 and 244 m). Basin fill is less than 500 ft (152 m) thick in northern Red Light Draw, increasing to more than 2,000 ft (610 m) along the Rio Grande.

Well-Numbering System

With few exceptions, all wells are referenced according to the State well-numbering system adopted by the Texas Water Development Board (TWDB) (White and others, 1980). Exceptions are monitor wells and stratigraphic tests drilled by the Bureau of Economic Geology on and near Faskin Ranch (for example, YM-7A, YM-8, YM-18, YM-19, and YM-63, in which YM refers to Yucca Mesa). In addition, well 48-64-BTH was drilled by the Bureau of Economic Geology along the hydrologic divide between Northwest Eagle Flat and Southeast Eagle Flat Watersheds, and other wells were located that had not been previously included and numbered in the TWDB data base. These wells were assigned unique numbers and letters consistent with the State well-numbering system (for example, 47-49-GHM and 48-62-BOR). The three letters are mnemonics based on a prominent local landmark or the surname of the landowner. Locations of wells and springs are shown in figure 3.

Water-Bearing Units

The Cretaceous Cox Sandstone is the primary water-bearing unit in Northwest Eagle Flat Watershed (Albritton and Smith, 1965). Albritton and Smith (1965) describe the formation as "a

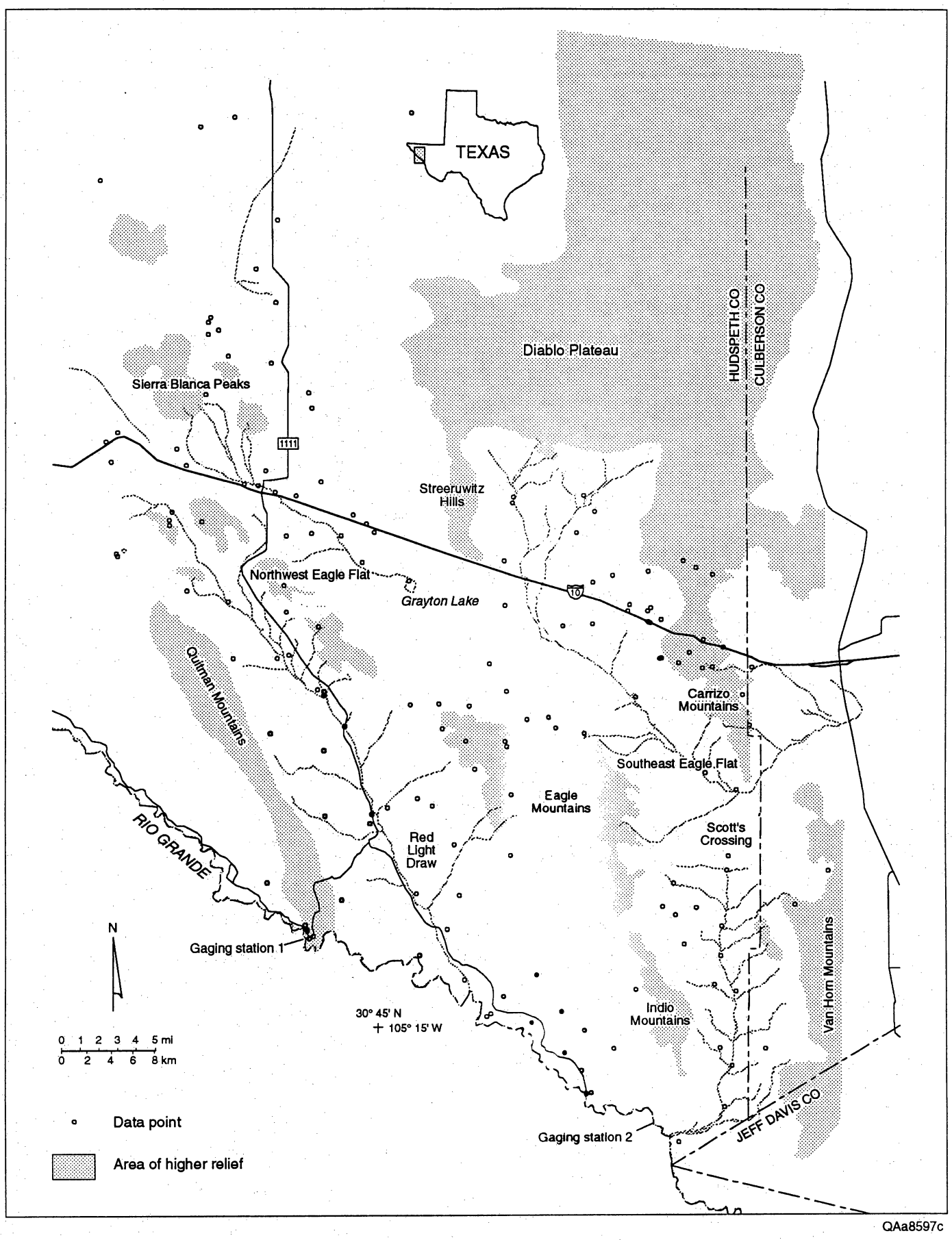

Figure 3. Locations of wells and springs.

heterogeneous body of sandstone and associated clastic rocks which is varied in detail and not entirely of the same age from place to place." Outcrops expose fine- to coarse-grained, yellowish-gray, quartzitic, cross-laminated, and ferruginous sandstone. Silt and shale are interbedded with medium-gray flaggy limestone (Underwood, 1962; Albritton and Smith, 1965). Cuttings and core from monitor wells YM-7A, YM-19, and YM-63 show the Cox in the subsurface to be white to reddish fine- to coarse-grained sandstone, with interbeds of gray limestone and green and yellow siltstone.

Two monitor wells at the Faskin Ranch Site (YM-8 and YM-18) produce water from the Cretaceous Finlay Limestone. In the Sierra Blanca area, exposures of the Finlay range from massive beds of gray fossiliferous limestone to a medium-gray pale-yellowish, brown-weathering, thin- to thick-bedded, finely crystalline, nodular limestone having a few thin beds of shale, siltstone, and extremely fine grained quartz sandstone (Underwood, 1962; Albritton and Smith, 1965). The lower part of the formation is marly, often giving way to beds of white sandstone, 0.5 to 3 ft (0.15 to 0.91 m) thick (Albritton and Smith, 1965). Cuttings from the two aforementioned monitor wells indicate that the Finlay consists of yellow siltstone and gray limestone with thin beds of white sandstone. In both wells, clean white sandstone occurs at the base of the formation. A well drilled to a depth of 1,300 ft (396 m) on the northeast side of Devil Ridge (48-62-TEX) (fig. 3) produces water from either the Bluff Mesa Formation or the underlying Yucca Formation.

Precambrian rocks form the principal aquifer in the northern and eastern areas of Southeast Eagle Flat Watershed. Well depths range from 80 to 480 ft (24 to 146 m), with water depths as much as 214 ft (65 m). In other areas of the Southeast Eagle Flat Watershed, wells that are as deep as 2,000 ft (610 m) produce water from basin fill. Only well 48-63-601 is reported to have pumped water from an unspecified Cretaceous unit (White and others, 1980).

In Red Light Draw, wells produce water from Cretaceous rocks and basin-fill material. Cretaceous rocks make up the water-bearing unit in the northern part of the basin. Wells in the central and southern reaches of Red Light Draw produce water from basin fill. At Indian Hot Springs

and Red Bull Spring near the southern end of the Hueco Bolson, ground-water discharge might be focused in fault zones in lower Cretaceous rocks (Henry, 1979).

Climate

The climate is subtropical arid (Larkin and Bomar, 1983). Average annual precipitation is 12 inches (30.5 cm), and mean annual evaporation is 84 inches (213 cm), based on measurements of lake-surface evaporation (Larkin and Bomar, 1983). Average annual low temperatures are nearly 48°F (8.9°C), and average high temperatures are close to 80°F (26.7°C). Most precipitation occurs during the months of July through October (Larkin and Bomar, 1983; Bedinger and others, 1984) as widely scattered thunderstorms with moisture originating primarily in the Gulf Coast (Elliot, 1949; Nativ and Riggio, 1990). Because of the convective nature of thunderstorms, most summer precipitation in West Texas and southern New Mexico increases with elevation (Gile and others, 1981). Winter rainfall, which accounts for less than one-third of total precipitation (Larkin and Bomar, 1983), is associated with widespread Pacific frontal systems (Elliot, 1949; Nativ and Riggio, 1990), which do not display a significant orographic effect.

Population and Water Use

The study area is sparsely populated. Sierra Blanca, the largest community, had a population of 700 in 1990. The economic base of the community is sustained predominantly by the ranching industry, interstate travel, and government services.

Sierra Blanca formerly depended upon local wells to satisfy municipal water needs but currently has most of its water piped in from Van Horn. Van Horn derives its water supplies from a basin-fill aquifer at Wild Horse Flat, a bolson aquifer east of the study area. In rural areas, water use is mostly limited to domestic and livestock consumption. A small number of low-capacity water wells satisfies the needs of the local population and livestock industry. A few springs issue from bedrock formations in the mountains and augment livestock water supplies.

SOURCES OF INFORMATION

Geologic Studies

King and Flawn (1953) studied the geology and mineral deposits of Precambrian rocks of the Van Horn area. Underwood (1962) described the geology of the Eagle Mountains and surrounding area. Albritton and Smith (1965) conducted a detailed evaluation of the geology around Sierra Blanca and the northern Quitman Mountains. Jones and Reaser (1970) compiled a geologic map of the Quitman Mountains. More recently, Raney and Collins (1993) conducted a field study of the regional geologic setting of the Eagle Flat area, and Collins and Raney (1993) mapped late Cenozoic faults of northwestern Trans-Pecos Texas.

Hydrological Studies

Although there have been many studies of ground-water hydrology in Trans-Pecos Texas, few have concentrated on the Northwest Eagle Flat, Southeast Eagle Flat, and Red Light Draw Watersheds. Kreitler and others (1986), Fisher and Mullican (1990), Scanlon and others (1991), and Mullican and Senger (1992) conducted ground-water studies in the Hueco Bolson, the Diablo and Culberson Plateaus, and the Salt Basin during an earlier effort by the Texas Low-Level Radioactive Waste Disposal Authority to evaluate potential repository sites in Hudspeth and Culberson Counties. The earliest regional study was by Richardson (1904), who surveyed ground-water resources in Trans-Pecos Texas north of the Texas and Pacific Railway. In a joint program between the U.S. Geological Survey and the Texas Department of Water Resources, Gates and White (1976) conducted a drilling program for ground-water resources in Hudspeth, Culberson, and Presidio Counties. Subsequently, Gates and others (1980) completed a reconnaissance of the availability of potable water resources in the westernmost counties of Texas. They drew the first water-table maps for the area representing the elevation of ground water measured in water wells and test borings. White and others (1980) compiled a data base of water depths and major-ion chemistry in Eagle

Flat, Red Light Draw, Green River Valley, Lobo Valley, the Salt Basin, and Hueco Bolson. Henry (1979) studied the geologic setting and geochemistry of thermal waters in Trans-Pecos Texas and adjacent parts of Mexico, and Hoffer (1978) directed an exploratory evaluation of geothermal energy potential. Other studies of significance addressed the distribution of stable isotopes in precipitation and in ground water in West Texas and southeastern New Mexico (Hoy and Gross, 1982; Chapman, 1986; Lambert and Harvey, 1987; Nativ and Riggio, 1990; Nativ and Gutierrez, 1988; Chapman and others, 1992).

METHODS

Methods used to characterize the regional flow system included (a) measuring water levels in wells and gauging Rio Grande streamflow, (b) analyzing aquifer and specific-capacity tests, (c) acquiring and interpreting water quality and isotopic data, and (d) modeling ground-water flow.

Water-Level Measurements and Stream Gauging

A composite potentiometric surface map was made on the basis of water-level measurements from all hydrostratigraphic units. There are insufficient data to separately map the regional potentiometric surfaces of each distinct hydrostratigraphic unit or even of separate bedrock and basin-fill aquifer units. In addition, historical data were pooled with recent measurements. Some old water-level measurements could not be repeated because the wells had been destroyed, were inaccessible, or could not be located. An electric probe was used to measure the depth to water relative to the measuring point, usually the top of well casing. Table 1 lists the wells and springs used as a basis for contouring the potentiometric map, along with corresponding surface elevations, water depths, well depths, casing diameters, measurement dates, and agencies reporting the measurements.

Water levels in observation wells drilled for hydrologic tests were measured with pressure transducers. Transducers were hung at a given depth in the water column and connected to a data

Table 1. List of water level measurements in southeast Eagle Flat, northwest Eagle Flat, and Red Light Draw.

ID no.	Chemical data*	Water-shed**	Date	Measured by†	Well depth (ft)	Casing diameter (inches)	Water-bearing unit††	Surface elevation (ft)	Depth to water (ft)	Water-level elevation (ft)
47-49-GHM	5, 6	SEEF		BEG			pCamb.			nm
47-49-GHW	5, 6	SEEF		BEG			pCamb.			nm
47-49-GTM	5, 6	SEEF		BEG			pCamb.			nm
47-57-401	5, 6	SEEF	10/7/72	TDWR	257	10	QTal	4,526	106.1	4419.9
47-57-501		SEEF	11/28/72	TDWR	400	6	QTal	4,521	75.0	4446.0
47-57-502		SEEF	12/14/72	TDWR	80	8	QTal	4,598	19.0	4579.0
47-57-702		SEEF	10/4/72	TDWB	84	10	QTal	4,472	46.3	4425.7
47-57-703		SEEF	10/4/72	TDWR	180	6	pCamb.	4,560	47.7	4512.3
47-57-801		SEEF	10/4/72	TDWR	160	6	pCamb.	4,578	29.9	4548.1
47-57-802		SEEF	10/5/72	TDWR	6	6	pCamb.	4,623	0.0	4623.0
47-57-803		SEEF	11/29/72	TDWR	335	6	pCamb.	4,380	51.4	4328.6
47-57-902		SEEF	11/28/72	TDWR	200	6	Qal, pCamb.	4,364	40.7	4323.3
47-57-KHN	5, 6	SEEF	12/18/92	BEG		8	QTal	4,472	44.0	4428.0
48-36-601		NWEF								4375.0
48-37-301		NWEF								4377.0
48-37-302		NWEF								4198.0
48-38-701		NWEF								3525.0
48-39-101		NWEF								3621.0
48-45-601		NWEF	5/30/72	TDWR	1,018	14	K	4,570	943.0	3627.0
48-45-602	5	NWEF	5/16/72	BEG	1,060	14	K	4,570	943.0	3627.0
"	"	"	9/19/74	BEG	"	"	"	"	938.0	3632.0
"	"	"	1/11/93	BEG	"	"	"	"	946.9	3623.1
48-45-603	5, 6	NWEF	3/26/74	TDWR	1,096	14	K	4,589	945.0	3644.0
"	"	"	6/1/74	TDWR	"	"	"	"	966.0	3623.0
"	"	"	5/17/75	TDWR	"	"	"	"	961.0	3628.0
48-45-604		NWEF	7/26/74	TDWR	1,110		K	4,608	979.0	3629.0
48-45-901	5, 6	NWEF	4/11/72	TDWR	1,126	5	K	4,740	1111.0	3629.0
48-46-101		NWEF								3610.0
48-46-401		NWEF	3/23/72	TDWR	1,093	6	K	4,678	1040.0	3638.0
48-46-701		NWEF	3/29/72	TDWR	1,137	6	K	4,600	1120.0	3480.0
48-53-101		NWEF								4036.0
48-53-104		NWEF								4597.0
48-53-301		NWEF	na	TDWR	1,341	6	K	4,993	1130.0	3863.0
"	"	"	1/12/93	BEG	"	"	"	"	1158.5	3834.5
48-53-401		NWEF	na	TDWR	175	5	Ti	4,737	148.0	4589.0
48-53-501	5, 6	NWEF	3/15/72	TDWR	1,110	10	K	4,656	369.7	4286.3
"	"	"	12/17/92	BEG	"	"	"	"	371.7	4284.3
48-53-503		NWEF	3/16/72	TDWR	645	7	K	4,698	454.0	4244.0
48-53-802	5, 6	NWEF	2/3/72	TDWR	286	8	K	4,695	154.6	4540.4
"	"	"	7/20/73	TDWR	"	"	"	"	176.0	4519.0
"	"	"	8/23/73	TDWR	"	"	"	"	197.0	4498.0
"	"	"	10/30/73	TDWR	"	"	"	"	223.0	4472.0
48-53-803	5, 6	NWEF	2/10/72	TDWR	298	6	K	4,681	165.2	4515.8
"	"	"	7/17/73	TDWR	"	"	"	"	224.0	4457.0
"	"	"	12/11/73	TDWR	"	"	"	"	242.0	4439.0
"	"	"	12/18/92	BEG	"	"	"	"	165.2	4515.8
48-53-804	5	NWEF	7/20/73	TDWR	970	7	K	4,655	355.9	4299.1
"	"	"	11/19/73	TDWR	"	"	"	"	364.0	4291.0
"	"	"	2/6/74	TDWR	"	"	"	"	372.0	4283.0
"	"	"	12/18/92	BEG	"	"	"	"	359.0	4296.0
48-53-805		NWEF	7/20/73	TDWR	298	6	K	4,697	176.3	4520.7
"	"	"	12/1/73	TDWR	"	"	"	"	236.2	4460.8
"	"	"	6/21/74	TDWR	"	"	"	"	259.0	4438.0
48-53-902		NWEF	2/9/72	TDWR	263	5	K	4,654	214.9	4439.1
"	"	"	12/18/92	BEG	"	"	"	"	209.5	4444.5
48-54-201		NWEF	3/30/72	TDWR	947	6	K	4,517	889.0	3628.0
48-54-202		NWEF	3/30/72	TDWR	906		K	4,498	902.0	3596.0
48-54-401	5	NWEF	6/6/57	TDWR	1,102	7	K	4,595	965.0	3630.0
"	"	"	7/19/92	BEG	"	"	"	"	973.5	3621.5

Table 1 (cont.)

ID no.	Chemical data*	Water-shed**	Date	Measured by†	Well depth (ft)	Casing diameter (inches)	Water-bearing unit††	Surface elevation (ft)	Depth to water (ft)	Water-level elevation (ft)
48-54-402	5	NWEF	7/23/43	TDWR	950	6	K	4,540	920.0	3620.0
48-54-404	5, 6	NWEF	3/23/72	TDWR	1,000	6	K	4,478	810.0	3668.0
48-54-408		NWEF	na	TDWR	988	6	K	4,580	960.0	3620.0
48-54-502	5, 6	NWEF	3/31/72	TDWR	950	6	K	4,408	781.0	3627.0
48-54-503	5	NWEF	na	OWNER	1,350	10	K	4,445	887.0	3558.0
48-54-701		NWEF	7/6/72	TDWR	920	6	K	4,487	905.0	3582.0
48-54-801	5	NWEF	7/6/72	TDWR	945	8	K	4,406	920.0	3486.0
48-54-901	5	NWEF	3/31/72	TDWR	1,150	na	K	4,380	788.0	3592.0
48-55-901		SEEF	8/31/72	TDWR	397	10	pCamb.	4,649	207.0	4442.0
"		"	1/11/93	BEG	"	"	"	"	214.1	4434.9
48-55-902	5, 6	SEEF	8/31/72	TDWR	190	9	pCamb.	4,638	151.2	4486.8
48-56-501		SEEF	9/1/72	TDWR	121		pCamb.	4,770	67.0	4703.0
48-56-803	5, 6	SEEF	9/1/72	TDWR	130	6	pCamb.	4,757	73.6	4683.4
48-56-DES	5, 6	SEEF	1/11/93	BEG			pCamb.	4,655	56.3	4598.8
48-61-101		RLD	5/4/72	TDWR	442	6	Ti	5,028	269.0	4759.0
48-61-103		RLD	5/4/72	TDWR	425	8	Ti	5,180	414.0	4766.0
48-61-104		RLD	5/4/72	TDWR	500	10	Ti	5,211	480.8	4730.2
48-61-201	5, 6	RLD	7/25/31	TDWR	690	6	K	4,372	538.0	3834.0
48-61-302	5	RLD	5/16/72	TDWR	740	6	QTal	4,280	421.4	3858.6
48-61-901		RLD	11/1/64	TDWR	290	10	K	4,383	190.0	4193.0
48-62-501	5	RLD	3/14/94	BEG	750	4	K	4,376	637.7	3738.3
48-62-701	5	RLD	5/10/72	TDWR	525	6	QTal	4,110	448.0	3662.0
48-62-801		RLD	5/12/72	TDWR	598	9	QTal	4,018	323.8	3694.2
48-62-802		RLD	11/9/66	TDWR	540	10	QTal	4,010	367.1	3642.9
"		"	5/16/72	TDWR	"	"	"	"	364.5	3645.5
"		"	5/16/72	TDWR	"	"	"	"	365.2	3644.8
48-62-804		RLD	5/16/72	TDWR	540	10	QTal	4,005	355.0	3650.0
48-62-805	5, 6	RLD			400	6	QTal	4,007		nm
48-62-807		RLD	10/28/64	TDWR	497	6	QTal	4,095	438.0	3657.0
"		"	5/17/72	TDWR	"	"	"	"	437.1	3657.9
48-62-BOR	5, 6	RLD				8	K	4,230		nm
48-62-TEX	5, 6	NWEF	1/15/92	BEG	1,250	8	K	4,575	842.0	3733.0
"		"	7/8/92	BEG	"	"	"	"	842.0	3733.0
48-63-302	5, 6	NWEF	8/30/72	TDWR	602	8	pCamb.	4,506	354.4	4151.6
48-63-601		NWEF	1959	OWNER	899	6	K	4,391	700.0	3691.0
48-63-802		NWEF	7/10/72	TDWR	124	5	K	4,314	120.7	4193.3
48-63-803		NWEF	7/10/72	TDWR	213	8	K	4,532	24.7	4507.3
48-63-901		NWEF	1941	TDWR	1,000	6	K	4,540	900.0	3640.0
48-63-902	5, 6	NWEF	6/8/73	TDWR	238	6	QTal	4,757	227.0	4530.0
48-64-201		SEEF	9/12/72	TDWR	226	8	pCamb.	4,504	143.7	4360.3
48-64-301	5, 6	SEEF	8/24/72	TDWR	200	5	pCamb.	4,676	156.0	4520.0
48-64-302	5, 6	SEEF	9/12/72	TDWR	193	6	pCamb.	4,560	157.8	4402.2
"		"	1/11/93	BEG	"	"	"	"	142.0	4418.0
48-64-501		SEEF	4/3/73	TDWR	477	6		4,388	229.6	4158.4
"		"	3/15/94	BEG	"	"	"	"	141.0	4247.0
48-64-601		SEEF	8/24/72	TDWR	177	6	pCamb.	4,511	174.0	4337.0
48-64-602	5, 6	SEEF	8/24/72	TDWR	239	5	pCamb.	4,538	190.3	4347.7
48-64-604	5, 6	SEEF	8/24/72	TDWR	220	6	pCamb.	4,490	163.7	4326.3
48-64-605		SEEF	9/13/72	TDWR	220	6	pCamb.	4,556	173.2	4382.8
48-64-901	5	SEEF	4/12/72	TDWR	1,001	10	QTal	4,271	610.3	3660.7
48-64-902		SEEF		TDWR	1,000	10	QTal	4,271		nm
48-64-BTH	5	NWEF	8/30/93	BEG	1,100	8	QTal	4,363	698.0	3665.0
48-64-HW3		SEEF	12/18/92	BEG		6	QTal	4,271	619.8	3651.3
48-64-LOV	5, 6	SEEF								nm
50-06-101		RLD	5/17/72	TDWR	115	6	K	4,342	72.5	4269.5
50-06-102		RLD	1964	TDWR	150	6	K	4,342	95.0	4247.0
50-06-203	5, 6	RLD	5/17/72	TDWR	667	6	K	4,039	391.2	3647.8
50-06-301	5, 6	RLD	12/4/61	TDWR	390	6	QTal	3,941	326.1	3614.9
"		"	5/17/72	TDWR	"	"	"	"	319.6	3621.4
"		"	1/16/92	BEG	"	"	"	"	316.3	3624.7
50-06-801	5, 6	RLD	7/18/72	TDWR	190	6	K	4,005	172.0	3833.0

Table 1 (cont.)

ID no.	Chemical data*	Water-shed**	Date	Measured by†	Well depth (ft)	Casing diameter (inches)	Water-bearing unit††	Surface elevation (ft)	Depth to water (ft)	Water-level elevation (ft)
50-06-901		RLD	10/30/64	TDWR	354	6		3,758	292.1	3465.9
"		"	7/19/72	TDWR	"	"	"	"	289.0	3469.0
50-06-LOV	5, 6	RLD				6	QTal			nm
50-07-201		RLD	5/24/72	TDWR	284	5	K	4,381	271.0	4110.0
50-07-202		RLD	na	TDWR	270	na	K	4,690	15.0	4675.0
50-07-301	5	NWEF	6/8/73	TDWR	200	6	K	5,760	96.0	5664.0
50-07-302		NWEF	6/8/73	TDWR	200	4	K	5,900	191.0	5709.0
50-07-401	5, 6	RLD	10/30/64	TDWR	510	5	QTal	3,966	460.0	3506.0
50-07-402		RLD	7/18/72	TDWR	370	10	QTal	3,785	300.0	3485.0
50-07-501		RLD	12/10/73	USGS	1,185	6	QTal	4,045	575.0	3470.0
50-07-601	5, 6	RLD	6/27/72	TDWR	264	6	K	4,787	192.0	4595.0
50-07-801		RLD	6/29/72	TDWR	510	6	QYAL	3,924	465.9	3458.1
50-07-901		RLD	7/29/72	TDWR	610	4	Tv,K	4,483	350.0	4133.0
50-07-FRC	5, 6	RLD	7/3/92	BEG	100	4	Tv	5,135	65.0	5070.0
50-07-MCM	5, 6	RLD	7/18/92	OWNER	319	6	K	4,071	290.0	3781.0
50-08-101	5, 6	SEEF	9/14/72	TDWR	237	5	K	4,941	79.0	4862.0
50-08-102	5, 6	SEEF	12/12/92	BEG	spring		K	4,761	0.0	4761.0
50-08-103		NWEF	9/14/72	TDWR	112	5	K	5,105	65.0	5040.0
50-08-201		SEEF	9/13/72	TDWR	90	5	QTal	4,762	37.4	4724.6
50-08-202	5, 6	SEEF	9/13/72	TDWR	40+	5	QTal	4,762	33.4	4728.6
50-14-301		RLD	1/26/73	TDWR	100	5	K	3,590	50.0	3540.0
50-14-501	5, 6	RLD		BEG	spring		K	3,312	0.0	3312.0
50-14-503	5, 6	RLD	7/6/92	BEG	spring		K	3,312	0.0	3312.0
50-14-509	5	RLD	4/1/69	TDWR	80	16	Qal	3,300	6.5	3293.5
50-14-RBL	5, 6	RLD	1/28/93	BEG	spring		K	3,510	0.0	3510.0
50-15-101	5	RLD	6/27/72	TDWR	114	6	QTal	3,510	29.0	3481.0
50-15-201	5, 6	RLD	6/29/72	TDWR	460	5	QTal	3,628	186.0	3442.0
50-15-401		RLD	7/19/72	TDWR	23	5	QTal	3,235	13.6	3221.4
50-15-801	5	RLD	11/10/64	TDWR	47	4	Qal	3,236	31.3	3204.7
"		"	6/29/72	TDWR	"	"	"	"	32.8	3203.2
"		"	12/14/92	BEG	"	"	"	"	32.4	3203.6
50-15-902		RLD	5/11/61	TDWR	40	15	Qal	3,190	7.2	3182.8
"		"	11/15/73	TDWR	"	"	"	"	4.7	3185.3
"		"	12/14/92	BEG	"	"	"	"	3.1	3186.9
50-15-903		RLD	10/29/64	TDWR	182	5	QTal	3,269	32.5	3236.5
"		"	6/30/72	TDWR	"	"	"	"	35.5	3233.5
"		"	12/14/92	BEG	"	"	"	"	17.4	3251.6
50-15-904		RLD	6/30/72	TDWR	104	5	QTal	3,269	74.5	3194.5
"		"	12/14/92	BEG	"	"	"	"	17.3	3251.7
50-15-905		RLD	11/15/73	TDWR	65	18	Qal	3,190	6.3	3183.7
50-15-905	5	RLD	12/14/92	BEG	65	18	Qal	3,190	2.2	3187.8
50-15-WBG	5	RLD	1/16/92	BEG	na	8	QTal	3,410	72.4	3338.0
50-16-701		RLD	10/29/64	TDWR	261	6	QTal	3,549	167.1	3381.9
"		"	1/24/73	TDWR	"	"	"	"	162.5	3386.5
"		"	1/9/93	BEG	"	"	"	"	162.8	3386.3
50-16-702		RLD	11/10/64	TDWR	56	6	QTal	3,215	45.0	3170.0
"		"	1/25/73	TDWR	"	"	"	"	40.6	3174.4
50-16-703	5	RLD	11/10/64	TDWR	224	6	QTal	3,352	127.8	3224.2
"		"	1/25/73	TDWR	"	"	"	"	195.3	3156.7
"		"	1/9/93	BEG	"	"	"	"	32.3	3319.7
50-16-901		RLD	10/19/72	TDWR	306	6	K	4,040	209.0	3831.0
50-24-201		RLD	11/10/64	TDWR	66	6	QTal	3,180	37.9	3142.1
"		"	1/25/73	TDWR	"	"	"	"	32.0	3148.0
50-24-202	5, 6	RLD	11/10/64	TDWR	66	6	Qal	3,204	52.4	3151.6
"		"	1/25/73	TDWR	"	"	"	"	45.1	3158.9
"		"	1/9/93	BEG	"	"	"	"	42.3	3161.8
50-24-301	5, 6	RLD	11/16/73	TDWR	330	8	QTal	3,465	198.2	3266.8
"		"	1/9/93	BEG	"	"	"	"	190.0	3275.0
50-24-501		RLD	5/11/61	TDWR	52	14	Qal	3,155	7.0	3148.0
"		"	11/16/73	TDWR	"	"	"	"	5.0	3150.0
50-24-502		RLD	5/11/61	TDWR	70	16	Qal	3,155	7.4	3147.6

Table 1 (cont.)

ID no.	Chemical data*	Watershed**	Date	Measured by†	Well depth (ft)	Casing diameter (inches)	Water-bearing unit††	Surface elevation (ft)	Depth to water (ft)	Water-level elevation (ft)
"		"	11/16/73	TDWR	"	"	"	"	5.6	3149.4
50-24-503	5, 6	RLD	5/11/61	TDWR	65	6	Qal	3,185	48.0	3137.0
50-24-504		RLD	10/11/64	TDWR	150	7	QTal	3,162	43.9	3118.1
"		"	11/16/73	TDWR	"	"	"	"	39.8	3122.2
50-24-505	5	RLD	11/16/73	TDWR	50	16	Qal	3,153	5.0	3148.0
"		"	1/9/93	BEG	"	"	"	"	5.0	3148.0
50-24-SHT	5, 6	RLD	10/22/92	BEG	200+	4	QTal	3,260	0.0	3260.0
51-01-301		SEEF	11/29/72	TDWR	80	5	Qal	4,242	40.4	4201.6
51-01-501	5, 6	SEEF	na	TDWR	501	6	QTal	4,146	484.0	3662.0
51-01-503	5, 6	SEEF	1973	TDWR	530	6	QTal	4,166	481.0	3685.0
51-01-801	5, 6	SEEF	11/14/72	TDWR		8	QTal	4,253	646.5	3606.5
51-09-101		SEEF	10/13/72	TDWR	305	6	K	4,525	263.7	4261.3
51-09-102		SEEF	11/12/64	TDWR		6	QTal	4,347	537.6	3809.4
"		"	11/11/72	TDWR	"	"	"	"	530.9	3816.1
51-09-103	5	SEEF	10/18/72	TDWR	193	6	K	4,284	130.5	4153.5
51-09-104		SEEF	10/18/72	TDWR	142	6	K	4,320	117.0	4203.0
51-09-201		SEEF	na	TDWR	1,600	na	K	4,230	428.0	3802.0
51-09-401		SEEF	10/18/72	TDWR	462	6	K	4,308	462.0	3846.0
51-09-501	5	SEEF	12/13/92	BEG		6		4,348	513.5	3834.5
51-09-503		SEEF	11/11/64	TDWR	344	8	QTal	4,085	234.4	3850.6
"		"	10/18/72	TDWR	"	"	"	"	230.0	3855.0
51-09-801		SEEF	10/19/72	TDWR	97	6	Qal	3,972	23.0	3949.0
51-09-802		SEEF	11/12/64	TDWR	100	6	QTal	3,865	24.1	3840.9
"		"	11/16/72	TDWR	"	"	"	"	24.1	3840.9
51-10-103	5, 6	SEEF					K	4,684		nm
51-17-201		SEEF	3/13/74	TDWR	113	6	QTal	3,600	110.8	3489.2
51-17-202		SEEF	3/13/74	TDWR	234	6	QTal	3,719	227.6	3491.4
51-17-301		SEEF	3/13/74	TDWR	455	5	QTal	3,906	432.0	3474.0
51-17-501		SEEF	3/17/93	BEG	spring		Qal	3,383	0.0	3383.0
51-17-701	5	SEEF	3/12/74	TDWR	100	16	Qal	3,152	31.0	3121.0
YM-18	5, 6	NWEF	12/17/92	BEG	835	8	K	4,376	751.1	3624.9
"		"	6/26/93	BEG	"	"	"	"	751.5	3624.5
YM-19	5, 6	NWEF	1/13/93	BEG	822	8	K	4,350	725.7	3624.3
"		"	6/26/93	BEG	"	"	"	"	725.0	3625.0
YM-63	5, 6	NWEF	7/3/93	BEG	920	8	K	4,359	733.3	3625.7
YM-7A	5, 6	NWEF	6/23/92	BEG	882	8	K	4,271	651.0	3620.0
YM-8	5, 6	NWEF	12/17/92	BEG	1,018	8	K	4,316	667.6	3648.4
"		"	6/26/93	BEG	"	"	"	"	667.6	3648.4
50-14-502	5			BEG						nm
50-14-505	5			BEG						nm
50-14-508	5			BEG						nm
51-09-301	5			BEG						nm

* Chemical and isotopical analyses reported in tables 5 and 6, respectively

** SEEF - Southeast Eagle Flat, NWEF - Northwest Eagle Flat, RLD - Red Light Draw

† BEG - Bureau of Economic Geology, TDWR - Texas Department of Water Resources, TWDB - Texas Water Development Board

†† Qal, Quaternary alluvium; QTal, Quaternary-Tertiary alluvium; Ti, Tertiary intrusive; K, undifferentiated Cretaceous; pCamb., Precambrian

na Data not available

nm Data not measured

logger. The data logger converts strain across the pressure transducers measured by electrical current to pressure of the water column overlying the transducers and stores the reading in internal memory. Stored pressure data were downloaded from the data logger and converted to water-level elevations. Pressure gauged in units of pounds per square inch (psi) was converted to hydraulic head in units of feet of water (assuming specific weight of water to be 0.433 psi/ft). Water-level elevation was determined by subtracting depth to water from measuring-point elevation.

Stream discharge was measured in the Rio Grande at Indian Hot Springs (gauging station 1) and at Green River Valley (gauging station 2). The objective of stream gauging was to determine whether ground-water discharge from the Red Light Draw Watershed could be measured (fig. 3). Stream discharge was measured using an AA-type current meter. At each station, a straight stream reach with a relatively symmetrical channel cross section and shallow depth of flow (less than 2.5 ft [0.8 m]) was chosen. A cloth measuring tape strung across the stream perpendicular to the direction of flow was used to divide the stream into uniform increments of 2 to 2.5 ft (0.6 to 0.8 m). At the midpoint of each increment, the depth of water was measured and the bucket wheel of the current meter placed at 0.6 times the depth of flow. The number of revolutions of the bucket wheel was counted over an interval of time and recorded. A U.S. Geological Survey rating table was used to convert revolutions per unit time to flow velocity. The velocity was multiplied by the width and depth of the increment to arrive at a value of stream discharge for that increment. The sum of at least 20 incremental discharges gave the total stream discharge for the stream reach. Measurement error is ± 3.9 ft^3/s.

Several discharge measurements were made at Indian Hot Springs (gauging station 1) on March 18, 1993. The following day, several measurements were performed at Green River Valley (gauging station 2). These measurements were arithmetically averaged to estimate daily stream discharge.

Aquifer Testing

Aquifer tests were performed to estimate transmissivity. Single well pump tests were performed in six wells for periods varying from 22 to 68 h. Qualitative and quantitative methods were used to evaluate aquifer test data. Qualitative examination of the drawdown curves helped to distinguish between confined, leaky confined, and unconfined aquifers (fig. 4). Quantitative interpretations were assisted with a curve matching computer program, AQTESOLV (Duffield and Rumbaugh, 1989). Where appropriate, drawdown curves were matched using (1) the modified Theis (1935) method (discussed in Kruseman and De Ridder, 1979) for analysis of drawdown in an unconfined aquifer, (2) the Cooper-Jacob (1946) method for drawdown in a confined aquifer and (3) the Hantush (1960) and Hantush-Jacob (1955) methods for analysis of drawdown in leaky confined aquifers with and without storage in confining layers. Recovery data were analyzed using the Theis (1935) recovery method. For the purpose of analysis, wells were considered fully penetrating. Hydraulic conductivity was determined by dividing transmissivity by the saturated aquifer section occupied by the well. Such an approximation overestimates hydraulic conductivity if the well only partially penetrates the entire saturated thickness of the aquifer.

Where aquifer test data of suitable quality were not available, specific capacity data were used to provide preliminary estimates of transmissivity. Specific capacity data were collated from TWDB files. The modified nonleaky artesian formula (Walton, 1962) was used to relate the specific capacity of a well to the aquifer transmissivity:

$$\frac{Q}{s} = \frac{T}{\left[264 \log (Tt / 2{,}693\, r^2 S) - 65.5\right]}, \qquad (1)$$

where Q/s is specific capacity in units of gal min^{-1} ft^{-1}, T is transmissivity in units of gal day^{-1} ft^{-1}, S is storage coefficient (dimensionless), r is effective well radius in feet, and t is pumping period in days. Coefficients in equation (1) convert between units. A graphical solution for transmissivity is obtained by plotting Q/s for various values of T on log-log paper while all other parameters are held

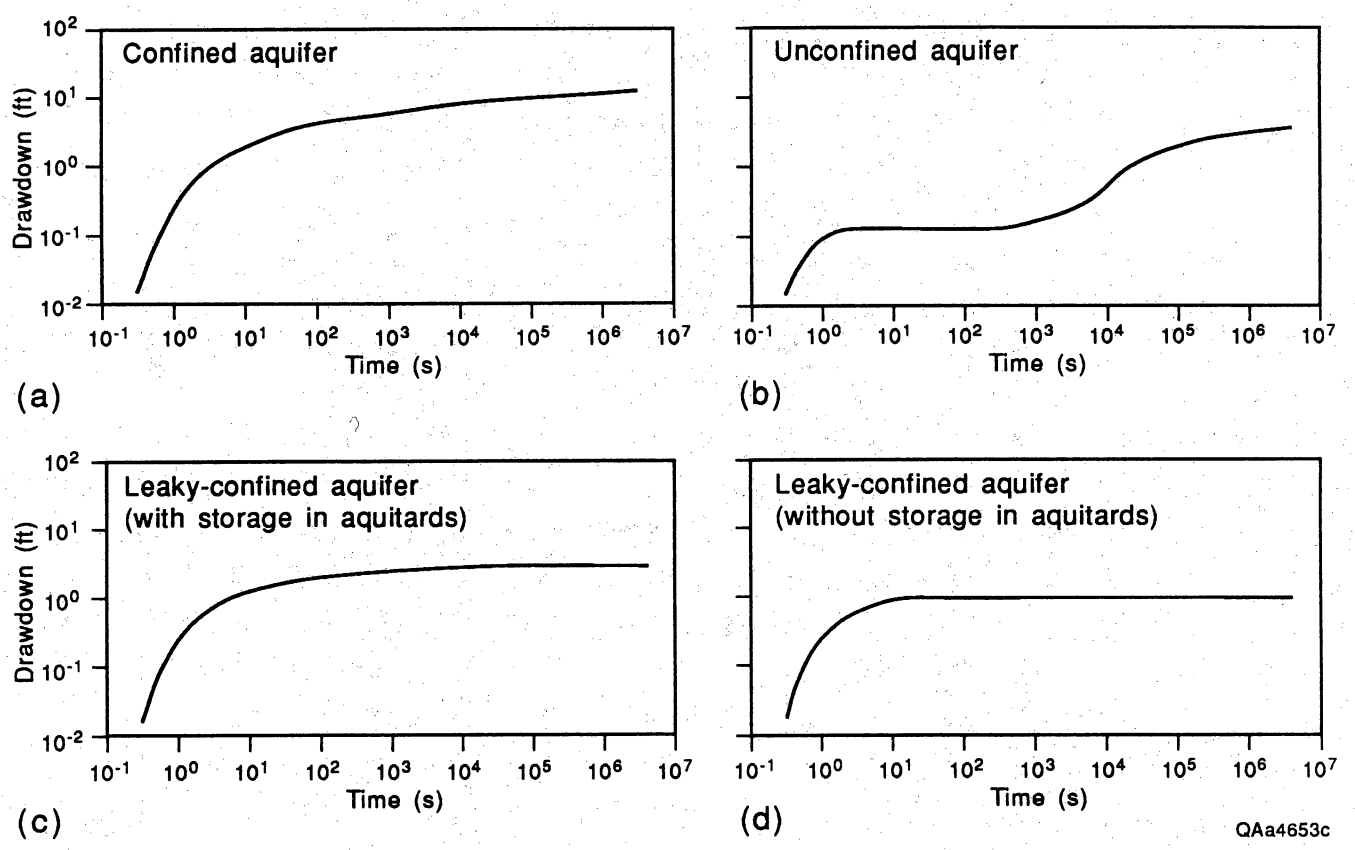

Figure 4. Representative time-drawdown curves for confined, leaky confined, and unconfined aquifers observed during aquifer testing. The nonequilibrium time-drawdown curve for a fully confined aquifer is a parabola (a). The time-drawdown curve for a unconfined aquifer often is an s-shaped curve (b). The time-drawdown curves for leaky confined aquifers (c and d) are suppressed parabolas because a leaky confined aquifer is replenished by vertical flow from lower permeability bounding strata. Modified from Kruseman and De Ridder (1979).

constant. Storage coefficients of 0.14 (unconfined) and 0.0005 (confined) were used to bracket possible ranges where the degree of aquifer confinement was unknown.

Water Sampling for Chemical and Isotopical Analyses

Water samples were collected during September 1991 through August 1993. Analytical results from this study were supplemented by data from White and others (1980) and Henry (1979). All sampling followed guidelines in Technical Program Manual, Specific Work Instruction 3.1 (Bureau of Economic Geology, 1989). Wells were pumped until pH, Eh, and temperature stabilized. Measurements of pH, Eh, and temperature were made in flow cells, with electrodes calibrated with buffer solutions that had been equilibrated to sample temperature (Wood, 1976). Time required for Eh to reach equilibration varied substantially from 20 to 120 minutes. Alkalinity was determined by acid (1.60 N H_2SO_4) titration of filtered samples to a pH of 3.5 to 3.0. Dissolved oxygen was determined by a modified Winkler titration method with 0.20 N sodium thiosulfate and an indicator starch solution (HACH, 1989). Samples for ionic analysis were filtered through a 0.45-m in-line filter and collected in separate 500 mL polyethylene bottles. Samples for cation analyses were treated with 5 mL of 6 N HNO_3. The sample containers were sealed and kept on ice. Samples that could not be filtered in the field were kept in ice-filled coolers until delivered to the laboratory, where they were filtered; cation samples were then treated with 6 N HNO_3.

Waters to be analyzed for δD, $\delta^{18}O$, and tritium were filtered through 0.45-µm cartridge filters and sealed in sample bottles without other treatment. Samples collected for analysis of tritium (^3H) and stable isotopes (D and ^{18}O) were stored in 1-L and 500-mL glass bottles, respectively. Dissolved inorganic carbon for ^{14}C and $\delta^{13}C$ analyses was collected by direct precipitation using a 30-percent ammonium hydroxide solution saturated with $SrCl_2$ (Hassan, 1982). The $SrCO_3$ slurry was decanted from carboys and later filtered and washed in the laboratory with negligible exposure to the atmosphere. The $SrCO_3$ powder was analyzed by liquid scintillation counting for ^{14}C and mass spectrometry for $\delta^{13}C$ at Beta Analytic, Inc., of Miami, Florida. ^{14}C is reported as uncorrected pmc

activity and $\delta^{13}C$ relative to Peedee belemnite (PDB). Details of this procedure are reported by Dutton (1993).

Chemical analyses for cations and silica were performed by chemists at the Mineral Studies Laboratory (MSL) of the Bureau of Economic Geology using inductively coupled plasma-optical emission spectrometry (ICP-OES). Chloride, fluoride, sulfate, and nitrate were measured by ion chromatography; bromide was determined by spectrophotometry. In some cases, nitrate was measured by distillation-titration, and fluoride by an ion-selective electrode.

δD and $\delta^{18}O$ measurements were made by means of gas-source mass spectrometry. To determine δD, water samples were reacted with hot zinc metal to generate hydrogen gas; to determine $\delta^{18}O$, water samples were equilibrated with CO_2. δD and $\delta^{18}O$ are reported relative to standard mean ocean water (SMOW). None of the $\delta^{18}O$ measurements required adjustment because of high ionic strength (Sofer and Gat, 1972). Tritium was determined on electrolytically enriched water samples by low-level proportional counting; results are reported as tritium units (1 TU is 1 ^{3}H atom/10^{18} H atoms) with a typical error of ±0.1 TU.

Mineral saturation states were computed by WATEQF, incorporated into the interactive geochemical reaction path modeling program NETPATH (Plummer and others, 1991). WATEQF calculates a saturation index, which represents the degree of equilibrium between water and minerals on the basis of the amount of dissolved ionic species in solution and the amount that would be present if the water-solute system were at equilibrium with specific minerals at the sample temperature. Equilibrium with respect to a given mineral is indicated by a value of zero; negative values suggest undersaturation and positive values, oversaturation.

Numerical Flow Modeling

MODFLOW, a block-centered, finite-difference computer program (McDonald and Harbaugh, 1988), was used to simulate steady-state flow of ground-water flow on the basis of a two-dimensional cross-sectional model in the x-z plane (profile model). The profile model was used to test hypotheses regarding flow and to estimate pathlines, residence times, and ground-water

velocities. The model's governing equation is the three-dimensional, partial differential equation describing ground-water flow

$$\partial/\partial x(K_{xx}\partial h/\partial x) + \partial/\partial y(K_{yy}\partial h/\partial y) + \partial/\partial z(K_{zz}\partial h/\partial z) = S_s\,\partial h/\partial t, \quad (2)$$

where x, y, and z are Cartesian coordinates of the system, Kxx, Kyy, and Kzz are hydraulic conductivities in the x, y, and z directions, h is the hydraulic head, S_s is specific storage, and t is time. To apply the cross-sectional model, it was assumed that (1) Darcy's law applies and discharge is linearly related to the hydraulic-head gradient; (2) flow in the aquifer is two-dimensional and restricted to the plane of the model; (3) density of water is spatially and temporally constant; (4) aquifer recharge, flow, and leakage are constant with time; and (5) water levels are constant and $\partial h/\partial t = 0$.

MODPATH (Pollock, 1989a) was used to find ground-water pathlines and residence times. MODPATH uses hydraulic head and cell-by-cell flow output files from MODFLOW along with a porosity file to calculate pathlines. The program assumes that each directional velocity component varies linearly within a model cell along a coordinate axis (Pollock, 1989a, b). Pathlines are defined within a grid matrix by tracking a "particle" specified in a cell to a model boundary or user-specified zone. By counting the travel time along the flowpath, velocities and residence times are estimated.

RESULTS OF ANALYSES

Water-Level Measurements

All wells with water-level measurements cited by Gates and others (1980) and White and others (1980) were posted in the potentiometric surface map along with measurements made during this study (fig. 5, pl. 1). Table 1 gives an exhaustive list of wells in which water levels have been measured. The version of the potentiometric surface depicted in figure 5 and plate 1 also takes into account the influence of topography on water levels and uses topography as a guide for drawing equipotential contours in data-poor areas. A regional divide that runs approximately subparallel to

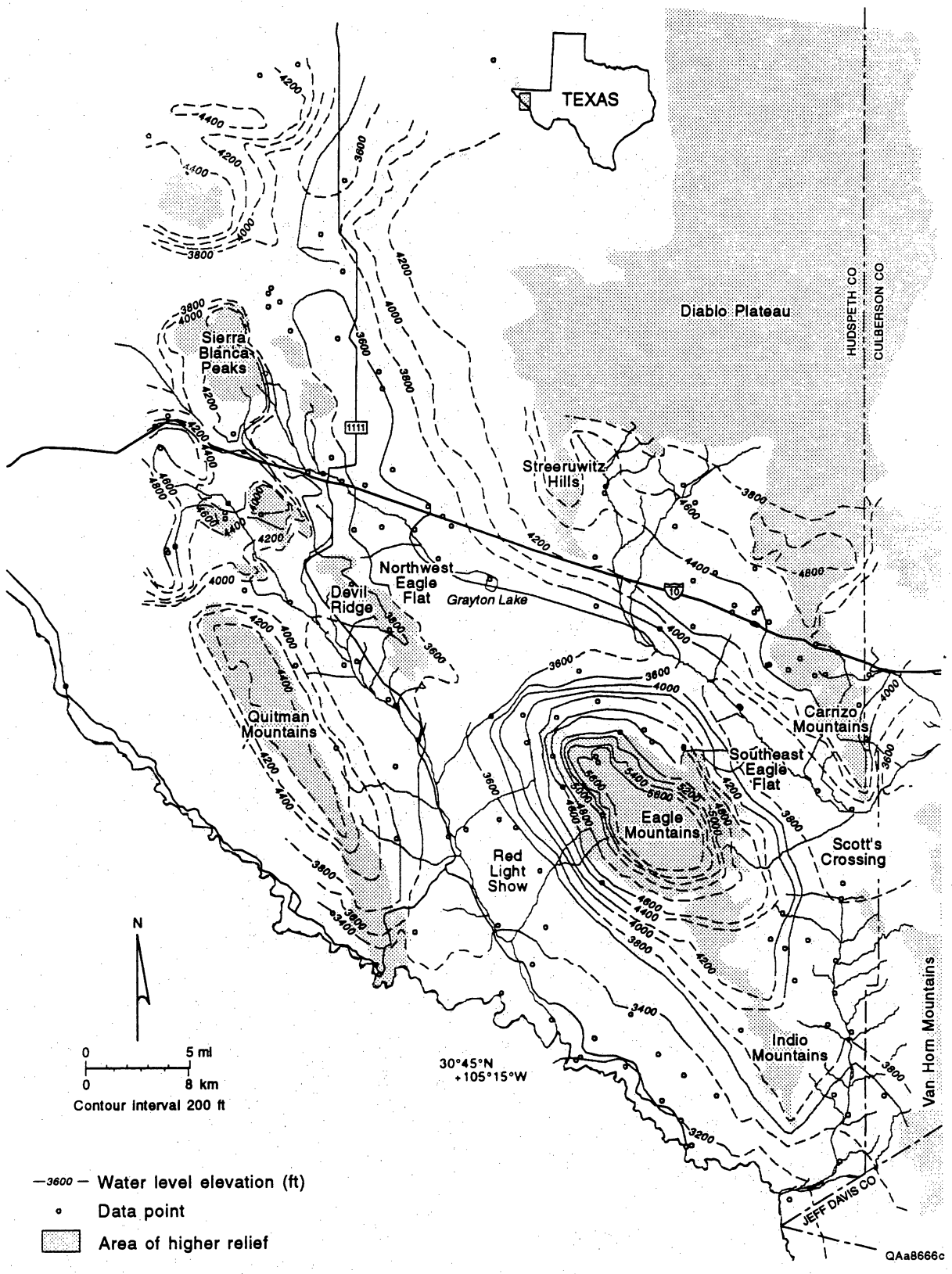

Figure 5. Composite potentiometric surface map generated with recent and historical water-level measurements in the study area. Quasi-steady flow in undeveloped aquifers suggests that historical measurements can be used with recent measurements to develop an acceptable potentiometric map (see fig. 6).

the Diablo Plateau escarpment (Kreitler and others, 1990; Fisher and Mullican, 1990) bounds the Northwest and Southeast Eagle Flat Watersheds along the northern side of the study area.

There are several main features to be seen in the potentiometric surface. First, hydraulic head is at high elevations beneath the Eagle Mountains, Quitman Mountains, Devil Ridge, Sierra Blanca Peaks, Streeruwitz Hills, and Carrizo Mountains and at low elevations beneath northwest Eagle Flat, southeast Eagle Flat, the Green River Valley, and Red Light Draw. Hydraulic gradients are as great as 0.066 in the mountains and as little as 0.005 in the flats and draws. Second, the valleys in the potentiometric surface are long and narrow between the elevated areas. Third, the potentiometric surface is lowest along the Rio Grande, at an elevation of less than 3,200 ft (975 m) at the southern end of Red Light Draw, whereas beneath northwest Eagle Flat the potentiometric surface is at an elevation of approximately 3,600 ft (1,097 m). Fourth, ground-water flow systems beneath the Northwest and Southeast Eagle Flat Watersheds are separated by a hydrologic divide, as are those beneath the Southeast Eagle Flat Watershed and the Green River Valley.

The ground-water divide drawn between Northwest and Southeast Eagle Flat Watersheds, approximately 10 to 11 miles (16 to 17.7 km) east-southeast of Grayton Lake, essentially coincides with the surface-water divide. Freeze and Cherry (1979) stated that ground-water and surface-water divides coincide in most symmetric flow systems. The location of the hydrologic divide is supported by water-level measurements at wells 48-64-BTH, 48-64-501 (an open, cased borehole), and Hot Wells 48-64-901 (pl. 1, table 1). Well 48-64-BTH was drilled and completed in August 1993 to help define the location of the ground-water divide. Gates and others (1980) drew a long narrow valley in the potentiometric surface, represented by 3,700-ft (1,127-m) equipotential contours, between the Eagle Mountains and Millican Hills. Ground water flowing northward from the Eagle Mountains and ground water flowing southward from the Streeruwitz, Bean, and Millican Hills most likely converges beneath southeast Eagle Flat, resulting in a "bridge" in the potentiometric surface and divergence of ground-water flow in opposite directions at either end of the valley.

Figure 5 and the potentiometric surface map by Gates and others (1980) both show northward-directed gradient in hydraulic head beneath the northern part of the Green River Valley.

Inasmuch as ground water cannot flow toward the north underneath the Carrizo Mountains nor toward the northwest toward the inferred hydrologic divide beneath southeast Eagle Flat between the Eagle Mountains and Millican Hills, the only logical discharge for water beneath southeast Eagle Flat and the northern part of the Green River Valley is through Scott's Crossing.

No ground-water divide is shown between Grayton Lake and Red Light Draw (fig. 5, pl. 1), and the equipotential contours are not closed beneath northwest Eagle Flat, unlike those shown by Gates and others (1980). Gates and others (1980) state that "available data are not sufficient to trace the movement of ground water in northwestern Eagle Flat." They go on to suggest that "water may discharge through the Cretaceous rocks in the subsurface, probably toward the Rio Grande to the south." Although data are insufficient to separately map the regional potentiometric surfaces of bedrock and basin-fill aquifer units, communication of ground waters in between these units might occur. Enough regional data exist, however, to suggest that there might not be a divide in the potentiometric surface between the Northwest Eagle Flat and Red Light Draw Watersheds (fig. 5, pl. 1).

These observations indicate that ground water is recharged mainly in the upland areas of the Eagle Mountains, Quitman Mountains, Devil Ridge, Sierra Blanca Peaks, Streeruwitz Hills, and Carrizo Mountains. Ground water flows outward from the recharge areas to beneath the valley floors of northwest Eagle Flat, southeast Eagle Flat, the Green River Valley, and Red Light Draw. Flow most likely occurs in both basin fill and bedrock, depending on the thickness of the former. The valleys are convergence zones of ground-water flow systems dominated by adjacent mountainous recharge areas. The potentiometric surface map also suggests that the Rio Grande is the discharge area for waters in the Northwest Eagle Flat and Red Light Draw Watersheds and beneath the southern part of Green River Valley. Ground waters in the Southeast Eagle Flat Watershed most likely flow through the Scott's Crossing area to Lobo Valley via interbasin flow. The lowest hydraulic head in the area is found in the gap between the Carrizo Mountains to the north and the Van Horn Mountains to the south.

A flowing well (50-24-SHT) documents artesian conditions in southern Red Light Draw. Well 50-24-SHT was one of several shot holes drilled as part of a geophysical survey of southern Hudspeth County in the late 1970's (Mann Bramblett, personal communication, 1993). Well 50-24-SHT and two other holes drilled to depths of approximately 200 ft (61 m) immediately yielded water. The holes were fitted with PVC to augment the water supply from other wells, but only 50-24-SHT was flowing in November 1992 (Mann Bramblett, personal communication, 1993). The authors estimated discharge from 50-24-SHT ranged from 2 to 3 gpm on three site visits during the spring of 1993.

Water-Level Fluctuations

Over the past several decades, water levels obviously have varied. Figure 6 presents selected hydrographs for wells in Eagle Flat, Blanca Draw, and Red Light Draw. There have been very few repeated water-level measurements at a given well such that only a few simple conclusions might be drawn. First, the fluctuations in water level generally are small to moderate, less than 10 ft (3 m). Greater change for well 50-16-703 (fig. 7) most likely results from deepening of the well. Pumping yield from this well reportedly was very low (1 gpm) prior to 1980. When the well was deepened in 1980, water levels rose nearly 150 ft (46 m) and well yields increased (Mann Bramblett, personal communication, 1993). This indicates that the well was recompleted in strata under a higher water pressure. The presence of different hydraulic heads in adjacent layers requires a confining layer and implies a permeable connection of the deeper, high-pressure zone with a recharge zone.

Stream Gauging

Although ground-water discharge to the Rio Grande is inferred from the potentiometric surface map (fig. 5), the one stream gauging survey did not detect a significant change in surface flow that could be attributed to ground-water discharge (table 2). Average surface-water flow was 129.22 ± 3.88 ft^3/s (3.66 ± 0.11 m^3/s) at Indian Hot Springs and 125.69 ± 3.77 ft^3/s (3.56

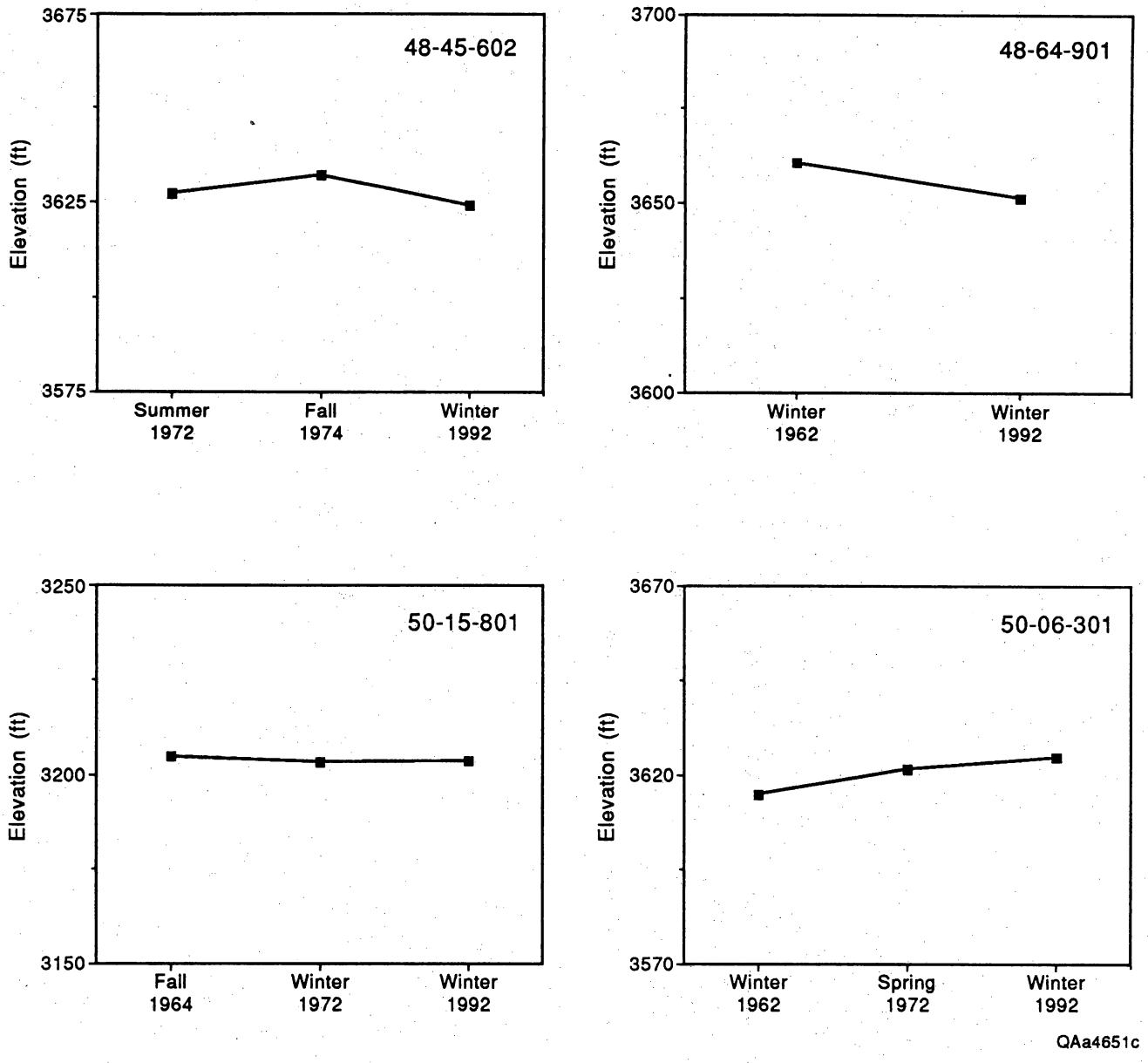

Figure 6. Hydrographs for wells in Eagle Flat, Red Light Draw, and Blanca Draw comparing historical and recent water-level measurements (1962 to 1992). Moderate to small water-level fluctuations (for example, 1 to 10 ft) with no consistent patterns are shown.

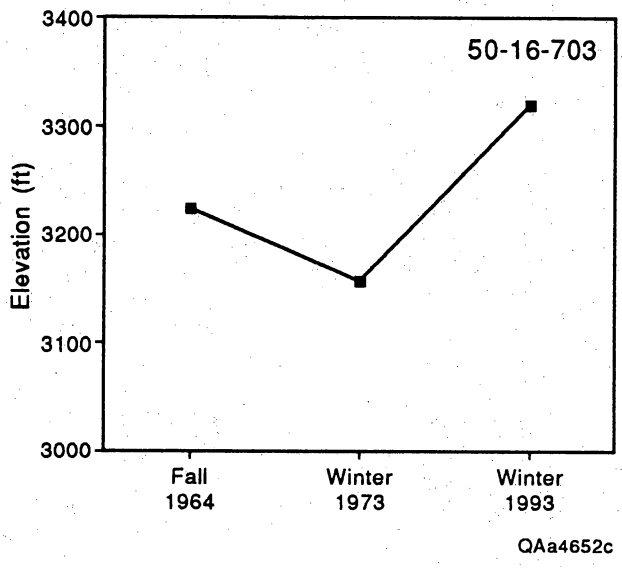

Figure 7. Hydrograph for well 50-16-703 in lower Red Light Draw, showing significant variation in water levels. Well yields in this well were very low initially (for example, 1 gpm). In 1980 the well was deepened to increase its capacity. The well yield increased and the water level rose when the well was recompleted in more permeable basin-fill material.

Table 2. Results of stream gauging at station 1 (Indian Hot Springs) and station 2 (Green River Valley).

	Measurement	Date	Time	Streamflow (cfs)
Station 1	1	3/18/93	10:35	129.262
	2	3/18/93	11:52	129.359
	3	3/18/93	13:10	131.006
	4	3/18/93	14:23	129.718
	5	3/18/93	15:40	126.96
	6	3/18/93	17:20	129.034
Average station 1 streamflow				129.223
Station 2	1	3/19/93	11:01	125.607
	2	3/19/93	13:20	127
	3	3/19/93	15:10	124.46
Average station 2 streamflow				125.689

±0.11 m^3/s) at Green River Valley. Change in flow rate is less than the ±3 percent accuracy of the technique. A preliminary conclusion allowed by these limited data is that aquifer discharge or recharge was less than 10 ft^3/s (0.3 m^3/s) along that reach of the Rio Grande; that is, there was no significant gain or loss of flow between the two gauging stations.

Aquifer Test Results

Aquifer time-drawdown curves for single-well pump tests are presented in figure 8. Results of quantitative analysis of aquifer tests are presented in table 3. All curves except that for well 48-64-BTH are for bedrock aquifers in the Northwest Eagle Flat Watershed. The shape of these time-drawdown curves most likely reflects a leaky confined aquifer (see fig. 4). Well 48-64-BTH is completed in the bolson aquifer. Drilling information and time-drawdown data indicate the aquifer at 48-64-BTH is locally unconfined to leaky confined; therefore, both unconfined and confined curve matches are provided (fig. 9). The match of data and type curve is acceptable for late-time drawdown but poor for early-time drawdown (1 to 50 s). The latter probably reflects well-bore storage and pumping effects. For semi-log analysis, the Theis (1935) recovery method and the Cooper-Jacob (1946) method provide estimates with apparently fair precision and accuracy (fig. 10). For log-log analysis, the Hantush-Jacob (1955) method for leaky aquifers with no storage in aquitards provided similar transmissivity estimates and, during late-time drawdown, excellent curve fits (fig. 11, column a). For early-time drawdown (first 10 to 500 s), curve fits are generally poor because of well-bore storage effects. The Hantush (1960) method for leakage with storage in aquitards usually provided a poor curve match for early- and late-time drawdown phases (fig. 10, column b).

Table 4 (columns 2 and 3) presents raw estimates from Walton's (1962) specific capacity analysis for wells having aquifer test data (for example, YM-18, YM-19, etc.). In this study, results using Walton's (1962) method are generally between 140 and 500 percent higher than results using conventional methods (table 4, compare tables 3 and 4). The specific capacity analyses provided fair precision and moderate to somewhat poor accuracy. Because of its precision, Walton's (1962)

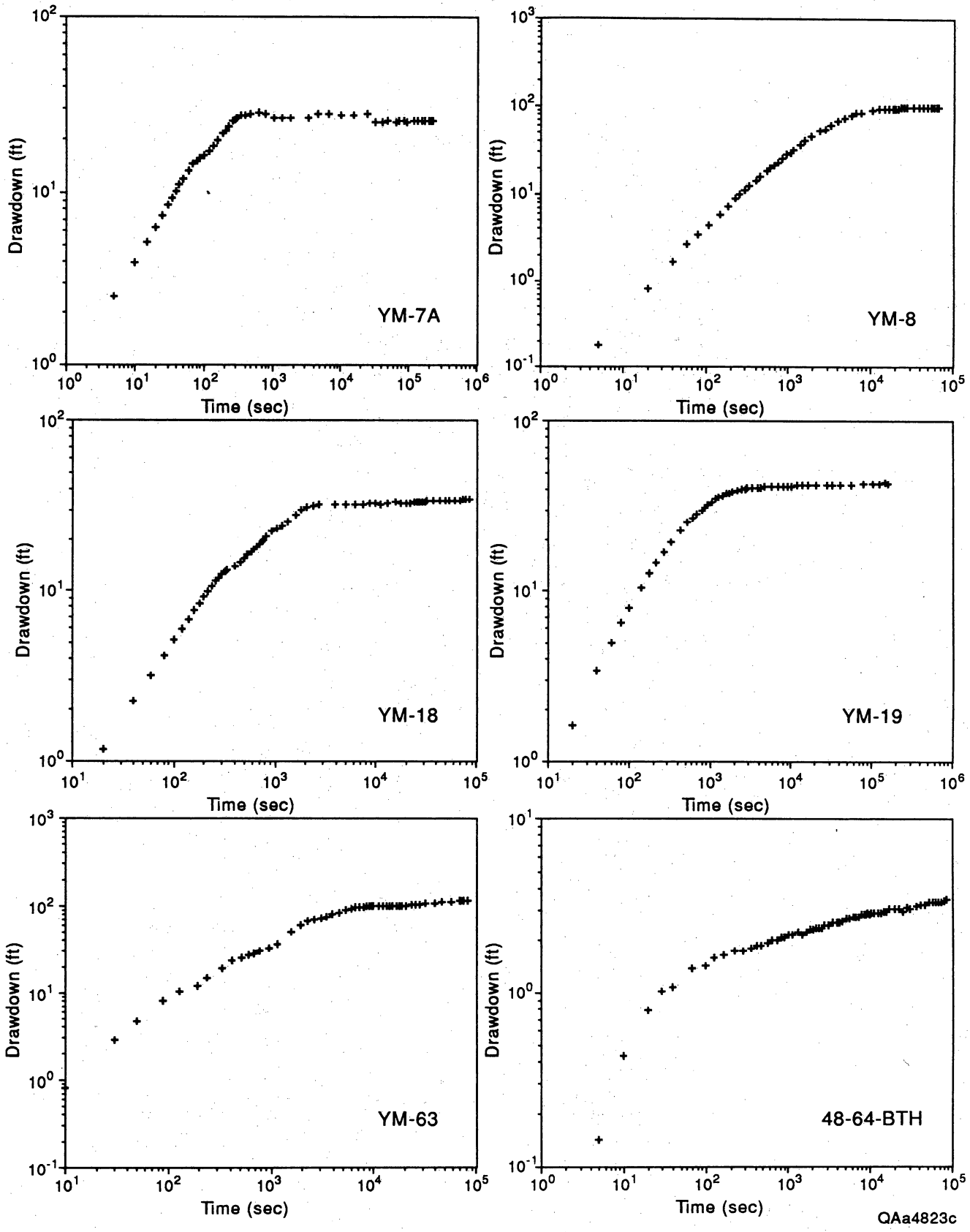

Figure 8. Time-drawdown curves for pump tests performed at Eagle Flat. All curves except 48-64-BTH are for bedrock aquifers in northwest Eagle Flat. Curve 48-64-BTH is for the bolson aquifer in southeast Eagle Flat. Time-drawdown curve shapes in northwest Eagle Flat are most representative of a leaky confined aquifer (see fig. 4). Drilling information and time-drawdown data indicate a locally unconfined to leaky confined aquifer at 48-64-BTH.

Table 3. Aquifer test results for wells in northwest and southeast Eagle Flat.

Transmissivity (ft^2/day)

Well no.	Hantush-Jacob (leaky confined)	Hantush (leaky confined)	Theis Recovery (confined)	Modified Theis (unconfined)	Cooper-Jacob (confined)
YM-7A	67.82	277.76	80.74	-	103.18
YM-8	2.40	3.19	2.50	-	3.12
YM-18	9.49	16.61	10.85	-	9.40
YM-19	10.23	23.48	10.19	-	15.00
YM-63	2.65	3.43	2.45	-	2.88
48-64-BTH	243.25	216.16	-	270.53	-

Hydraulic conductivity (ft/day)

Well no.	Hantush-Jacob (leaky confined)	Hantush (leaky confined)	Theis Recovery (confined)	Modified Theis (unconfined)	Cooper-Jacob (confined)
YM-7A	0.33	1.37	0.40	-	0.51
YM-8	0.0074	0.0099	0.0077	-	0.0097
YM-18	0.12	0.21	0.14	-	0.12
YM-19	0.11	0.25	0.11	-	0.16
YM-63	0.014	0.018	0.013	-	0.015
48-64-BTH	4.68	4.16	-	5.20	-

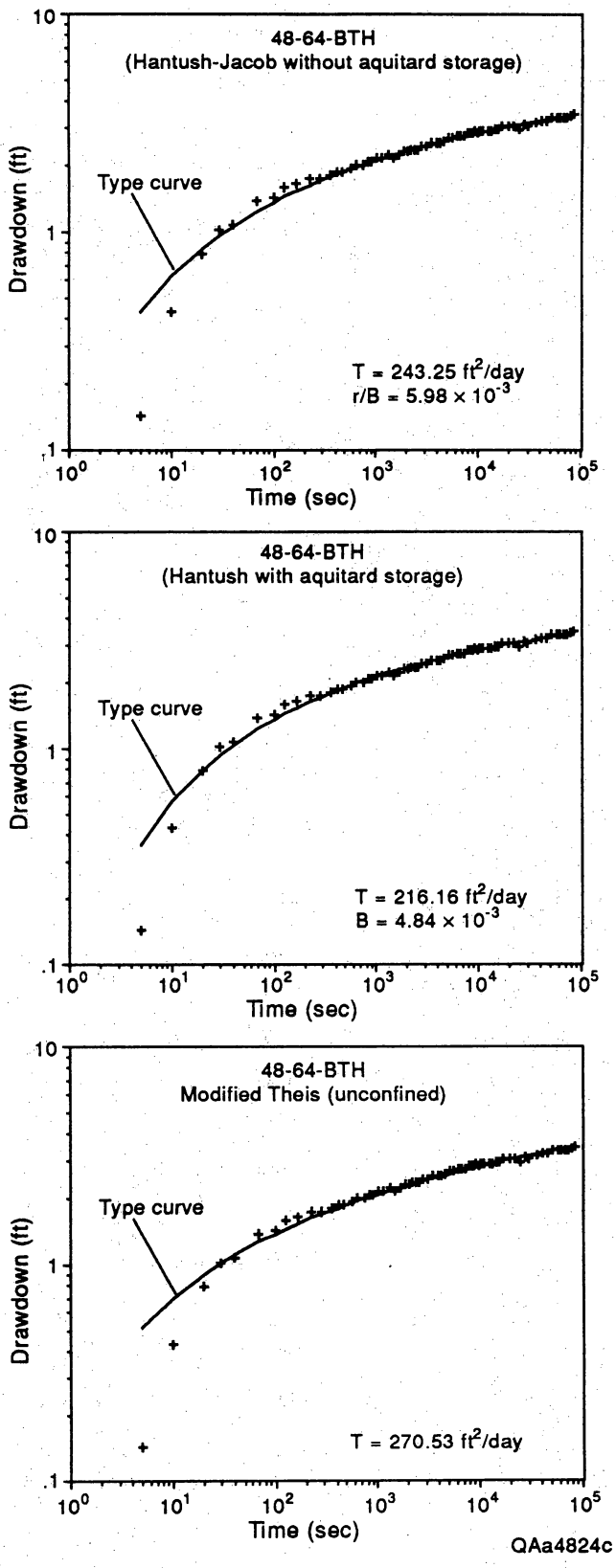

Figure 9. Aquifer test results for 48-64-BTH in southeast Eagle Flat. Curve matches provided by the Hantush-Jacob (1955) and Hantush (1960) methods for leaky confined aquifers and the modified Theis method (discussed in Kruseman and De Ridder, 1979) for an unconfined aquifer. During early-time drawdowns (for example, the first 30 s) the curve fits are poor, probably due to well-bore storage effects. After early-time drawdowns, the curve fits are good for all interpretive methods. Drilling information and time-drawdown data indicate a locally unconfined to leaky confined aquifer at 48-64-BTH.

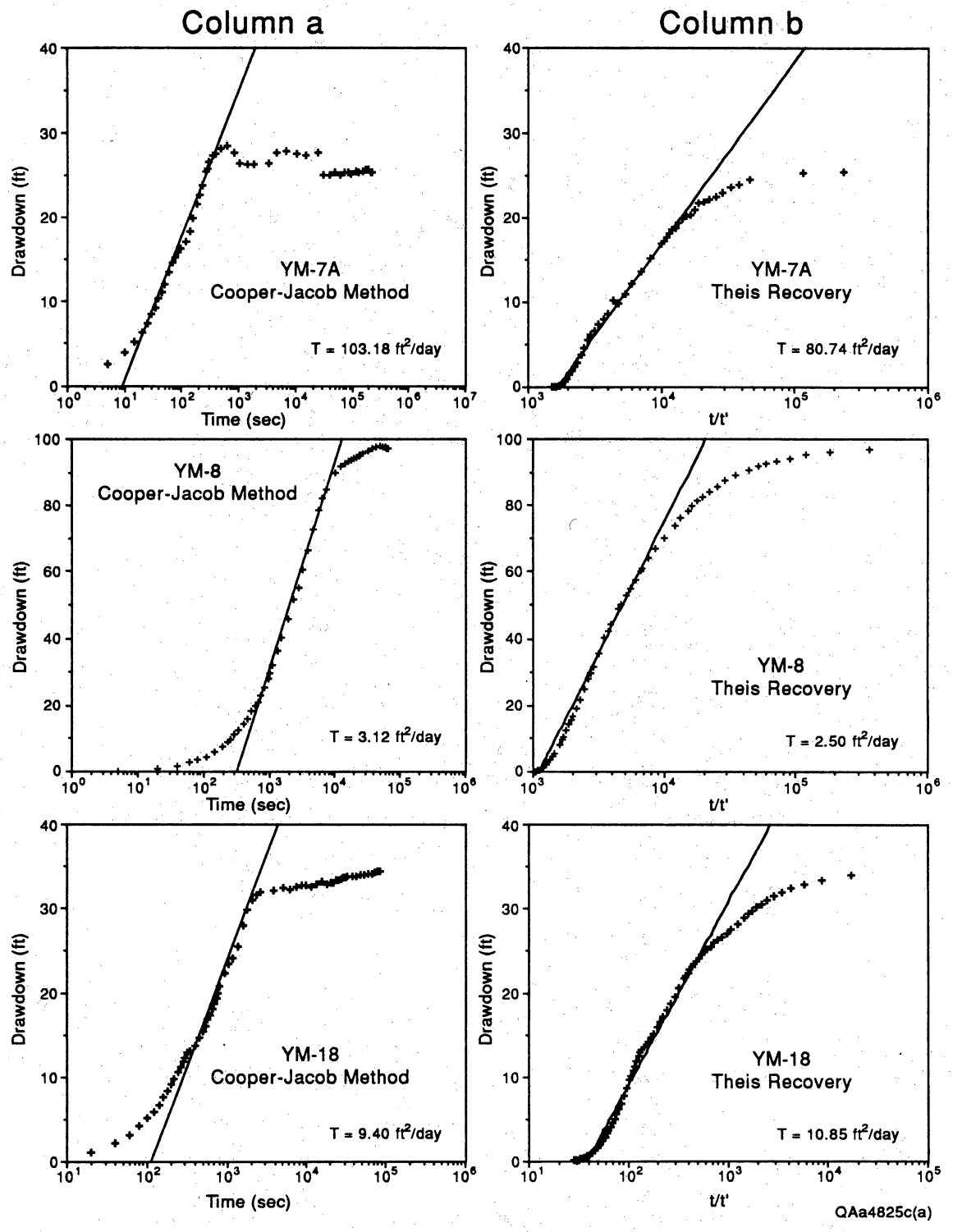

Figure 10. Semilog match of straight line segments of drawdown and recovery data for wells in northwest Eagle Flat. Semilog analysis provided by the Cooper-Jacob (1946) method (drawdown phase; column a) and the Theis (1935) recovery method (column b). For Cooper-Jacob (1946) interpretations, well-bore storage effects during early-time drawdowns probably causes the nonlinear curve segment to drift to the left of the linear segment. The sharp inflection away from the linear segment during late-time drawdowns is due to vertical leakage from the semipermeable confining layers. The straight line segment matched during intermediate times represents the withdrawal of water from storage in the confined aquifer, no part of which was contributed from the semipermeable confining layers (that is, during intermediate times, all the water pumped comes from storage in the confined aquifer). After intermediate times, leakage from the semipermeable units forms a significant part of the water pumped.

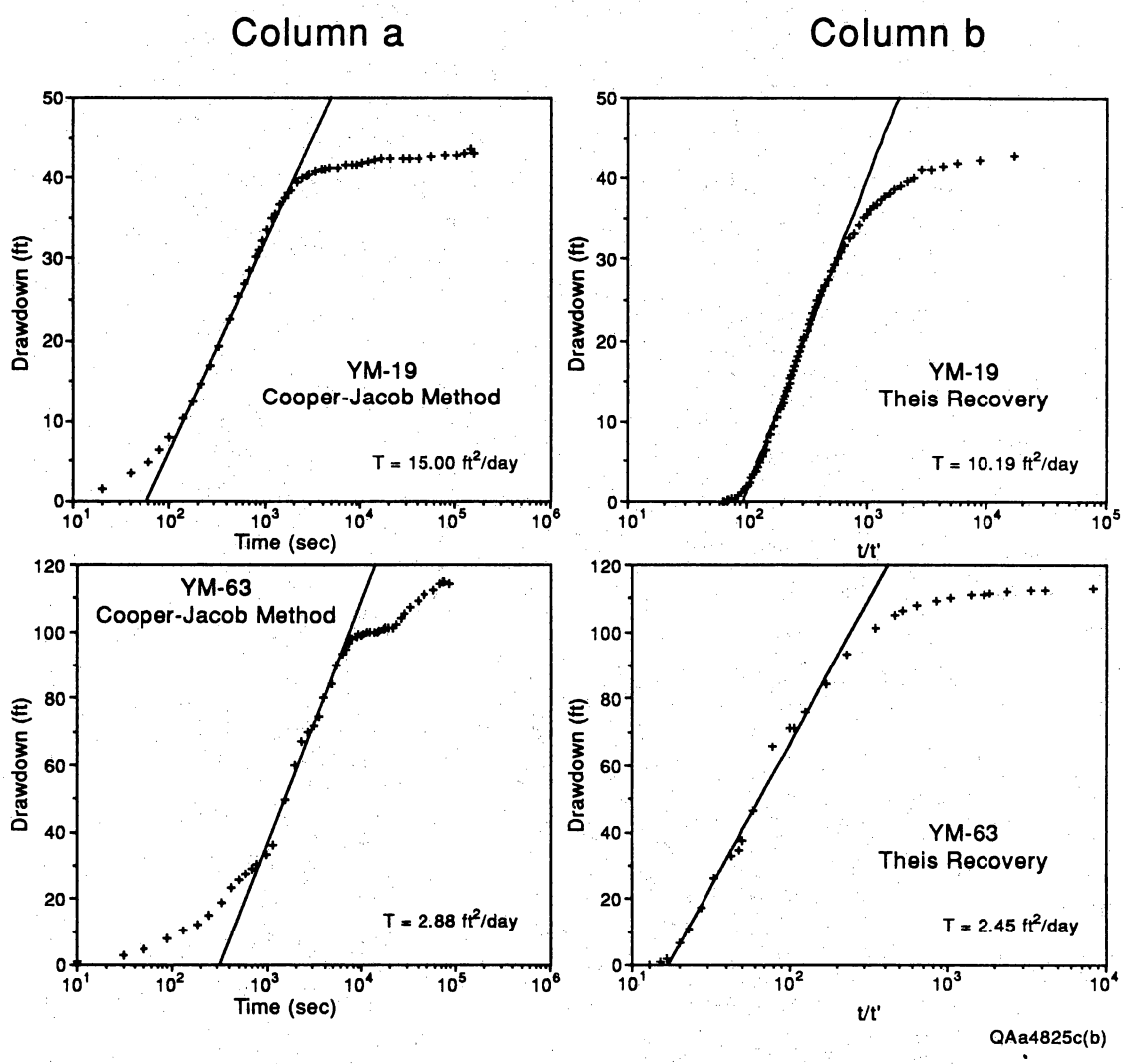

Figure 10 (cont.).

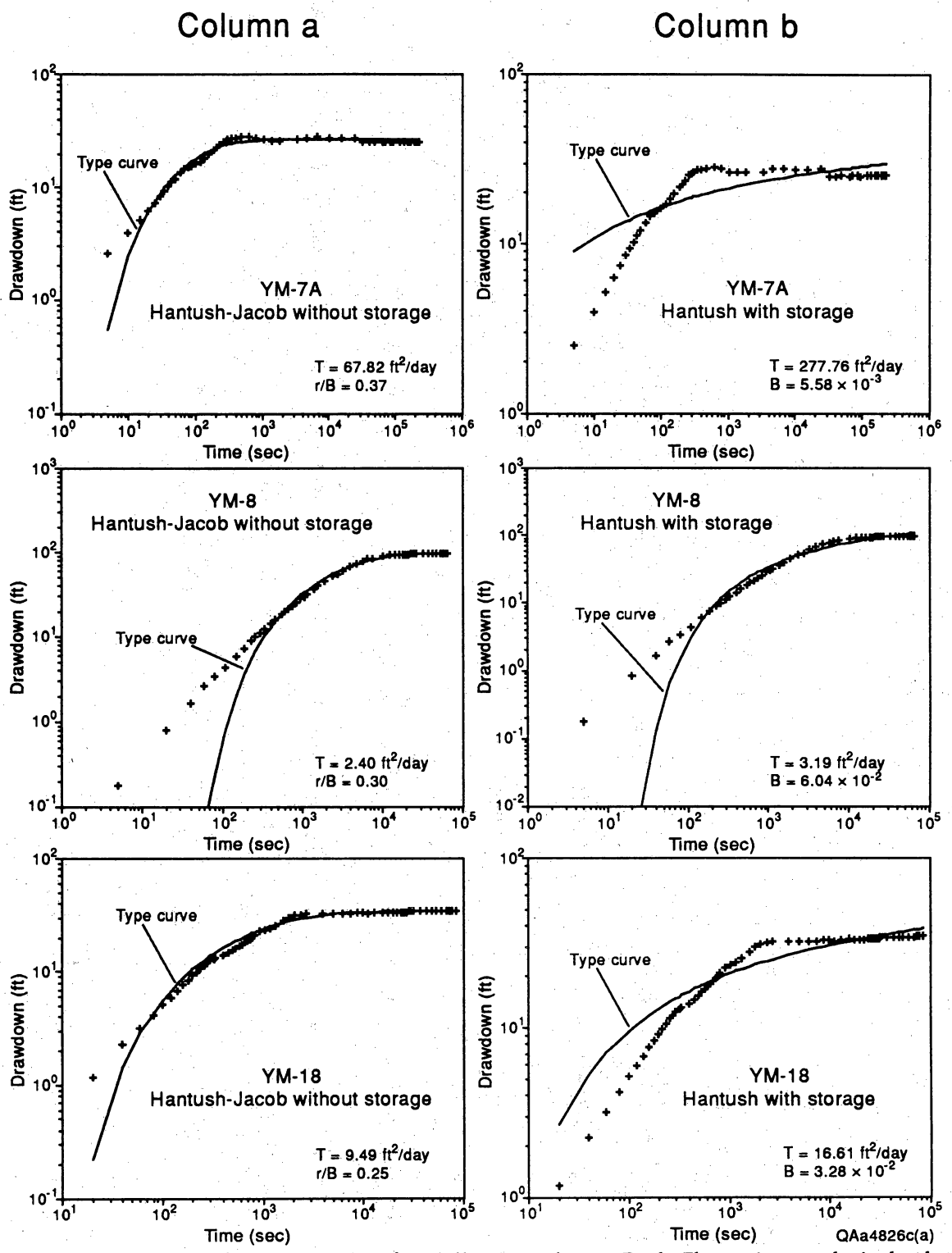

Figure 11. Comparison of curve matches for wells in northwest Eagle Flat, using analytical solutions for leaky confined aquifers. Curve matches for leaky aquifers without storage in aquitards (Hantush-Jacob, 1955) typically provided the best curve fit (column a). Curve matches for leaky aquifers with storage in aquitards (Hantush, 1960) generally provided a poor curve fit (column b). During early-time drawdowns (for example, 10 to 500 s) curves matches are poor, probably as a result of well-bore storage. Very good fits were provided for intermediate- and late-time drawdowns using the Hantush-Jacob (1955) method (column a). Poor curve fits generally were provided by the Hantush (1960) method for early-, intermediate-, and late-time drawdowns.

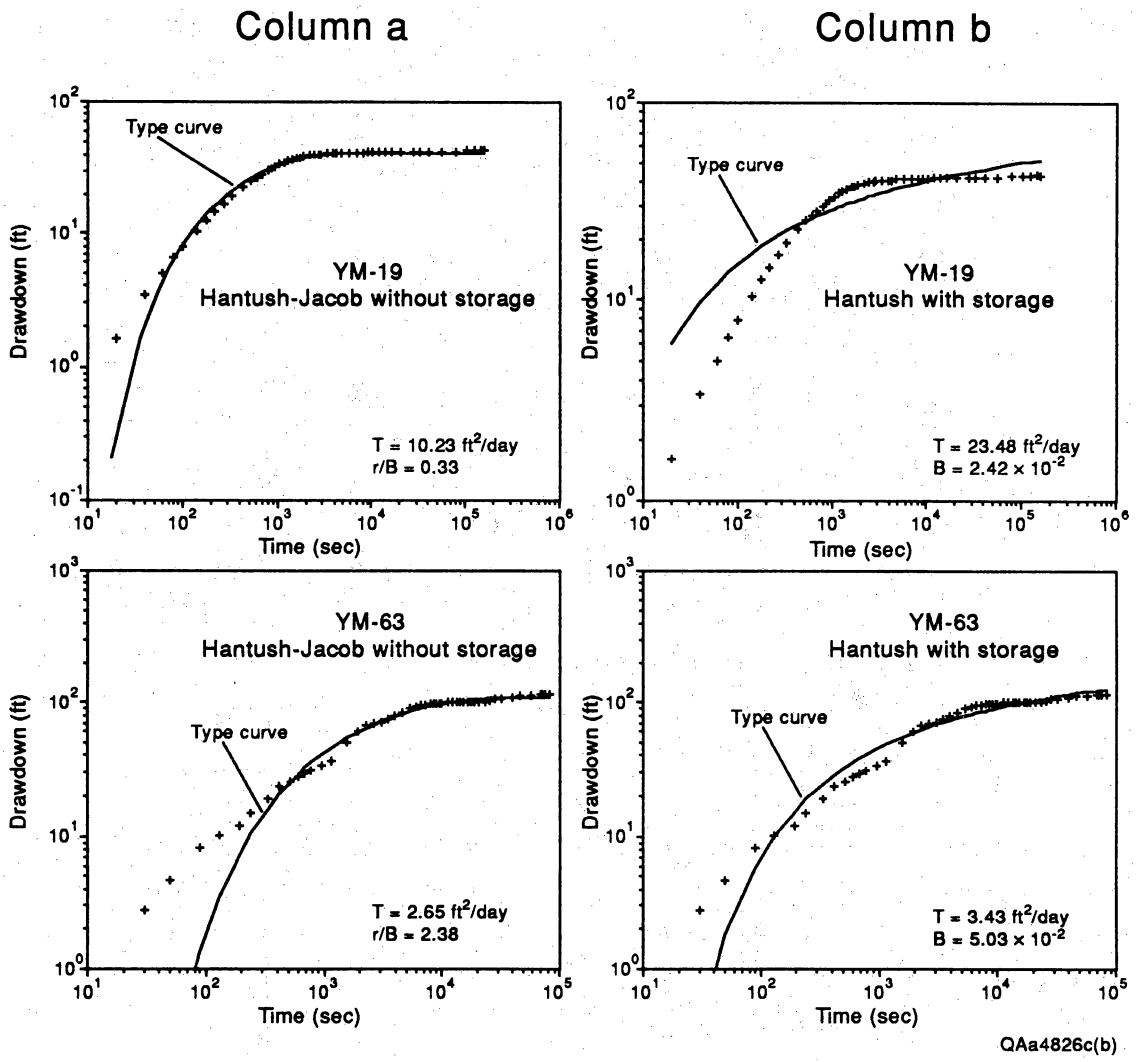

Figure 11 (cont.).

Table 4. Estimates of transmissivity and hydraulic conductivity provided by specific capacity data and Walton's (1962) method.

TRANSMISSIVITY ESTIMATES FROM SPECIFIC CAPACITY DATA (FT^2/DAY)

Well no.	Raw estimates (S = 0.0005)	Raw estimates (Sy = 0.14)	Calibrated estimates (S = 0.0005)	Calibrated estimates (Sy = 0.14)
YM-7A	384.36	199.20	128.12	66.40
YM-8	10.96	5.61	3.65	1.87
YM-18	44.12	26.07	14.71	8.69
YM-19	61.50	36.10	20.50	12.03
YM-63	10.70	5.76	3.57	1.92
48-64-BTH	401.07	256.68	133.69	85.56
48-45-603	2673.80	1537.43	891.27	512.48
48-53-101	1.20	0.46	0.40	0.15
48-53-801	7620.32	5347.59	2540.11	1782.53
48-53-802	1671.12	989.30	557.04	329.77
48-53-902	2807.49	1898.40	935.83	632.80
48-54-201	61497.33	43048.13	20499.11	14349.38
48-54-401	167.25	106.95	55.75	35.65
48-56-802	244.65	140.37	81.55	46.79
48-62-TEX	7085.56	4278.07	2361.85	1426.03

HYDRAULIC CONDUCTIVITY ESTIMATES FROM SPECIFIC CAPACITY DATA (FT/DAY)

Well no.	Raw estimates (S = 0.0005)	Raw estimates (Sy = 0.14)	Calibrated estimates (S = 0.0005)	Calibrated estimates (Sy = 0.14)
YM-7A	1.89	0.98	0.63	0.33
YM-8	0.034	0.017	0.011	0.0058
YM-18	0.56	0.33	0.19	0.11
YM-19	0.65	0.38	0.22	0.13
YM-63	0.058	0.031	0.019	0.01
48-64-BTH	7.71	4.94	2.57	1.65
48-45-603	17.94	10.32	5.98	3.44
48-53-101	0.0028	0.0011	0.00094	0.00035
48-53-801	357.76	251.06	119.25	83.69
48-53-802	55.70	32.98	18.57	10.99
48-53-902	58.49	39.55	19.50	13.18
48-54-201	1618.35	1132.85	539.45	377.62
48-54-401	1.22	0.78	0.41	0.26
48-56-802	2.05	1.18	0.68	0.39
48-62-TEX	12.77	7.71	4.26	2.57

method provides useful relative comparisons. A calibration factor is used to improve accuracy. The calibrated values (table 4, columns 4 and 5) are obtained by multiplying raw transmissivity values (table 4, columns 2 and 3) by 1/3, an average multiplier that accounts for overestimates in transmissivity. Estimates of aquifer parameters having specific capacity data for wells without aquifer tests are presented in table 4. Estimates in columns 2 and 3 (uncorrected) are multiplied by the calibration factor (1/3). Columns 4 and 5 (table 4) present calibrated results.

Results indicate heterogeneity in the bedrock units in the regional study area (for example, hydraulic conductivity estimates vary from 0.00094 ft/day to 539.45 ft/day [0.00029 m/day to 164.42 m/day] using calibrated hydraulic conductivity estimates and a storage coefficient of 0.0005). This heterogeneity probably arises as a result of different rock types in the stratigraphic column and localized areas of more intensive fracturing resulting from Laramide or younger tectonism. Beneath Faskin Ranch, transmissivity values are extremely low (see tables 3 and 4; wells YM-8, YM-63, YM-18, and YM-19). The small range of transmissivity (2.4 to 10.2 ft^2/day [0.2 to 0.95 m^2/day]; Hantush-Jacob [1955] method, for example), indicates fairly homogeneous water-bearing units beneath the ranch.

Saturation Indices, Hydrochemical Facies, and Temperatures

The results of water-chemistry analyses are found in table 5. WATEQF analyses (fig. 12) indicate that ground water is typically at equilibrium with respect to calcite and dolomite, although there is a much wider range of values for the latter. Despite the high sulfate content of many samples, none of the areas appears to be consistently within the range of values indicating equilibrium with respect to gypsum. Many samples are either at or very near saturation with respect to fluorite. In all cases, waters are undersaturated with respect to halite.

Ground water beneath the Northwest Eagle Flat Watershed (fig. 13, table 5) is marked by relatively high total dissolved solids (TDS) and warm temperatures. Ground water is characteristically of the Na-SO_4-Cl to Na-Cl type with salinities between 1,000 mg/L and 4,000 mg/L. The highest salinities are associated with the SO_4-dominated waters of 48-54-901,

Table 5. Hydrochemical analyses of ground-water samples from southeast Eagle Flat, northwest Eagle Flat, and Red Light Draw.

Southeast Eagle Flat

Sample ID Number	Date Collected	Collected by	pH	Temp. Deg. C	SiO2	Na	K	Mg	Sr	Ca	Cl	F	Br	NO3	SO4	Field HCO3	Lab HCO3
47-49-GTM	1/12/92	BEG	7.4	20.2		80	1.52	56.7		104	76	0.8		29.4	242	325	320
47-49-GHM	1/12/92	BEG	7.1	21.5		33	1.54	15.6		85.1	12	0.4		10.8	43	342	331
47-49-GHW	1/13/92	BEG	7.4	19.8		101	1.49	47.4		53.8	40	0.7		24.8	127	525	412
47-57-401	10/29/91	BEG	7.5	18.8		284	5.58	65.3		47.6	107	5.8		14.9	449	526	494
47-57-KHN	11/3/91	BEG	7.1	21.1		77	2.07	33.1		80.1	43	1.1		9.02	110	369	386
47-57-KHN	1/8/92	BEG	7.2	21.8												370	
48-55-902	5/28/92	BEG	7.3	20.9	59.3	57	2.07	33.8	0.64	58.2	20	0.9	0.25	18.7	59	361	386
48-56-803	1/10/92	BEG	7.3	19.2		63	1.54	30.0		55.4	39	0.4		27	79	284	287
48-56-DES	1/10/92	BEG	6.9	18.7		178	1.54	81.2		88.9	178	0.9		28.4	262	456	460
48-56-DES	8/11/92	BEG	7.1	20.2	34.2	182	1.9	85.4	1.42	91.6	166	2.2	1.41	28.3	293	502	467
48-64-302	10/31/91	BEG	7.4	19.1		106	3.44	57.4		54.6	68	1.3		30.9	217	335	310
48-64-301	10/29/91	BEG	7.4	20.1		121	2.05	56.3		65.4	83	2.2		39.6	189	366	376
48-64-602	10/28/91	BEG	7.3	21.8		161	4.62	108.0		140	145	1.3		38.7	717	228	234
48-64-602	12/18/91	BEG	7.2	21.6												230	
48-64-604	10/28/91	BEG	7.4	20.5		115	2.24	37.4		45.9	54	1.8		17	175	305	315
48-64-604	8/14/92	BEG	7.6	22.2	25.0	127	3.32	41.7	0.64	49.6	57	2.1	0.54	14.8	201	356	315
48-64-LOV	10/29/91	BEG	7.4	21.4		74	2.2	36.7		49.3	45	0.9		14.5	99	311	320
48-64-LOV	12/15/91	BEG	7.3	21.4												311	
48-64-901	7/23/43	TDWR		41.0		151		8.2		10	32			6.9	135		238
50-08-101	11/1/91	BEG	7.0	18.7		30	2.26	7.7		95	21	1.5		5.8	74	326	271
50-08-102	12/12/92	BEG	7.1	16.8	35.7	131	4.53	47.5	1.95	172	41	2.9	0.33	0.11	491	464	353
50-08-202	11/2/91	BEG	7.1	18.7		20	1.38	9.3		113	16	1.0		78.7	107	285	207
51-01-501	6/25/92	BEG	8.3	29.7	38.7	132	1.54	1.2	0.15	8.09	8	3.4	0.30	4.76	43	384	287
51-01-501	1/9/92	BEG	8.1	14.0		132	1.53	1.1		7.83	8	3.9		4.26	43	280	279
51-01-501	5/31/92	BEG	8.0	24.5	37.4	134	1.54	1.2	0.16	8.41	9	3.6	0.25	3.98	44	336	283
51-01-503	10/12/72	GS	7.9	26.0	18.0	94		2.9		9.5	6	2.2		1.8	35		230
51-01-503	10/31/91	BEG	8.3	23.3	18.0	98	2.36	3.2	0.22	7.53	5	2.4		3.01	34	307	232
51-01-503	12/18/91	BEG	7.8	23.2													
51-01-801	8/31/64	GS	7.4	27.0	18.0	83		2.1		7.8	15	1.7		3.2	37		174
51-01-801	6/28/92	BEG	8.7	26.9	16.9	82	1.67	1.9	0.27	7.5	17	1.5	0.25	5.5	35	215	163
51-09-103	10/18/72	TDWR	7.6	21.5	21.0	160		68.0		200	30	0.7		1.3	810		302
51-09-301	12/1/72	TDWR	8.3	17.0	13.0	140		12.0		15	32	1.9		1.8	130		244
51-09-501	10/18/72	TDWR	7.9	22.0	31.0	21		15.0		63	4	0.7		6.2	19		284
51-10-103	2/8/93	BEG	7.6	28.2	25.0	101	6.74	10.3	0.38	29.1	21	2.8	0.23	7.66	80	253	245
51-17-701	9/16/64	TDWR	7.2	23.0	63.0	126		7.4		52	38	1.9		16	95		322

Table 5 (cont.).

Northwest Eagle Flat

Sample ID Number	Date Collected	Collected by	pH	Temp. Deg. C	SiO2	Na	K	Mg	Sr	Ca	Cl	F	Br	NO3	SO4	Field HCO3	Lab HCO3
48-45-602	2/10/75	TDWR	7.6			520	36	47.0		109	590	3.8		3.2	434		434
48-45-603	8/10/92	BEG	7.4	27.4	16.0	577	20.9	41.1	2.41	91.2	546	4.1	1.12	3.91	485	477	405
48-45-901	5/24/92	BEG	7.3	27.5	26.9	226	3.01	27.1	1.17	63.5	87	3.2	0.64	16.4	316	373	347
48-53-501	1/13/92	BEG	7.2	23.2		751	2.03	34.1	4.79	85.6	149	3.0	0.70	0.1	1,170	703	649
48-53-501	5/26/92	BEG	7.0	25.1	16.7	779	2.08	36.1		92.3	154	2.2	1.48	0.1	1,250	670	627
48-53-802	6/26/92	BEG	7.2	23.3	20.8	64	1.54	12.9	0.82	112	35	1.4	0.32	7.73	146	329	321
48-53-803	5/28/92	BEG	7.2	20.6	25.7	52	1.69	13.9	1.01	141	22	1.3	0.25	1.86	158	361	361
48-53-804	8/23/73	GS	7.6	26.0	19.0	100		25.0		76	39	1.8		3.1	190		316
48-54-401	9/27/68	TDWR	7.5			540		36.0		97	650	4.5		0.4	362		356
48-54-402	7/23/43	GS		38.0		303		9.8		27	202			8.4	184		346
48-54-404	10/30/91	BEG	7.2	32.0		402	22.6	13.4		44.4	357	5.1		15.1	289	385	328
48-54-404	6/1/92	BEG	7.2	32.0	22.9	433	25	14.2	1.50	51.3	361	4.9	0.87	13.1	332	356	370
48-54-502	8/13/92	BEG	7.5	26.8	13.3	582	27	25.5	2.68	77	600	5.0	5.00	5	410	450	597
48-54-503	8/23/72	GS	7.8	28.0	27.0	610		26.0		86	650	4.9		4.2	390		372
48-54-801	9/15/72	GS	8.0	22.0	19.0	600		30.0		81	610	4.8		1.1	400		426
48-54-901	7/23/43	GS				1,103		65.0		128	775			26	1,498		380
48-62-TEX	3/3/93	BEG	7.8	24.0	14.1	163	2.88	27.4	1.87	64.3	70	2.2	0.55	5.69	277	313	301
48-62-TEX	5/27/93	BEG	7.6	25.3	15.4	165	2.2	26.4	2.05	67.3	68	2.2	0.67	6.07	265	333	303
48-62-TEX	7/28/93	BEG	8.2	27.1	28.8	185	8.65	5.9	0.59	10.8	25	5.5	0.17	0.23	128	339	315
48-63-302	8/31/72	GS	7.6	26.0	27.0	154		44.0		41	58	1.1		6.5	185		410
48-63-302	10/31/91	BEG	7.6	23.1		148	2.85	40.9		43	62	2.4		8.7	197	387	354
48-63-302	12/17/91	BEG	7.3	23.6													
48-63-302	5/30/92	BEG	7.5	25.5	24.4	153	3.12	45.5	0.95	44.1	68	2.1	0.57	6.46	221	374	354
YM-7A	6/23/92	BEG	7.2	29.5	20.2	305	20.3	26.6	1.23	69.6	316	3.2	0.79	0.8	161	439	393
YM-7A	11/20/92	BEG	7.0	31.8	21.6	308	19.8	26.4	1.22	69	314	2.6	0.71	0.8	181	462	387
YM-7A	3/5/93	BEG	7.1	33.4	20.3	303	20.4	25.0	1.15	71.2	320	2.3	0.54	1.42	202	380	386
YM-7A	5/25/93	BEG	7.2	33.4	21.2	298	21.1	24.5	1.26	71.3	319	2.7	0.54	1.99	171	406	389
48-63-902	6/8/73	GS	8.2	21.0	37.0	94		23.0		30	20	2.8		8	55		334
48-63-902	11/2/91	BEG	7.6	16.1		96	2.21	24.4		30.8	22	3.8		10.2	63	348	331
48-63-902	1/8/92	BEG	7.5	21.4													
48-63-902	7/16/92	BEG	7.6	22.0	39.4	93	2.55	23.8	1.36	29	19	3.1	0.13	8.91	63	340	325
48-64-BTH	8/30/93	BEG	7.2	29.0	26.4	109	3.11	56.3	1.53	56.1	76	1.4	0.56	15.1	284	220	232
50-07-301	8/30/93	BEG	7.0	20.0	36.4	35	1.54	5.7	0.36	86.1	25	0.5	0.37	7.02	47		250
YM-18	3/1/93	BEG	7.5	28.2	12.4	934	17.5	26.7	2.11	74.6	464	4.9	2.33	24.8	1,170	370	389
YM-18	5/25/93	BEG	7.4	29.1	13.3	954	17.4	33.8	2.58	92.8	445	5.3	2.72	25.3	1,380	447	387
YM-18	7/29/93	BEG	7.2	29.0	13.1	962	16.5	29.5	2.07	79	457	6.3	2.31	24.8	1,233	477	394
YM-19	2/3/93	BEG	7.1	28.4	14.7	645	33.1	32.6	2.11	95.7	547	3.9	1.97	5.39	683	357	353
YM-19	5/27/93	BEG	7.3	29.3	15.2	625	33.3	32.2	2.07	99.9	483	4.9	1.34	5.29	671	385	347
YM-19	7/30/93	BEG	7.3	29.5	15.9	652	30.8	29.2	1.99	91.1	509	5.4	2.31	5.52	659	396	352
YM-63	8/20/93	BEG	7.1	30.4	14.1	1,200	28.6	59.3	4.36	180	779	6.5	3.91	46.3	1,716	306	315
YM-8	11/21/92	BEG	7.2	25.7	12.6	285	3.8	28.8	1.67	65.1	96	3.0	0.88	0.8	431	582	391
YM-8	5/26/93	BEG	7.2	26.8	13.0	280	3.57	31.3	1.99	77.9	95	2.7	0.66	0.96	445	433	398

Table 5 (cont.).

Sample ID Number	Date Collected	Collected by	pH	Temp. Deg. C	SiO2	Na	K	Mg	Sr	Ca	Cl	F	Br	NO3	SO4	Field HCO3	Lab HCO3
Red Light Draw																	
48-61-201	2/18/70	GS	7.8	21.0	11.0	106		33.0		53	30	2.1		0.4	212		298
48-61-201	7/7/92	BEG	7.2	25.4	21.4	117	2.41	33.9	3.49	56.7	32	1.8	0.37	0.8	218	316	317
48-61-302	8/17/72	GS	8.2		14.0	120		27.0		41	32	1.8		0.4	210		268
48-62-501	3/14/94	BEG		26.0							83		0.50				
48-62-BOR	7/7/92	BEG	7.4	22.5	14.8	1,008	3.31	62.3	4.73	88.9	525	8.2	3.62	53.4	1,390	539	523
48-62-701	8/18/70	TDWR	7.5	18.0	5.0	119		23.0		26	33	2.3		1.5	171		231
48-62-805	7/18/92	BEG	7.6	25.8	19.4	141	2.77	19.0	1.51	34.6	45	2.2	0.40	6.71	156	275	269
50-06-203	8/10/72	GS	7.9	22.0	16.0	240		38.0		62	85	2.6		18	410		322
50-06-203	7/2/92	BEG	8.6	27.8	15.5	206	4.44	37.1	3.30	54.2	65	3.0	0.33	0.8	355	386	344
50-06-301	6/27/60					94		21.0		46	39				132		259
50-06-301	5/29/92	BEG	7.6	27.3	22.9	131	2.24	18.2	1.70	36.7	39	1.9	0.25	4.74	164	336	274
50-06-LOV	7/2/92	BEG	7.5	26.7	39.8	140	3.5	30.2	3.00	56.2	71	2.0	0.76	11.6	191	283	289
50-06-LOV	5/14/93	BEG	7.3	25.9	44.5	134	3.18	27.3	3.12	58	73	2.1	0.53	10.2	203	323	274
50-06-801	8/10/72	GS	7.8	22.0				92.0		110	20				620		430
50-06-801	8/28/93	BEG	7.8	22.0	7.0	130	2.5	76.6	11.80	102	18	1.6	0.10	5.01	461	412	454
50-07-401	6/27/92	BEG	7.7	29.0	35.7	48	1.7	6.6	0.55	46.7	14	0.6	0.13	6.74	50	217	208
50-07-MCM	8/9/92	BEG	7.5	24.6	16.0	124	3.13	26.8	1.15	45.4	41	1.7	0.38	6.19	155	355	311
50-07-MCM	7/18/92	BEG	7.4	23.4	15.1	147	3.15	28.1	1.22	46.7	49	1.9	0.52	5.8	179	392	321
50-07-601	8/18/93	BEG	7.0	25.6	14.1	100	1.19	8.2	0.80	83.2	29	2.1	0.25	0.61	224	211	211
50-07-FRC	7/3/92	BEG	6.8	19.3	33.2	27	2.48	7.0	0.30	75.6	19	1.0	0.30	6.68	51	236	220
50-14-501	1976	BEG	6.6	47.2	40.0	2,185	134	27.0	3.80	150	2,680	2.8		0.1	1,090		906
50-14-501	12/4/61	GS	6.5	42.0	42.0	2,370		28.0		135	2,600				1,150		892
50-14-502	Jun-53	GS	7.1		21.0	885		17.0		43	738	2.6		1.2	505		645
50-14-502	12/4/61	GS	7.2	14.0	35.0	839		19.0		63	700				504		668
50-14-502	1976	BEG	8.0	27.2	20.0	725	40.9	14.4		62	605	3.6		0.4	440		623
50-14-503	Jun-53	GS	7.1		36.0	2,550		33.0		153	2,900	2.6			1,170		907
50-14-503	1/23/73	GS	7.2	50.0	42.0	2,600		31.0		58	2,900	2.3		3.1	1,200		628
50-14-503	1976	BEG	7.0	44.4	40.0	2,340	158	34.0	3.40	145	2,950	2.7		5.4	1,150		902
50-14-503	7/6/92	BEG	6.7	41.3	41.9	2,420	143	33.0	3.74	140	2,870	2.7	2.14	7.7	1,230	970	916
50-14-505	1976	BEG	6.9	33.6	35.0	2,375	160	29.0		160	3,000	2.8		1	1,190		962
50-14-508	1969	TDWR	7.1			2,370		24.0		180	2,740				1,075		915
50-14-509	1969	TDWR	7.9			2,870		182.0		380	4,520				1,425		122
50-14-RBL	1976	BEG	8.0	37.0	36.0	312	11	1.7	0.70	15.5	87	3.2		0.1	259		474
50-14-RBL	1/28/93	BEG	7.7	31.3	38.5	346	8.22	1.7	0.53	15.1	95	2.6	0.34	0.1	281	555	456
50-15-101	6/15/64	GS	7.4		43.0	11		19.0		15	3	0.7			18		139
50-15-101	5/15/93	BEG	7.7	22.0	46.0	12	1.2	14.5	1.47	55.2	2	1.6	0.10	18.5	14	220	227
50-15-201	10/30/64	GS	7.4	26.0	24.0	101		1.9		10	33	3.0		9.4	52		166
50-15-201	6/29/92	BEG	8.2	26.8	22.7	99	1.54	2.0	0.52	9.48	30	2.7		10.3	47	196	174
50-15-WBG	6/30/92	BEG	8.4	24.6	24.6	126	4.06	15.9	1.88	47.5	86	1.0	0.58	11.6	167	201	205
50-15-801	11/10/64	GS	7.8		47.0	361		29.0		44	171	2.7		6.9	420		394
50-15-801	5/12/93	BEG	7.7	23.0	62.9	240	3.82	12.9	1.53	36.5	101	3.3	0.41	14.5	202	343	370
50-15-905	4/15/74	GS	7.9	20.0	43.0	1,300	25	97.0		220	1,700	0.5		4.9	1,200		156
50-16-703	1/25/73	GS	8.3	26.0				0.8		7.8	11				39		182
50-16-703	5/13/93	BEG	8.4	26.6	32.3	62	2.29	3.5	0.53	11.3	17	2.8	0.23	8.97	25	223	138

Table 5 (cont.).

Sample ID Number	Date Collected	Collected by	pH	Temp. Deg. C	SiO2	Na	K	Mg	Sr	Ca	Cl	F	Br	NO3	SO4	Field HCO3	Lab HCO3
Red Light Draw (cont.)																	
50-24-202	1/25/73	GS	7.9	22.0	41.0	940		35.0		94	960	1.5		0.04	800		288
50-24-202	7/4/92	BEG	7.4	25.4	40.4	992	6.27	41.0	3.43	120	1,040	0.8	1.50	0.8	842	322	327
50-24-301	11/16/73	GS	8.0	22.0				4.1		17	16				46		204
50-24-301	7/4/92	BEG	8.5	33.2	20.3	80	3.68	4.2	0.82	11.6	14	1.2	0.13	6.38	40	263	191
50-24-503	11/10/64	GS	7.5		28.0	389		48.0		152	580	0.7		2.5	388	239	
50-24-503	1/9/93	BEG	7.0	23.0	29.9	811	13.4	150.0	22.00	585	1,810	0.5	1.90	0.8	1,040	196	211
50-24-503	5/12/93	BEG	7.0	23.5	31.7	770	12.7	138.0	24.10	589	1,894	0.4	1.68	0.8	1,010	209	213
50-24-505	11/16/73	GS	6.6	17.0	1.7	5,000	120	410.0		400	7,300	0.1		8.4	2,900		44
50-24-SHT	10/22/92	BEG	8.8	25.4	55.2	88	2.28	1.4	0.10	3.5	17	2.3	0.50	6.34	31	170	159

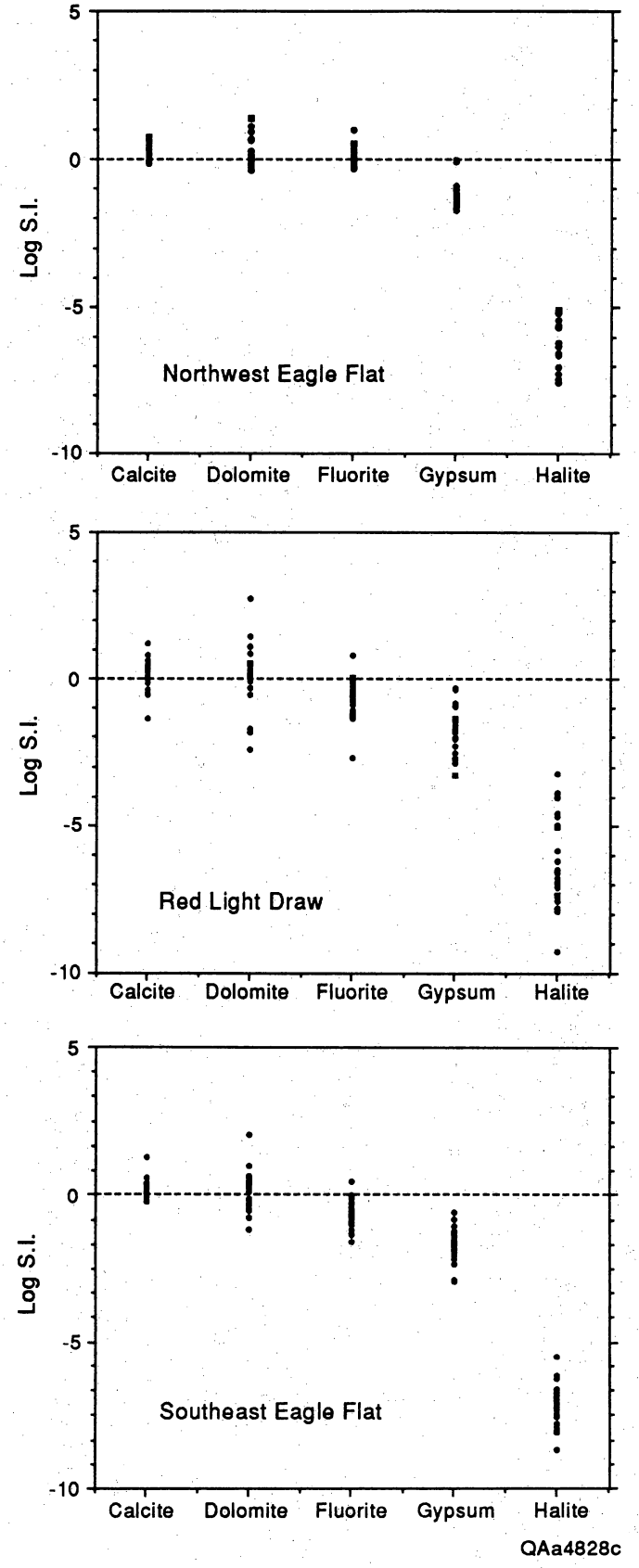

Figure 12. Range of saturation indices of calcite, dolomite, fluorite, gypsum, and halite for northwest Eagle Flat, Red Light Draw, and southeast Eagle Flat.

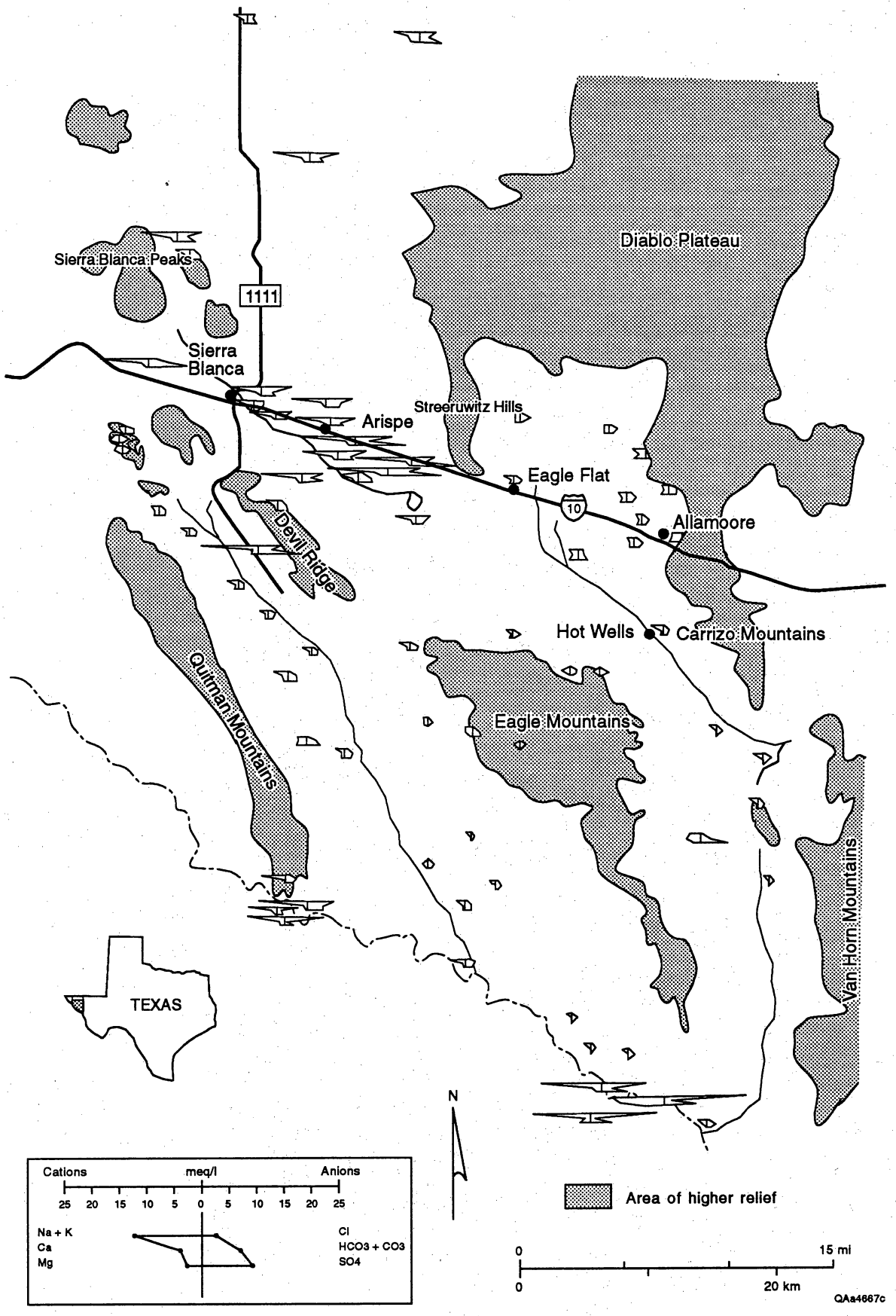

Figure 13. Hydrochemical composition of ground water in Eagle Flat and surrounding area. The hydrochemical composition is represented by Stiff diagrams.

YM-18, and YM-63 (figs. 13 and 14). Water wells beneath the Northwest Eagle Flat Watershed are among the deepest in the study area; many were drilled to depths of 1,000 ft to 1,300 ft (305 m to 396 m). Average temperature is 86°F (30°C). Lower water temperatures of approximately 77°F (25°C) and more dilute ground water occur in the vicinity of Devil Ridge, where wells YM-8 and 48-62-TEX are 900 to 1,500 ft (275 to 457 m) deep. Hoffer (1978) reported a temperature of 100.4°F (38°C) from a 950-ft-deep (290-m) well (48-54-402) at Sierra Blanca. Abandoned since Hoffer's (1978) study, the well is no longer usable, and the temperature could not be verified. Temperatures of 93.2°F (34°C) were recorded in an 880-ft-deep (268-m) monitor well (YM-7A) at Grayton Lake, 10 mi (16 km) east of Sierra Blanca. Ground water from areas west of Sierra Blanca is also highly variable in composition, ranging from dilute Ca-HCO_3 and Na-HCO_3 water in three wells (48-53-801, 48-53-801, and 48-53-804) in an abandoned municipal well field 5 mi (8 km) southwest of Sierra Blanca to higher-TDS Na-SO_4-Cl and Na-Cl water in deep wells (48-53-501, 48-45-602, and 48-45-603) near the Sierra Blanca Peaks.

Ground water in the northern half of Southeast Eagle Flat Watershed is a Ca-Mg-HCO_3 type except near the village of Allamoore, where SO_4 is the dominant anion (wells 48-64-602 and 47-57-401) (fig. 13). TDS range from 600 to 1,500 mg/L, and temperatures from 65.8° to 71.9°F (19° to 22°C) (table 5). Depth to water is between 50 to 200 ft (15 to 61 m) across much of the area. To the south, the proximal area of the Eagle Mountains fan is dominated by Ca-HCO_3 ground water, having TDS around 500 mg/L and temperatures of 57.2° to 71.6°F (14° to 22°C) (table 5). Water depths are typically less than 80 ft (24 m), and temperatures at these locations fluctuate monthly by several degrees centigrade.

Down-gradient from the Eagle Mountains fan in the Scott's Crossing area, Na-HCO_3 ground water is found at depths as great as 600 ft (183 m) in thick deposits of basin fill. TDS are less than 400 mg/L. Temperatures at Scott's Crossing are among the highest in southeast Eagle Flat. White and others (1980) reported a temperature of 107.8°F (42°C) and a geothermal gradient of 4.1°F/100 ft (75°C/km) at Hot Wells (48-64-901). Gates and White (1976) also reported a temperature of 100.4°F (38°C) and a geothermal gradient of 1.8°F/100 ft (32°C/km) in a 2,100-ft

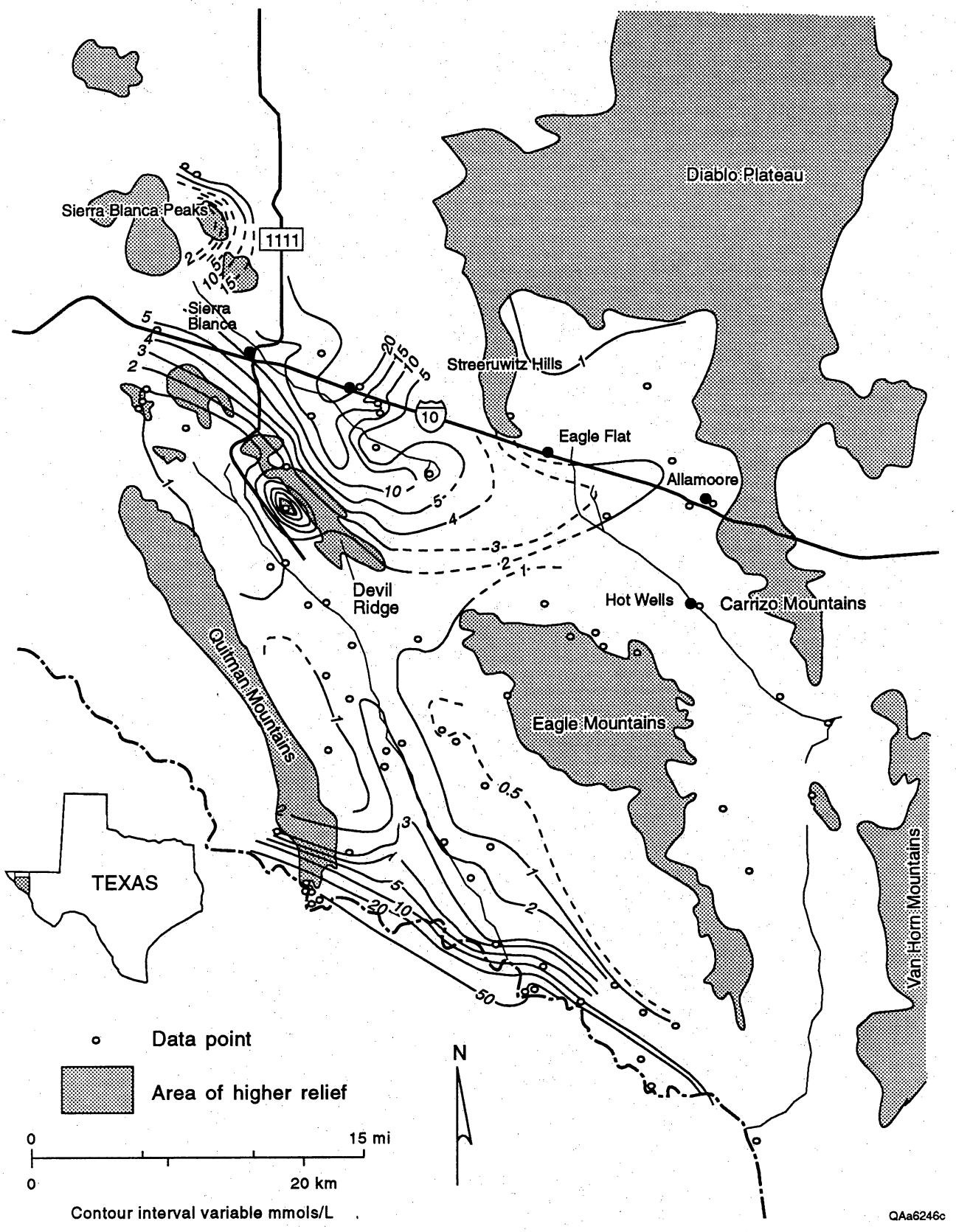

Figure 14. Chloride concentration (mmols/L) of ground water in Eagle Flat and surrounding area.

(641-m) water test well (50-01-504) 5.5 mi (8.8 km) southeast of Hot Wells. Temperatures between 75.2° and 86°F (24° and 30°C) were recorded at three other Scott's Crossing locations (51-01-501, 51-01-503, and 51-01-801) during this investigation.

Wells in the Eagle and Indio Mountains and in adjacent fans yield ground water that is of Ca-HCO_3 to Na-HCO_3 types with a TDS of typically 300 to 500 mg/L. The depths of wells range from less than 50 ft (15 m) in the mountains to more than 500 ft (152 m) in the fan deposits. Gates and White (1976) drilled a 1,185-ft (361-m) water test well (50-07-501) as part of their exploration program for potable ground-water resources in the Trans-Pecos region. A water sample collected from fan material at a depth of 1,100 ft (335 m) showed TDS (326 mg/L) not appreciably greater than other ground-water samples in the eastern half of the watershed (Gates and White, 1976). Samples from shallower depths were contaminated by drilling fluid (Gates and White, 1976).

Wells in the western half of the Red Light Draw Watershed yield water that is of a Na-HCO_3-SO_4 to Na-SO_4-HCO_3 type, with TDS and SO_4 increasing toward the south. Dissolved solids increase from 600 to 800 mg/L in the upper part of the draw to 1,200 mg/L in the lower part of the draw. Ground-water temperatures range from 71.6° to 91.4°F (22° to 33°C) in southeast Red Light Draw to more than 104°F (40°C) at Indian Hot Springs.

The highest TDS in the Red Light Draw Watershed is in the Rio Grande alluvium, an area once heavily irrigated by cotton farmers (Mann Bramblett, personal communication, 1993). At Indian Hot Springs, Na-Cl water having more than 7,000 mg/L of dissolved solids discharges along the Caballo fault into river alluvium (Henry, 1979). Five springs, including Stump Spring and Chief Spring (50-14-501 and 50-14-503), discharge a total of at least 400 L/min of Na-Cl-SO_4 water (TDS >7000 mg/L) into river alluvium at Indian Hot Springs. The discharge occurs near the point where the trace of the Caballo fault, which bounds the southwest flank of the Quitman Mountains, disappears beneath floodplain sediments of the Rio Grande (Henry, 1979). Temperature of the five springs (Soda, Chief, Stump, Squaw, and Beauty) ranges from 80.9° to 116.9°F (27.2° to 47.2°C) (Henry, 1979). Dorfman and Kehle (1974) reported temperatures greater than 140°F (60°C) from a nearby shallow well. Red Bull Spring (50-14-RBL), located 2.5 mi (4.0 km) northwest of Indian Hot

Springs, discharges 50 L/min of moderately saline (1,040 mg/L TDS) Na-HCO_3-SO_4 water, with temperatures of 93.2° to 98.6°F (34° to 37°C), through fractured calcareous claystone (Henry, 1979). The spring is situated at the point where the Red Bull fault terminates against the Caballo fault (Henry, 1979).

Three wells (50-15-801, 50-24-202, and 50-24-503) that provide water for livestock are located along the edge of the southernmost terrace overlooking the Rio Grande floodplain in Red Light Draw. The wells are shallow (45 to 65 ft [13.7 to 19.8 m]), with water depths between 35 and 48 ft (10.7 and 14.6 m). Temperatures are 73.4° to 77°F (23° to 25°C).

Chloride (Cl) concentration varies significantly in southern Hudspeth County (fig. 14). The lowest levels are in areas with HCO_3-dominant ground water. This includes all of southeast Eagle Flat, the abandoned well field west of Sierra Blanca, and most of Red Light Draw. In northwest Eagle Flat, Cl rises to more than 700 mg/L (20 mmol/L) at the proposed low-level radioactive waste disposal site, decreasing to less than 70 mg/L (2 mmol/L) at the northwest end of Devil Ridge (48-62-TEX). With the exception of 48-62-BOR, drilled to supply water to a 16,000-ft (4877-m) exploration well, most wells in Red Light Draw produce water with less than 50 mg/L (1.4 mmol/L) of chloride. Well 48-62-BOR lies on the southwest side of Devil Ridge, 2 mi (3.4 km) south of 48-62-TEX, a well with one of the lowest Cl levels in northwest Eagle Flat.

Cl rises sharply within 2 mi (3.4 km) north of the Rio Grande, but the increase is first seen nearly 10 mi (16.4 km) north of the river in 50-06-LOV, where the concentration is 72 mg/L (2.03 mmol/L) (fig. 14). From there southward, Cl rises to more than 1,000 mg/L in wells along the terrace overlooking the Rio Grande floodplain (table 5). The increased chlorinity in southern Red Light Draw is accompanied by a sharp rise in the Cl/Br molar ratio (fig. 15). Figure 16 shows the marked differences in Cl/Br ratios with increasing TDS. Wells and springs within the high-TDS zone form a distinct linear trend that extends upward from the cluster of low-TDS, low-Cl/Br points of lower Red Light Draw.

The ratio of sodium to chloride decreases with increasing salinity, approaching a value near 1.0 within the high-TDS zone of Red Light Draw (fig. 17A). The differences among the three basins

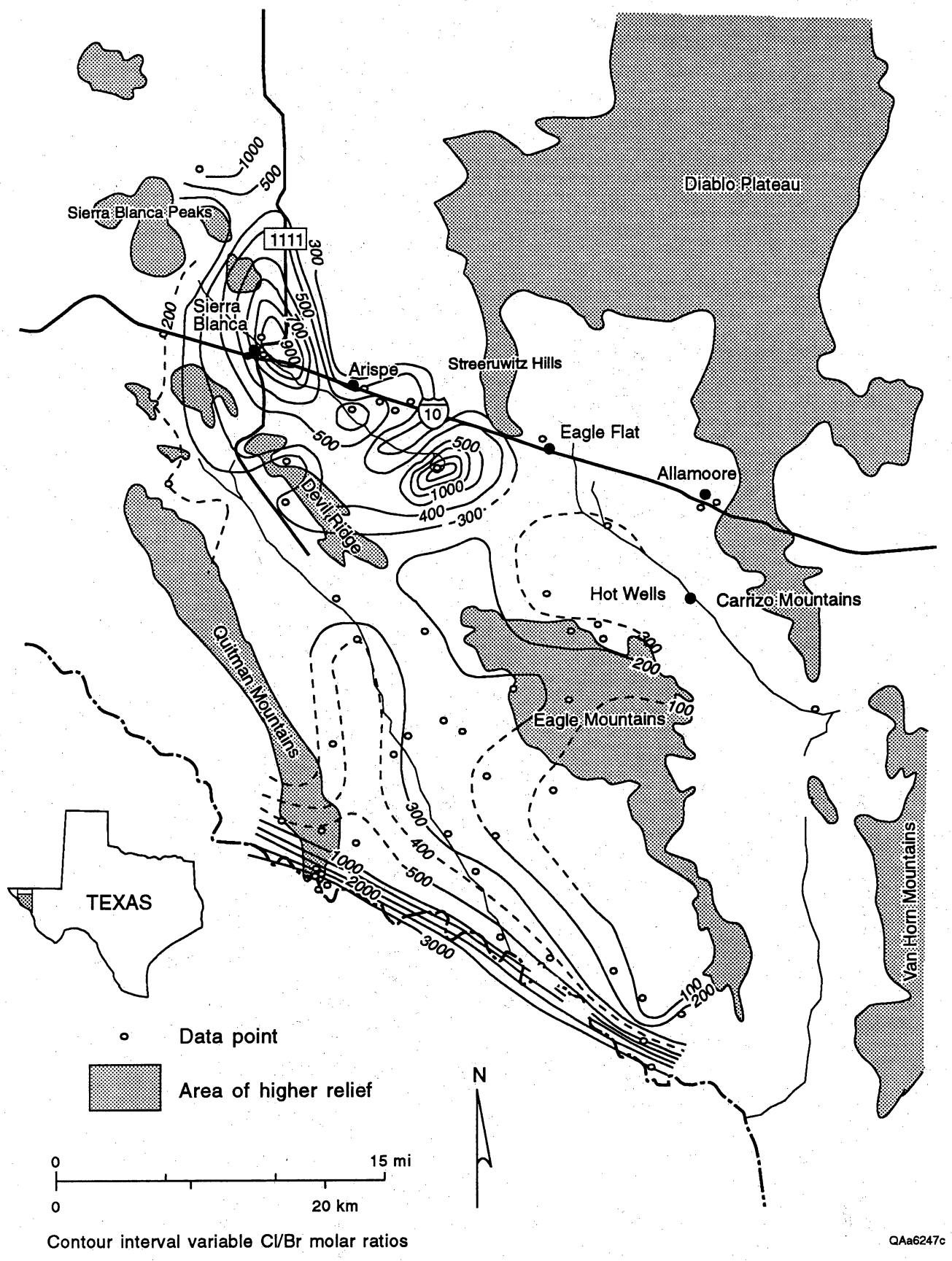

Figure 15. Map of Cl/Br mole ratios.

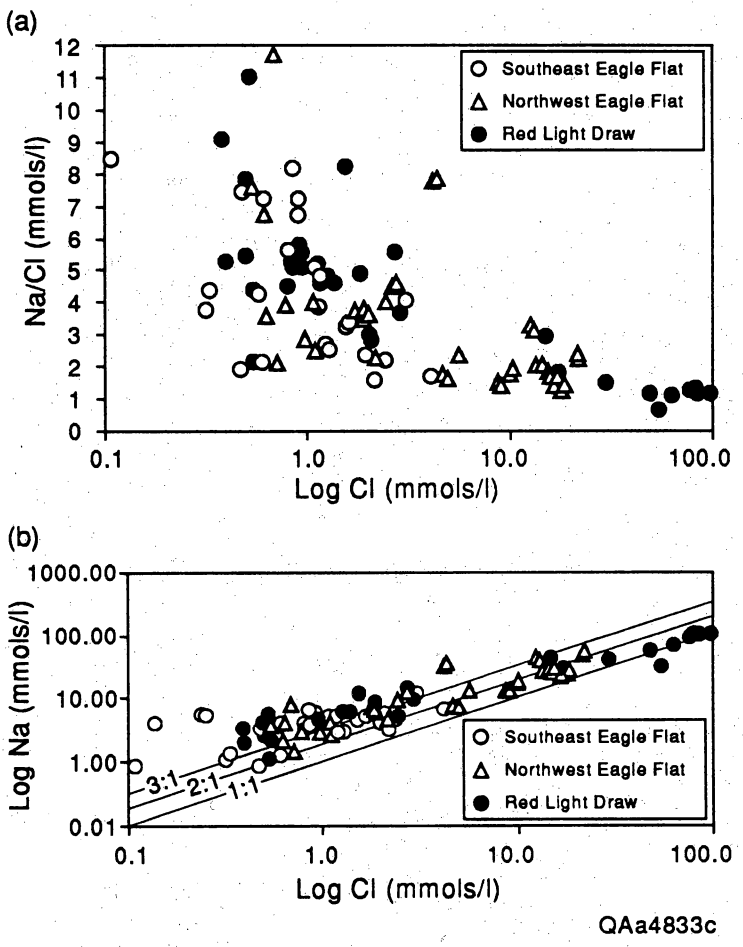

Figure 17. (a) Binary plot of Na/Cl mole ratios versus Cl (mmols/L). The downward-sloping trend approaches a value of 1.0 at the highest Cl levels in Red Light Draw. The trend toward decreasing Na/Cl ratios suggests the influence of NaCl on the hydrochemical composition of ground water in the study area. (b) Binary plot of Na versus Cl (mmols/L) for southeast Eagle Flat, northwest Eagle Flat, and Red Light Draw. Dissolution of NaCl produces equimolar concentrations of sodium and chloride. A 1:1 mole ratio would result in a line with a slope of 1:1, as indicated for Red Light Draw. Situations involving excess Na lead to higher Na/Cl ratios, and to lines with slopes greater than 1:1 (southeast Eagle Flat and northwest Eagle Flat). The excess sodium may be contributed by mineral weathering or by exchange of divalent cations for Na on mineral surfaces.

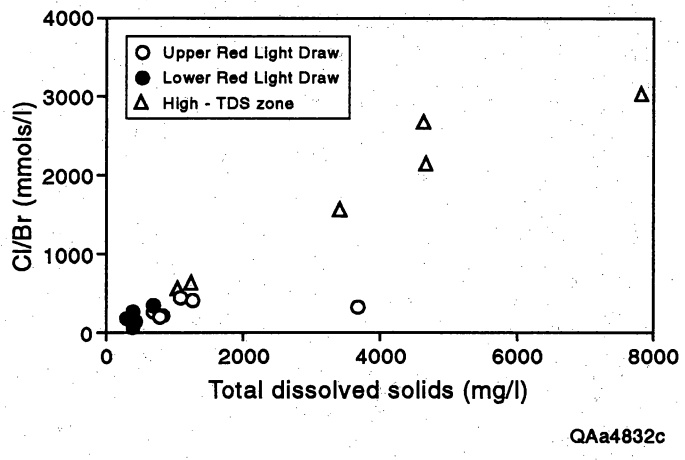

Figure 16. Plot of Cl/Br mole ratios versus TDS for Red Light Draw. The points within the high-TDS zone form an upward-sloping trend originating from within the lower TDS points of lower Red Light Draw. This is interpreted as an indicator of mixing between high-TDS, high-Cl/Br water with the more dilute ground water of lower Red Light Draw.

are further underscored by the plot of Na versus Cl (fig. 17B). Only among the high-TDS waters of Red Light Draw is there nearly a 1:1 relationship between Na and Cl. In northwest Eagle Flat, Na exceeds Cl by an average of 2:1; and the ratio is 3:1 or higher among the dilute ground waters of southeast Eagle Flat and Red Light Draw. Consistent with this observation is the increase in excess Na, estimated as (Na - Cl), with SO_4 (fig. 18).

The (Ca + Mg)/HCO_3 molar ratio (fig. 19) varies from 0.1 to >1.0 within each area. Similarly, subtracting SO_4 from total Ca and Mg yields an estimate of the amount of Ca and Mg not associated with sulfates. The composite variable of Ca + Mg - SO_4 is inversely related to the variable of excess Na (or Na - Cl) (fig. 20) with a slope near -0.5.

Carbon-14 and Tritium

The ^{14}C and ^{3}H values of southern Hudspeth County ground water are listed in table 6 and in figures 21 and 22. In southeast Eagle Flat, ^{3}H and ^{14}C values are among the highest in the study area, ranging from 0 to 7.69 for ^{3}H and 2.20 to 109.9 for ^{14}C (table 7). The highest ^{14}C and ^{3}H values occur in the Bean and Millican Hills, the Carrizo Mountains, and the Eagle Mountains—areas where the potentiometric surface is high (fig. 5), the depth to water is typically less than 200 ft (61 m) (table 1), and where bedrock is either exposed or covered by thin basin fill. Intermediate values of both isotopes occur in the Allamoore area, where wells draw water from basin fill. The lowest ^{3}H and ^{14}C levels are associated with samples from three Scott's Crossing area wells (51-01-501, 51-01-503, and 51-01-801) that extract water from depths as much as 600 ft (183 m) in basin fill.

Carbon-14 measurements decrease from levels near or greater than 100 pmc in bedrock exposures in the Bean and Millican Hills to 40 to 50 pmc at Allamoore and to less than 5 pmc near Scott's Crossing. The overall pattern is consistent with flowpaths inferred from the potentiometric map, as it suggests that ground-water age increases toward the east-southeast. Shallow low-yield windmills producing from gravels in the proximal area of the Eagle Mountains fan in southeast

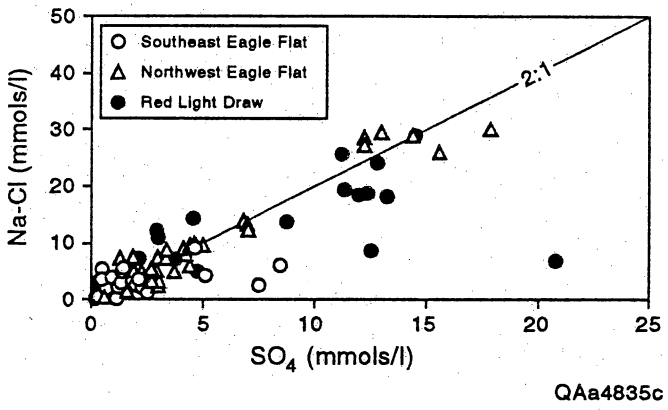

Figure 18. Binary plot of (Na-Cl) versus SO_4 for all areas. The quantity (Na-Cl) represents excess sodium, or that amount not attributable to dissolution of NaCl. The points form an upward-sloping trend with an approximate slope of 2:1. This is interpreted as an indicator of the gain of Na through exchange reaction with Ca derived from the dissolution of gypsum. The slope of 2:1 is what would be expected in a divalent/monovalent cation exchange process.

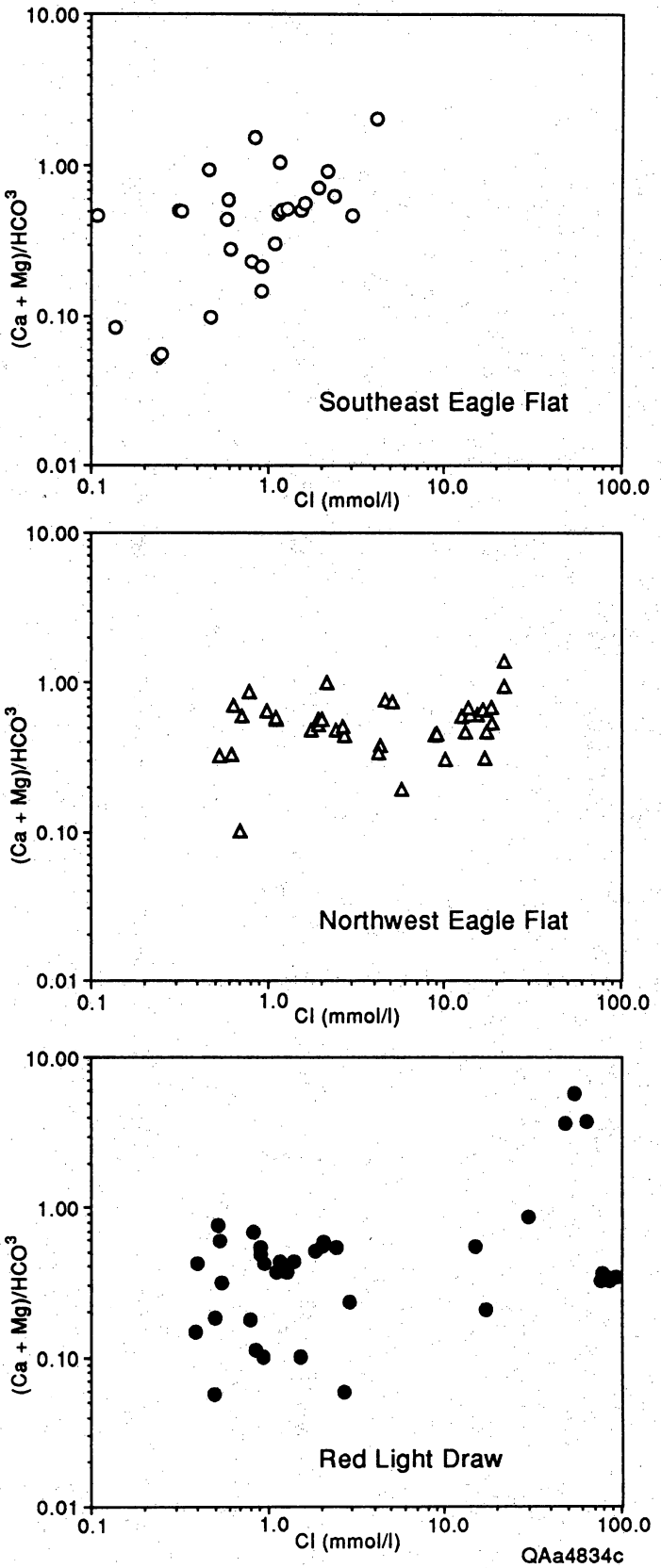

Figure 19. Binary plots of (Ca + Mg)/HCO_3 versus Cl (mmols/L) for (a) southeast Eagle Flat, (b) northwest Eagle Flat, and (c) Red Light Draw. If Ca and Mg were contributed only by calcite dissolution or by weathering of pyroxene and amphiboles, the (Ca + Mg)/HCO_3 ratio would equal 0.50. Lower ratios may indicate loss of Ca and Mg through exchange reactions for Na. Ratios greater than 0.5 indicate accessory sources of Ca and Mg, possibly from dissolution of evaporites.

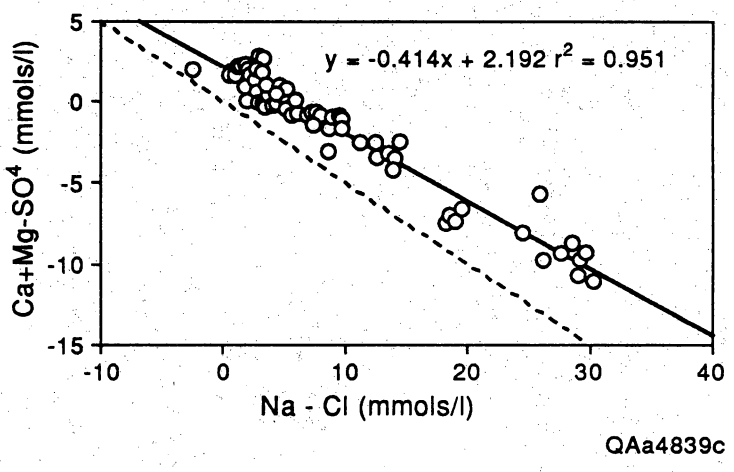

Figure 20. Binary plot of (Ca + Mg - SO_4) versus (Na - Cl). The quantity (Ca + Mg - SO_4) represents the molar concentration of Ca and Mg not associated with sulfates. The points for a downward trend interpreted to be the result of the loss of Ca and Mg in exchange reactions for Na. The quantity (Na-Cl) represents excess Na, as described in the text and in figure 14.

Table 6. Analyses of stable isotopes and unstable isotopes of ground-water samples from southeast Eagle Flat, northwest Eagle Flat, and Red Light Draw.

Basin*	ID Number	Date	$\delta^{18}O$ (‰)	δD (‰)	^{3}H (TU)	$\delta^{13}C$ (‰)	^{14}C (pmc)
SEEF	47-49-GTM	1/12/92	-6.7	-44	6.5	-9.4	103.3
SEEF	47-49-GHM	1/12/92	-6.6	-42	6.3	-11.8	109.9
SEEF	47-49-GHW	1/13/92	-7	-40	6	-10.1	108.5
SEEF	47-57-401	10/29/91	-6.9	-44	2.2		
SEEF	47-57-KHN	1/8/92	-7	-41	7.7	-12.6	100.8
SEEF	48-55-902	5/28/92	-5.2	-30			
SEEF	48-56-803	1/10/92	-7.6	-49	3.7	-6.6	62.8
SEEF	48-56-DES	1/10/92	-7.5	-40	4.5	-8.4	79.5
SEEF	48-64-302	10/31/91	-6.8	-49	3.1	-6.9	47.1
SEEF	48-64-301	10/29/91	-6.7	-46	5.2	-9.7	94.4
SEEF	48-64-602	12/18/91	-6.6	-42	1.5	-7	23.5
SEEF	48-64-604	12/15/91	-6.9	-49	3	-6.3	45.1
SEEF	48-64-604	8/14/92	-7.1	-46	2.7		
SEEF	48-64-LOV	12/15/91	-7.2	-49	0.4	-8.2	52.5
SEEF	50-08-101	11/1/91	-8.3	-56	6.8		
SEEF	50-08-102	12/12/92	-8.3	-55			
SEEF	50-08-202	11/2/91	-7.8	-52	7		
SEEF	51-01-501	6/25/92	-9.7	-52	0	-7	5.4
SEEF	51-01-501	1/9/92	-9.3	-59	0	-6.9	6.8
SEEF	51-01-501	5/31/92	-9.3	-56			
SEEF	51-01-503	12/18/91	-9.5	-56	0	-4.7	2.2
SEEF	51-01-801	6/28/92	-9.8	-63	0	-5.6	5.6
NWEF	48-45-603	8/10/92	-8.7	-59	0	-5	6.1
NWEF	48-45-901	5/24/92	-8.3	-51	1.4	-6.4	23
NWEF	48-53-501	1/13/92	-8	-52	0.4	-6.1	12.7
NWEF	48-53-501	5/26/92	-8.3	-52	0.3	-6.2	7.2
NWEF	48-53-802	6/26/92	-7.9	-47	2	-9.4	47.3
NWEF	48-53-803	5/28/92	-8.1	-45	1.7	-9.4	42.4
NWEF	48-54-404	6/1/92	-8.1	-54	0.7	-4.9	8.5
NWEF	48-54-502	8/13/92	-8.8	-54	0	-4.3	4.7
NWEF	48-62-TEX	3/3/93	-8	-55	1	-7.3	11.4
NWEF	48-62-TEX	5/27/93	-8.4	-53		-6.7	9.8
NWEF	48-62-TEX	7/28/93	-8.9	-57	0.9	-10.5	80.5
NWEF	48-63-302	12/17/91	-7.3	-46	0.4	-7.9	27.6
NWEF	48-63-302	5/30/92	-7.7	-34	0.4	-7.5	29.5
NWEF	YM-7A	6/23/92	-8.3	-47	0	-6	5.8
NWEF	YM-7A	11/20/92	-7.8	-54	0	-6.4	8.1
NWEF	YM-7A	3/5/93	-7.9	-55	0	-6.2	6
NWEF	YM-7A	5/25/93	-9.1	-57	0	-6.5	6
NWEF	48-63-902	1/8/92	-7.8	-52	0	-6.6	21.2
NWEF	48-63-902	7/16/92	-7.8	-45	0.2	-6.6	22.8
NWEF	48-64-BTH	8/30/93	-7.4	-50	0	-7.7	10.1
NWEF	50-07-301	8/30/93			4.1		
NWEF	YM-18	3/1/93	-8.3	-56	0	-5.7	3.8
NWEF	YM-18	5/25/93	-8.3	-53	0	-5.8	4.5
NWEF	YM-18	7/29/93	-8	-50	0	-5.9	1.7

Table 6 (cont.).

Basin*	ID Number	Date	$\delta^{18}O$ (‰)	δD (‰)	^{3}H (TU)	$\delta^{13}C$ (‰)	^{14}C (pmc)
NWEF	YM-19	2/3/93	-9.2	-61		-5.9	3.7
NWEF	YM-19	5/27/93	-9.2	-61	0		
NWEF	YM-19	7/30/93	-10	-64	0	-7.4	1.3
NWEF	YM-63	8/20/93	-8.3	-50	0	-7.2	1.3
NWEF	YM-8	11/21/92	-8.3	-56	1	-5.2	3.9
NWEF	YM-8	5/26/93	-8.6	-55	0	-5.3	4.6
RLD	48-61-201	7/7/92	-8.3	-52	0.4	-5	5.9
RLD	48-62-BOR	7/7/92	-6.1	-39	0	-4.2	26.1
RLD	48-62-805	7/18/92	-8.5	-55			
RLD	50-06-203	7/2/92	-8.1	-53	0		
RLD	50-06-301	5/29/92	-8.3	-50	0	-5.6	8
RLD	50-06-LOV	7/2/92	-8.4	-54	0		
RLD	50-06-LOV	5/14/93	-8.7	-55	0		
RLD	50-06-801	8/28/93	-6.8	-41	1.3	-3.6	11.7
RLD	50-07-401	6/27/92	-8	-47	0	-6.9	8
RLD	50-07-MCM	7/18/92	-8.1	-43	0	-7.9	15.2
RLD	50-07-601	8/18/93	-7.9	-44	1.3	-10.7	54.3
RLD	50-07-FRC	7/3/92	-8.5	-45	6.9		
RLD	50-14-501	1976	-7.9	-59			
RLD	50-14-503	1976	-7.7	-58			
RLD	50-14-503	7/6/92	-6.8	-49	0	-2.7	2.1
RLD	50-14-RBL	1976	-9.1	-63			
RLD	50-14-RBL	1/28/93	-8.6	-57			
RLD	50-15-101	5/15/93	-7.8	-49	6.2		
RLD	50-15-201	6/29/92	-8.5	-41	0	-5.4	3.7
RLD	50-15-WBG	6/30/92	-8.5	-58	0		
RLD	50-15-801	5/12/93	-8.1	-52	2.6		
RLD	50-16-703	5/13/93	-8.5	-54	0	-8.5	4.3
RLD	50-24-202	7/4/92	-10.4	-76	0		
RLD	50-24-301	7/4/92	-7.7	-42	0	-7.1	3.4
RLD	50-24-503	1/9/93	-9.3	-64			
RLD	50-24-503	5/12/93	-9.2	-67	4.2		
RLD	50-24-SHT	10/22/92	-8.5	-54			

* SEEF - Southeast Eagle Flat, NWEF - Northwest Eagle Flat, RLD - Red Light Draw

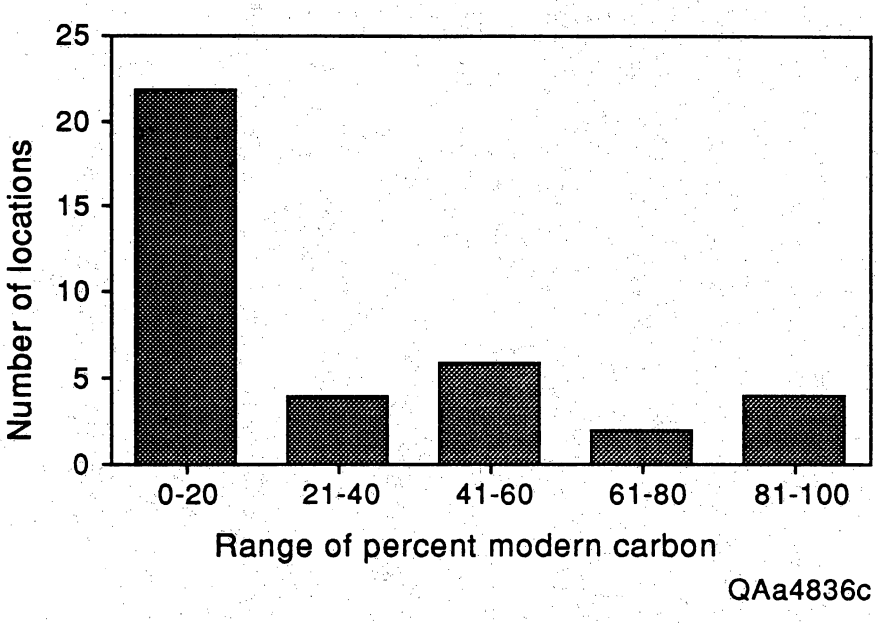

Figure 21. Histogram of Percent Modern Carbon (pmc) values in southern Hudspeth County ground water.

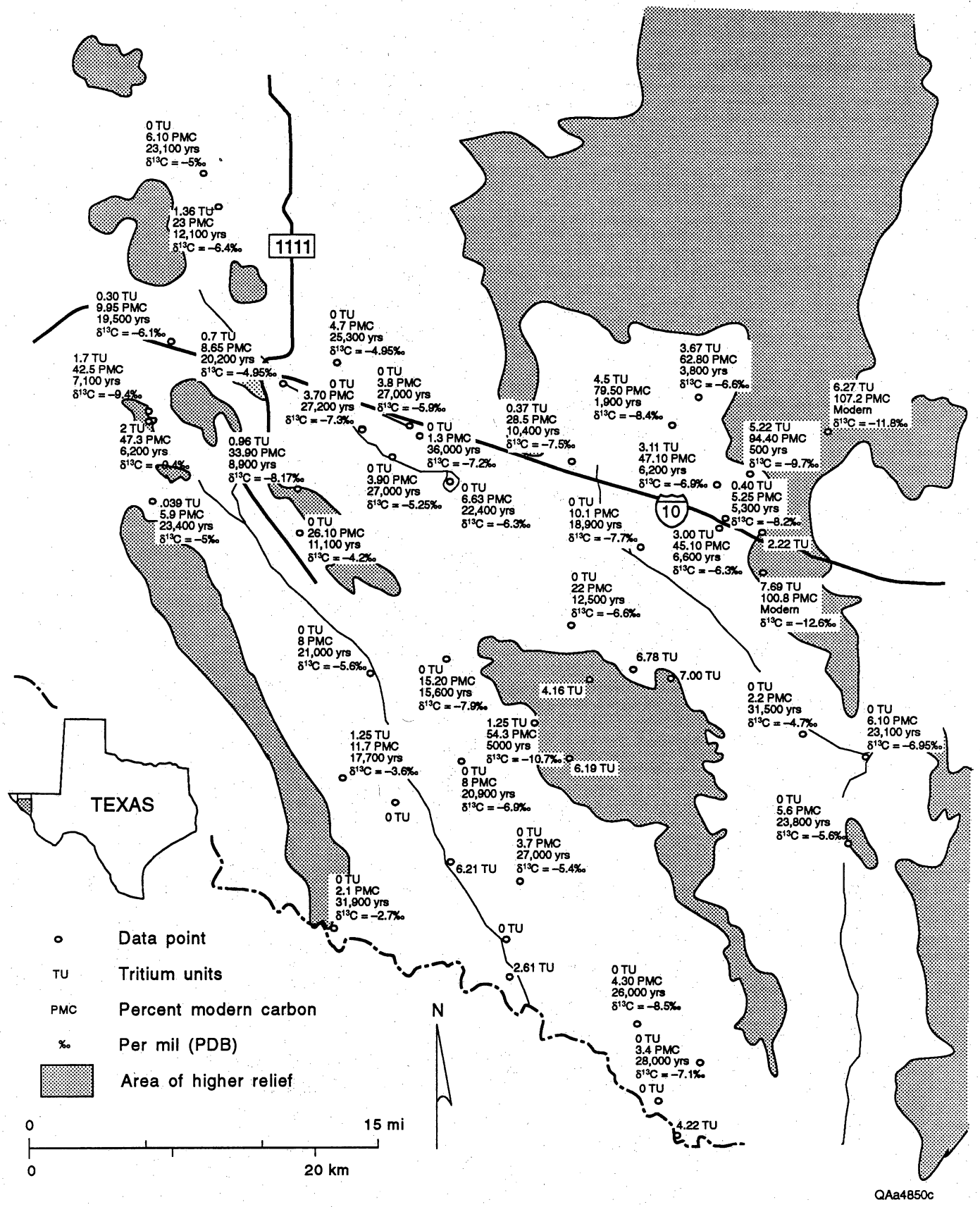

Figure 22. Map of ^{3}H, ^{14}C, and $\delta^{13}C$ in southern Hudspeth County ground water. Carbon-14 is shown as pmc, along with uncorrected ages. Tritium is reported as Tritium Units (TU). $\delta^{13}C$ is measured with respect to Peedee belemnite (PDB) standard.

Table 7. Range of tritium units and percent modern carbon in southern Hudspeth County ground water.

RANGE OF TRITIUM UNITS

AREA	WELLS	HIGH	LOW
S.E. Eagle Flat	17	7.69	0.00
N.W. Eagle Flat	17	4.16	0.00
Red Light Draw	19	6.91	0.00

RANGE OF PERCENT MODERN CARBON VALUES

AREA	WELLS	HIGH	LOW
S.E. Eagle Flat	14	109.90	2.20
N.W. Eagle Flat	16	80.50	1.30
Red Light Draw	11	54.30	2.10

Eagle Flat (50-08-101, 50-08-102, and 50-08-202) were not sampled for carbon isotopes, but tritium values were between 6 and 7 TU.

In northwest Eagle Flat, ^{3}H and ^{14}C range from 0 to 4.16 TU and 1.3 to 80.5 pmc, respectively (table 7). Tritium units and percent modern carbon are positively correlated (fig. 23), and some of the highest values are associated with ground-water samples from the abandoned well field west of Sierra Blanca. Two wells from this field (48-53-802 and 48-53-803) yielded samples with ^{14}C values of 47.30 and 42.4 pmc, respectively, and tritium concentrations of 1.99 and 1.73 TU. Seven miles (11.3 km) north of Sierra Blanca, an 1,100-ft well (48-45-901) on the north side of Triple Hill yielded a sample of $Na\text{-}SO_4\text{-}HCO_3$ ground water (1,040 mg/L) that had 23 pmc and 1.36 TU. Well 48-45-901 is adjacent to another deep well (48-45-603) having substantially higher dissolved solids (2,200 mg/L), no measurable tritium, and only 6.1 pmc.

The lowest ^{14}C and ^{3}H values in northwest Eagle Flat occur near the proposed repository site. Several wells were drilled in this area during the period September 1991 through August 1993 as part of the characterization and monitoring program. The wells range in depth from 880 to 1,100 ft (268 to 335 m) and produce water from the Cox Sandstone and the Finlay Limestone. Pumping tests indicate that the aquifer is leaky confined, with transmissivities of less than 11 ft^2/day (1.02 m^2/day) at the proposed waste disposal site (YM-8, YM-18, YM-19, and YM-63) to 70 ft^2/day (6.50 m^2/day) at Grayton Lake (YM-7A).

All of the monitor wells were sampled several times between June 1992 and August 1993 as part of the quarterly monitoring program. With the exception of 48-62-TEX, average ^{14}C is less than 6.63 pmc. Only YM-7A, YM-8, and YM-19 were in operation by November 1992. YM-19 and 48-62-TEX were added by February 1993, and YM-63 was completed in August 1993. YM-8 was not sampled in February and August of 1993 because of mechanical problems, and YM-7A was not accessible because of standing water at Grayton Lake in August 1993. Except for 48-62-TEX, no significant variation in ^{14}C is observed through August 1993.

There is no readily discernible pattern of decreasing ^{14}C along flowpaths in northwest Eagle Flat, as several key locations lie along the same potentiometric contour. YM-7A, YM-8, YM-19,

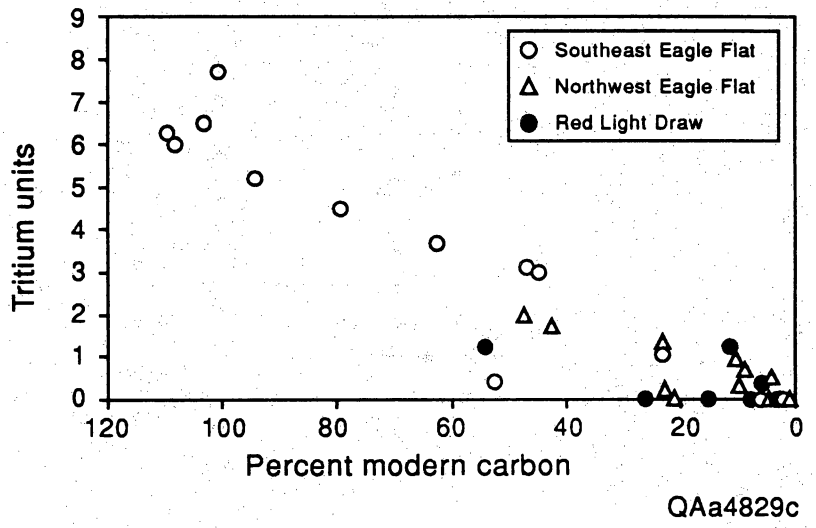

Figure 23. Plot of ^{3}H versus ^{14}C in study area. The downward-sloping trend for southeast Eagle Flat and northwest Eagle Flat indicates mixing between recent recharge water and older ground water. Points from Red Light Draw exhibit unapparent trend.

YM-63, and 48-54-502, for example, are close to the 3,600-ft (1,097-m) isopleth along the east side of the basin (fig. 5). Average ^{14}C measurements and uncorrected ages are 6.63 pmc (22,400 yr) at YM-7A, 3.9 pmc (26,800 yr) at YM-8, 3.7 pmc (27,300 yr) at YM-19, 3.8 pmc (27,000 yr) at YM-18, 1.3 pmc (36,000 yr) at YM-63, and 4.7 pmc (25,300 yr) at 48-54-502. These figures suggest significantly long residence time for ground water in the aquifer underlying northwest Eagle Flat.

Between May and August 1993, ^{14}C increased from 9.8 to 80.5 pmc at 48-62-TEX. The increase was accompanied by a change in $\delta^{13}C$ from -6.7 ‰ to -10.5 ‰ and a decrease in TDS from 923 to 713 mg/L. Tritium was 0.94 TU, essentially unchanged from the 0.96 TU reported for an earlier sample. The δD and $\delta^{18}O$ values were also consistent with earlier values.

In Red Light Draw, ^{3}H ranges from 0 to 6.91 TU, and ^{14}C is 2.1 to 54.3 pmc (table 7). The highest ^{14}C values are associated with wells in the Eagle Mountains and along the northwestern part of Devil Ridge (50-07-601, 54.3 pmc; 48-62-BOR, 26.1 pmc). Along flow lines from the Eagle Mountains, ^{14}C and ^{3}H decrease rapidly toward the axis of the basin (fig. 5). There is only one ^{14}C measurement within the high-TDS zone along the Rio Grande. A sample from 50-14-503 (Chief Spring) yielded 2.1 pmc and no tritium. Two other locations in the high-TDS zone (50-15-801 and 50-24-503) had 2.61 and 4.22 TU, respectively.

Stable Isotopes

The δD and $\delta^{18}O$ values of ground-water samples are found in table 6. Figures 24 and 25 present δD and $\delta^{18}O$ analyses of ground waters in which ^{14}C also was measured. The proximity of the points to the meteoric water line and the overlap with precipitation samples from Midland, Texas, collected by Nativ and Smith (1987), indicate that (1) the ground waters are of meteoric origin and (2) stable isotopes have not been altered significantly by rock-water interaction (Banner and Hanson, 1990). In addition, δD and $\delta^{18}O$ have more negative (more depleted in the heavy isotope) average values in ground waters in which ^{14}C activity is less than 20 pmc than in ground waters in which ^{14}C activity is greater than 20 pmc (compare figs. 24 and 25).

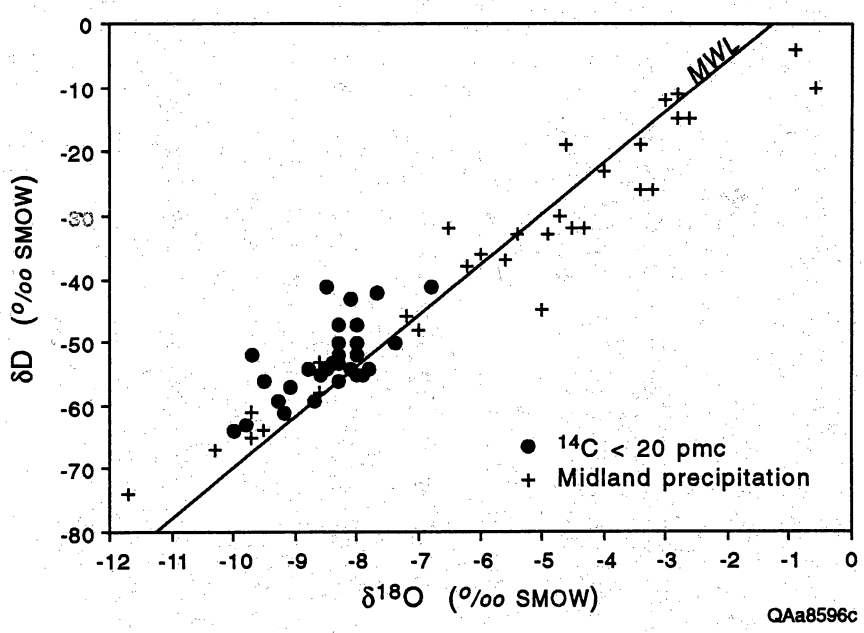

Figure 24. Plot of δD versus $\delta^{18}O$ for ground waters with ^{14}C activity less than 20 pmc. MWL is meteoric water line defined by $\delta D = 8\,\delta^{18}O + 10$ (Craig, 1961). Also shown are analyses of precipitation from Midland, Texas, collected by Nativ and Smith (1987) that show that local (Midland) meteoric water data are consistent with the global data.

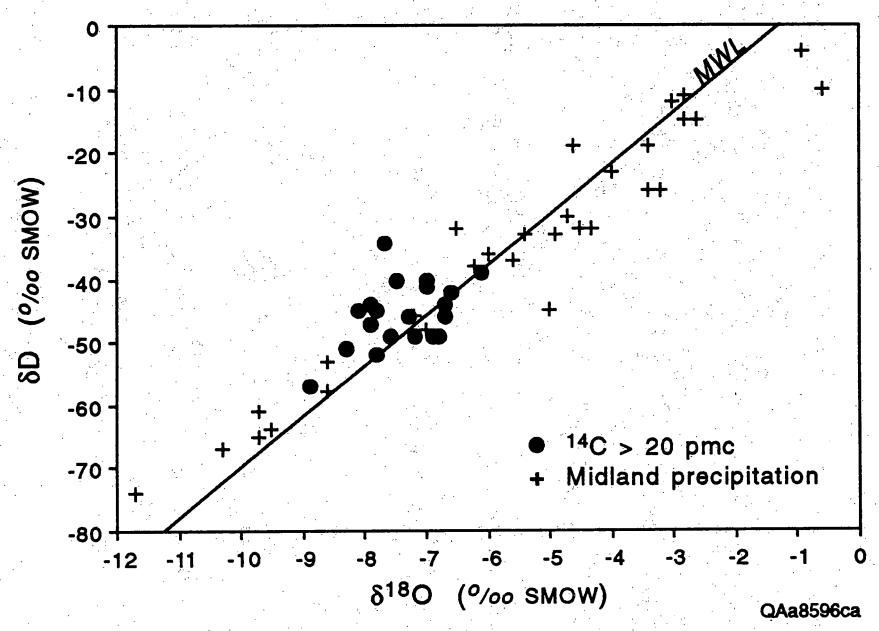

Figure 25. Plot of δD versus $\delta^{18}O$ for ground waters with ^{14}C activity more than 20 pmc. MWL and precipitation data from Midland, Texas, as defined in figure 24.

δD and $\delta^{18}O$ values vary along inferred flow paths from an upland recharge area to beneath the adjacent valley floor (fig. 26). The pattern shown in figure 26 is the map view of results shown in figures 24 and 25; that is, older ground water with lower ^{14}C activity has more negative δD and $\delta^{18}O$ values and lies farther along flow paths that originate at the recharge areas. Similarly, $\delta^{18}O$ is more positive beneath the Streeruwitz, Bean, Millican Hills (>-6 ‰) than down-gradient beneath northwest Eagle Flat (<-8 ‰).

Ground water in the Northwest Eagle Flat Watershed has δD and $\delta^{18}O$ values (fig. 26) that are between -64.0 and -34.0 ‰ and -10.0 and -7.3 ‰, respectively. The lowest ^{14}C and ^{3}H activities in the Northwest Eagle Flat Watershed coincide with the most depleted δD and $\delta^{18}O$ measurements. $\delta^{18}O$ is increasingly depleted toward the central part of the basin.

Ground water in the Southeast Eagle Flat Watershed (fig. 26) can be divided into three groups based on differences in δD, $\delta^{18}O$, ^{14}C, and ^{3}H data. The first group has δD between -49 and -30 ‰ and $\delta^{18}O$ between -7.6 and -5.2 ‰ and predominates where the Precambrian bedrock is either exposed or only thinly buried. Tritium values from samples collected over the period October 1991 through December 1992 are 0.4 to 7.7 TU, and ^{14}C measurements are between 23.5 and 109.9 pmc. Water depths in this area are as much as 214 ft (65 m), although 66 percent of water depth measurements in the area are less than 150 ft (46 m).

The second group of samples is from wells near Scott's Crossing (50-01-501, 50-01-503, and 50-01-801) that extract water from basin fill at depths as great as 600 ft (183 m). δD and $\delta^{18}O$ values are the lowest in southeast Eagle Flat, ranging between -63 and -52 ‰ and -9.8 and -9.3 ‰, respectively; ^{14}C is 6.8 to 2.2 pmc, and ^{3}H is zero.

The third group of samples in Southeast Eagle Flat Watershed (50-08-101, 50-08-102, 50-08-202) is found at the lower elevations of the Eagle Mountains ranging from 4,761 to 4,941 ft (1,451 to 1,506 m). Stable isotope values are intermediate to those of the above groups: δD of -55.6 to -52.1 ‰ and $\delta^{18}O$ of -8.3 to -7.8 ‰. Tritium is 6.8 to 7.0 TU. Because all of the above wells are low-yield windmills, samples were not collected for radiocarbon analysis.

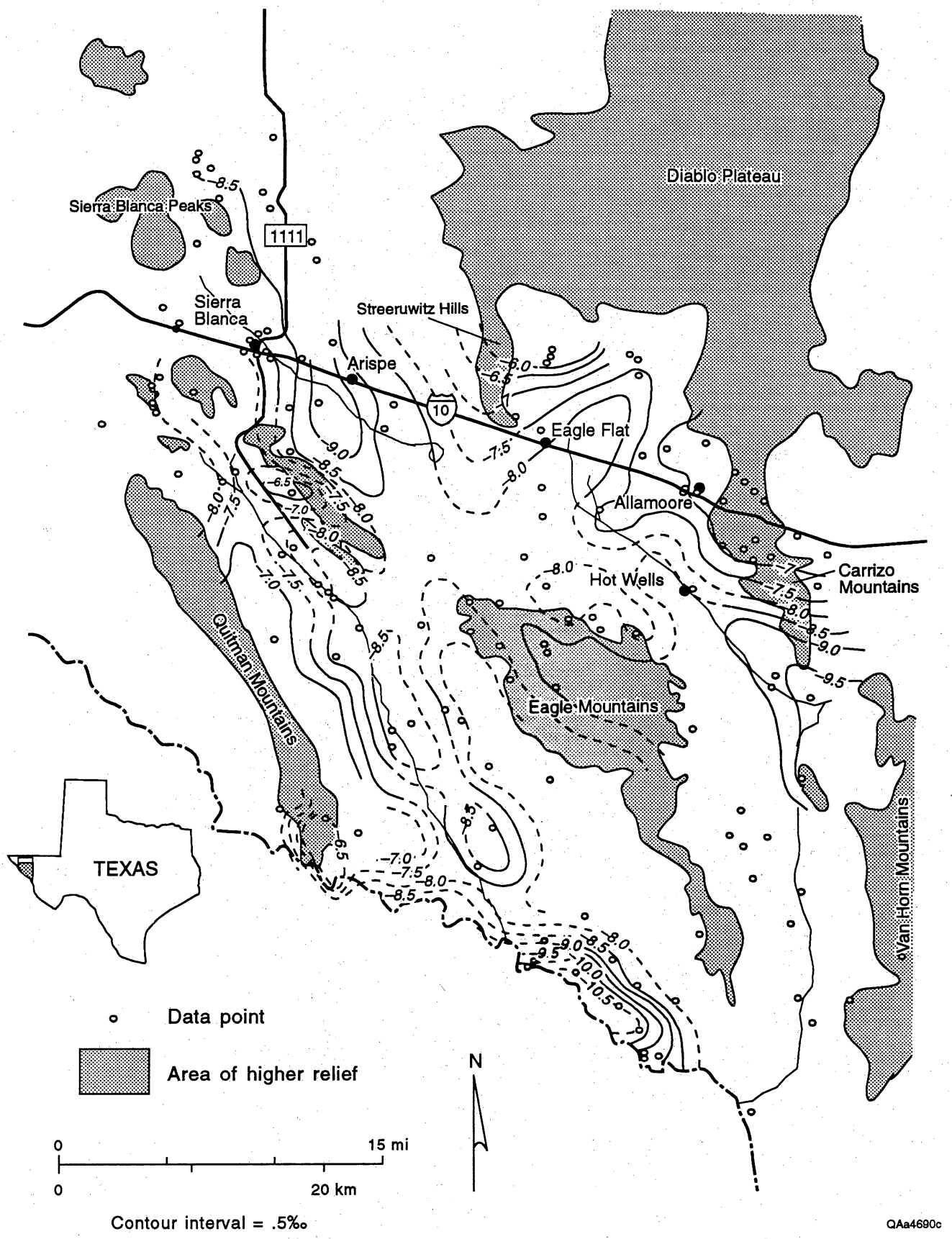

Figure 26. Map of $\delta^{18}O$ values in southern Hudspeth County ground water.

$\delta^{18}O$ also decreases along flow paths beneath Red Light Draw Watershed, with the most depleted δ-values at the center of the contour pattern. For example, $\delta^{18}O$ is more positive in the Quitman Mountains (>-7 ‰) and Eagle Mountains (>-8 ‰) but more negative down-gradient beneath Red Light Draw (<-8.5 ‰). Also, in the area between southeast Red Light Draw and Indian Hot Springs where TDS are high near the Rio Grande, δD and $\delta^{18}O$ values are among the lowest in the study area (-64 to -76 ‰ and -9.5 to -10.4 ‰, respectively).

Figure 27 shows the relationship between δD and $\delta^{18}O$ for ground waters with low (<100 mg/L) and high (>100 mg/L) dissolved Cl in the Red Light Draw Watershed. All these waters are meteoric in origin. The more saline waters (solid dots, fig. 27) appear to form a well-defined trend parallel with the meteoric water line. Other lower salinity samples from Red Light Draw form a more widespread cluster of data.

DISCUSSION

Origin of Solutes

The variable hydrochemical signature of southern Hudspeth County ground water (table 5, figs. 12 and 13) is attributable to the relative solubilities of aquifer materials, cation exchange, and mixing. Calcium (Ca) and magnesium (Mg) concentrations, for example, are controlled not only by the weathering of Ca- and Mg-bearing minerals, such as calcite, pyroxene, or amphiboles, but also by the dissolution of sulfates and by exchange for the monovalent cation Na.

If Ca and Mg originate entirely from dissolution of carbonates and from the weathering of pyroxene or amphiboles, the molar ratio of Ca and Mg to HCO_3 would be 0.50 (Sami, 1992). The governing equations for the weathering of the above minerals are

calcite: $$CaCO_3 + H_2O + CO_2 = Ca + 2HCO_3, \quad (3)$$

pyroxene: $$CaMg(Si_2O_6) + 4CO_2 + 6H_2O = Ca + Mg + 4HCO_3 + 2SI(OH)_4, \text{ and} \quad (4)$$

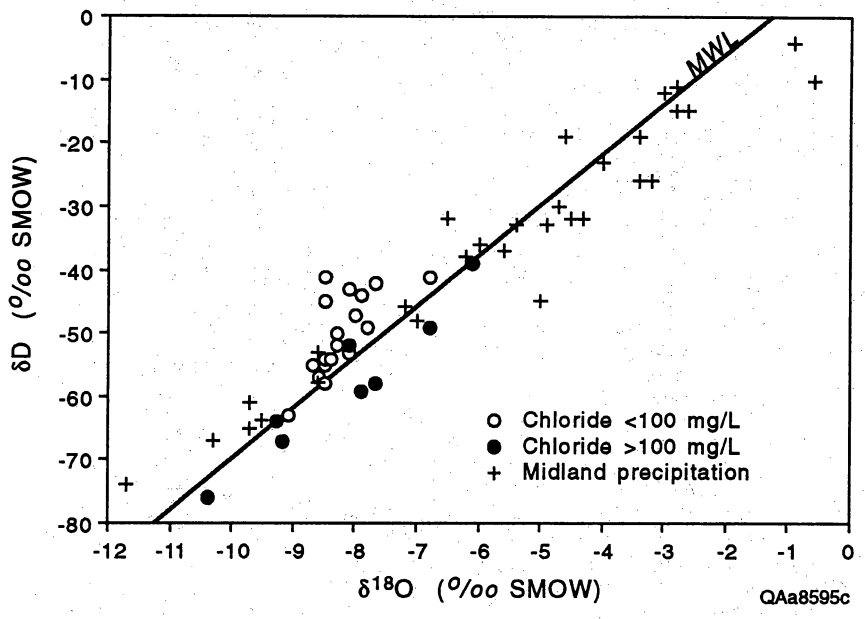

Figure 27. Plot of δD versus $\delta^{18}O$ for ground waters in lower Red Light Draw with varying total dissolved solids. Midland precipitation from Nativ and Smith (1987).

amphiboles: $Ca_2Mg_5Si_8O_{22}(OH)_2 + 14CO_2 + 22H_2O = 2Ca + 5Mg + 14HCO_3 + 8Si(OH)_4$. (5)

Each of the above reactions yields two moles of HCO_3 for every mole of Ca, or Ca and Mg. Ratios less than 0.5 may be attributed to the loss of Ca and Mg through cation exchange, and ratios greater than 0.5 may indicate additional sources of Ca and Mg, possibly associated with the dissolution of sulfates. Figure 19 shows the covariation between the (Ca + Mg)/HCO_3 ratio and Cl in each of the three basins. The wide scatter around a molar (Ca + Mg)/HCO_3 ratio of 0.5 indicates that Ca and Mg are not only lost by cation exchange but also gained by weathering of sources other than calcite, pyroxene, or amphiboles (Sami, 1992).

Furthermore, if all Cl originates as NaCl, then (Na - Cl) represents a maximum value of Na from cation exchange (Sami, 1992). The plot of (Na - Cl) versus SO_4 (fig. 18) offers support for the hypothesis that dissolution of sulfates is a factor accounting for regional hydrochemical patterns. In figure 18, points from all three basins form an upward trend with a slope of approximately 2.0. If Ca derived from the dissolution of gypsum replaces Na through exchange, then the molar ratio of Na to SO_4 should be 2:1, as traced by the line in figure 18.

Figure 20, a plot of (Ca + Mg - SO4) versus (Na - Cl), best illustrates the interrelationship between Ca, Mg, and Na because it allows for direct evaluation of the significance of exchange and mineral weathering on concentrations of the three cations (Sami, 1992). The linearity indicates a highly correlated relationship between the increase of Na and the loss of the divalent cations Ca and Mg. Specifically, Na increases at slightly more than twice the loss rate of Ca and Mg, as would be expected from cation exchange. The dashed line traces the amount of Ca and Mg lost solely as a result of cation exchange, and the position of the points above the dashed line indicates that Ca and Mg are also derived by processes other than dissolution of sulfates (Sami, 1992).

The trend of decreasing Na/Cl ratios (fig. 17a and 17b) with increasing chlorinity suggests the influence of NaCl on the chemistry of southern Hudspeth County ground waters, especially from the lowermost reaches of Red Light Draw. Dissolution of NaCl yields equimolar concentrations of Na and Cl, so that the Na/Cl ratio should equal 1.0. Ratios much greater than 1.0, especially at

lower salinities, signify additional sources of Na, such as weathering of albite or exchange of divalent cations (Ca and Mg) for Na.

Chloride/bromide (Cl/Br) molar ratios have significant implications for tracing sources of salinity in Red Light Draw, as illustrated by figure 16. In this figure, the Cl/Br ratios of wells and springs in the high-TDS zone along the Rio Grande fall along a line that extends upward from the cluster of low-TDS samples of Red Light Draw. Linear features such as this suggest two-component mixing processes involving parent waters of different hydrochemical compositions. In such cases, the compositions of all possible mixtures vary systematically, forming a straight line between end members on a binary plot such as figure 16 (Faure, 1986, 1991; Mazor, 1991; Mazor and others, 1993). The ground-water chemistry of the lowermost area of Red Light Draw is dominated by the high-TDS waters. Red Bull Spring (50-14-RBL) and well 50-15-801, with salinities and Cl/Br ratios that are intermediate to those of dilute Red Light Draw ground water and the more saline components at Indian Hot Springs and the southeastern areas Red Light Draw, are the first locations where the effects of the ground-water mixing can be seen.

The source of the high-TDS water is problematic because no other example of ground water of similar composition is found in Red Light Draw. Cl-Br systematics, however, offer some insight into a possible origin. As members of the halide group of elements, Cl and Br are conservative anions, and few processes other than precipitation or dissolution of salts and ground-water mixing will significantly affect their concentrations in natural waters, although Hem (1985) notes that clay-membrane effects may selectively concentrate bromide.

In a review of the trace-element geochemistry of evaporites, Holser (1979) observed that the molar ratio of Cl to Br is sensitive to the origin of water as marine (~300), as a second-cycle solution of marine salt (~1000), or as a brine residue from the precipitation of halite (<250). Cl/Br molar ratios in the high-TDS zone lie above the characteristic molar ratio of second-cycle evaporites, possibly indicating the presence of saline water linked to the dissolution of marine salt. Another, although less likely, possibility is the flushing of salts crystallized from recycled irrigation water in floodplain sediments along the Rio Grande (Kreitler and others, 1986). That the Na/Cl molar ratios

are approximately 1.0 for all wells within the high-TDS zone (fig. 17a and 17b) offers additional support for the hypothesis that salt dissolution accounts for the Cl/Br ratios.

Henry (1979) observed that Indian Hot Springs and Red Bull Spring lie near the edge of the Jurassic evaporite basin described by DeFord and Haenggi (1970). He concluded that meteoric water mixes with salt-dissolution brine before moving upward along the Caballo fault to discharge points near the Rio Grande. If waters from deeper aquifers in Mexico upwell and eventually discharge to the Rio Grande alluvium, there is reason to expect a similar phenomenon to occur from the north because flow systems on both sides of the Rio Grande will tend to be imperfect mirror images of each other. One regional flow system may dominate the overall pattern of flow, depending on its relative dimensions, hydraulic gradients, and permeabilities. Aquifers to the south presumably dominate patterns of flow because high Cl/Br molar ratios are found more than a mile north of the Rio Grande. Unfortunately, the geochemical signatures of waters from northwest Eagle Flat do not allow us to trace saline waters directly where they upwell near the Rio Grande. These waters, having evolved in areas where halite deposits are unknown, have only moderate Cl/Br ratios.

Paleoclimatic Inference

In many areas of southern Hudspeth County, ^{14}C signatures indicate that ground water was recharged many thousands of years ago (fig. 22). Highly accurate age estimates based solely on carbon isotopes, however, are difficult to derive because of the complex nature of carbon chemistry in ground-water systems. This problem may be traced to the effects of dilution and isotope exchange, which have been shown to alter significantly the carbon signature of ground water (Mook, 1980), leading to falsely old age estimates.

Many researchers have proposed the use of correction factors to adjust raw ^{14}C ages for the effects of dilution and isotope exchange. Fontes and Garnier (1979) reviewed the factors used in most ground-water age-dating studies, and Muller and Mayo (1986) evaluated the sensitivity of models to variations in input parameters, such as $\delta^{13}C$ of limestone and soil gas. It is clear that a correction factor should not be used without regard to the specific set of conditions that the model

was designed to address (Muller and Mayo, 1986). Use of an inappropriate correction factor may yield age estimates that are thousands of years older or younger than the true age of an unmixed sample.

No effort is made in this report to derive adjusted ^{14}C ages because of the many factors known to influence the chemistry of dissolved inorganic carbon. Absolute values of ^{14}C are accepted as conveying significant information only about relative differences in ground-water ages and flow directions (Siegel, 1991; Dutton, 1993). Unadjusted ages are assumed to represent maximum limits.

Despite the many problems involving the ^{14}C dating method in hydrological investigations, it is still possible to derive reasonable age estimates indirectly by comparing $\delta^{18}O$ in ground water with $\delta^{18}O$ of modern rainfall because the effects of climate and atmospheric temperature on the fractionation of deuterium and oxygen-18 are well documented (Dansgaard, 1964; Siegenthaler and Oeschger, 1980; Schoch-Fischer and others, 1983). The assumptions underlying this approach are that (1) low ^{14}C values indicate late Pleistocene ages and (2) the combination of significantly depleted δ-values and low ^{14}C activities may reflect the cooler and wetter climatic conditions of late Pleistocene glacial stages (Gonfiantini and others, 1974; Dutton and Simpkins, 1989). Other factors that may account for greater depletion of ^{18}O are elevation (Siegenthaler and Oeschger, 1980; Payne and Yurtsever, 1974; Musgrove, 1993) and distance from the source of moisture (Sonntag and others, 1979), but these are not related in any systematic manner to ^{14}C values.

Lambert and Harvey (1987) observed that the isotopic signatures of ground water in the confined aquifers of southeastern New Mexico are more depleted in $\delta^{18}O$ and δD than is observed for modern rainfall in the Carlsbad area. Lambert (1967) estimated ground-water ages of 12,000 to 16,000 yr using the correction method of Evans and others (1979) and Lambert and Harvey (1987) and concluded that the confined waters were recharged under a more humid climatic regime.

Weighted averages of $\delta^{18}O$ in precipitation from eight sample stations in West Texas (Alpine, Amarillo, Lubbock, and Midland) and southeast New Mexico (Carlsbad, Clovis, Elk, and Roswell) are shown in figure 28. The weighted averages, based on more than 500 samples representing wide ranges of temperature and elevation (Hoy and Gross, 1982; Lambert and Harvey, 1987; Nativ and

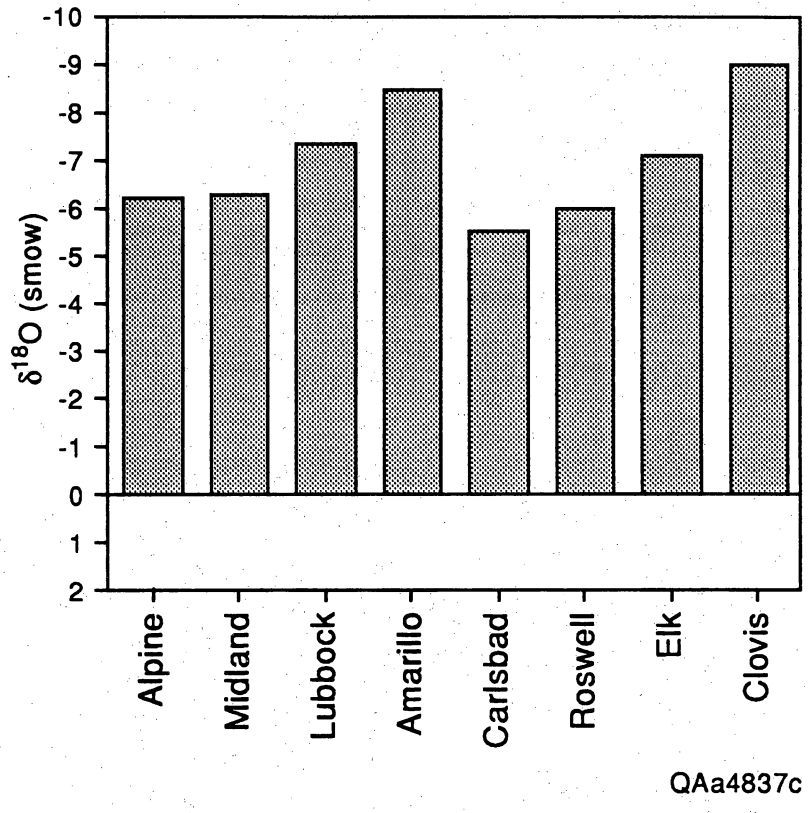

Figure 28. Weighted-average $\delta^{18}O$ values for precipitation from stations in West Texas and southeastern New Mexico.

Riggio, 1990; Lawrence, personal communication, 1993) establish a baseline against which the $\delta^{18}O$ of southern Hudspeth County ground water may be compared. Southern Hudspeth County lies between stations in Roswell (southeastern New Mexico) and Alpine and west-southwest of Midland. The stable isotope composition of rainfall in the study area may therefore be expected to resemble the composition of rainfall in surrounding stations more than that of distant locations, such as Amarillo and Clovis.

Figure 29A is a plot of $\delta^{18}O$ versus ^{14}C activity (pmc) for southern Hudspeth County ground waters. The ^{14}C axis is reversed, so that apparent ^{14}C age increases from left to right. The degree of depletion in ^{18}O is shown to increase with decreasing ^{14}C activity (increasing age). This downward shift of $\delta^{18}O$ is consistent with Lambert and Harvey's (1987) observations regarding the stable-isotope values of southeastern New Mexico ground waters. The probability that this is related to paleoclimatic factors is underscored by research on the Pleistocene climatic history of the desert Southwest, as summarized by Langford (1993):

> During the early Pleistocene, the climate of the southwestern United States was cooler and more moist than that of the present (Hall, 1985). The Late Wisconsinan glacial period from 25,000 to 14,000 yr B.P. was a time of moist and cooler climate throughout the southwestern United States (Wells and others, 1982; Hall, 1985). At the end of the Wisconsinan, 14,000 to 10,000 yr B.P., the climate became warmer and drier, although still cooler, and more moist than that of the present, and there was a gradual transition from glacial to post-glacial vegetation (Wells and others, 1982; Hall, 1985). Dry woodlands of juniper lasted in the deserts of the southwest until 8,000 to 10,000 yr ago (Alexrod and Bailey, 1976; Van Devender and Spaulding, 1979; Wells and others, 1982). Juniper woodlands persisted in the Hueco Basin, immediately to the west of Eagle Flat, until 8,000 to 4,000 yr ago, when they were replaced by grasses (Horowitz and others, 1981). Because the Eagle Flat and Red Light Draw Basins lie at generally higher elevations than the floor of the Hueco Basin, and therefore would have had higher rainfall, woodlands should have persisted as long as in the Hueco Basin. To the north, wetter climatic regimes with woodlands persisted even longer, to about 5,000 yr B.P. in the

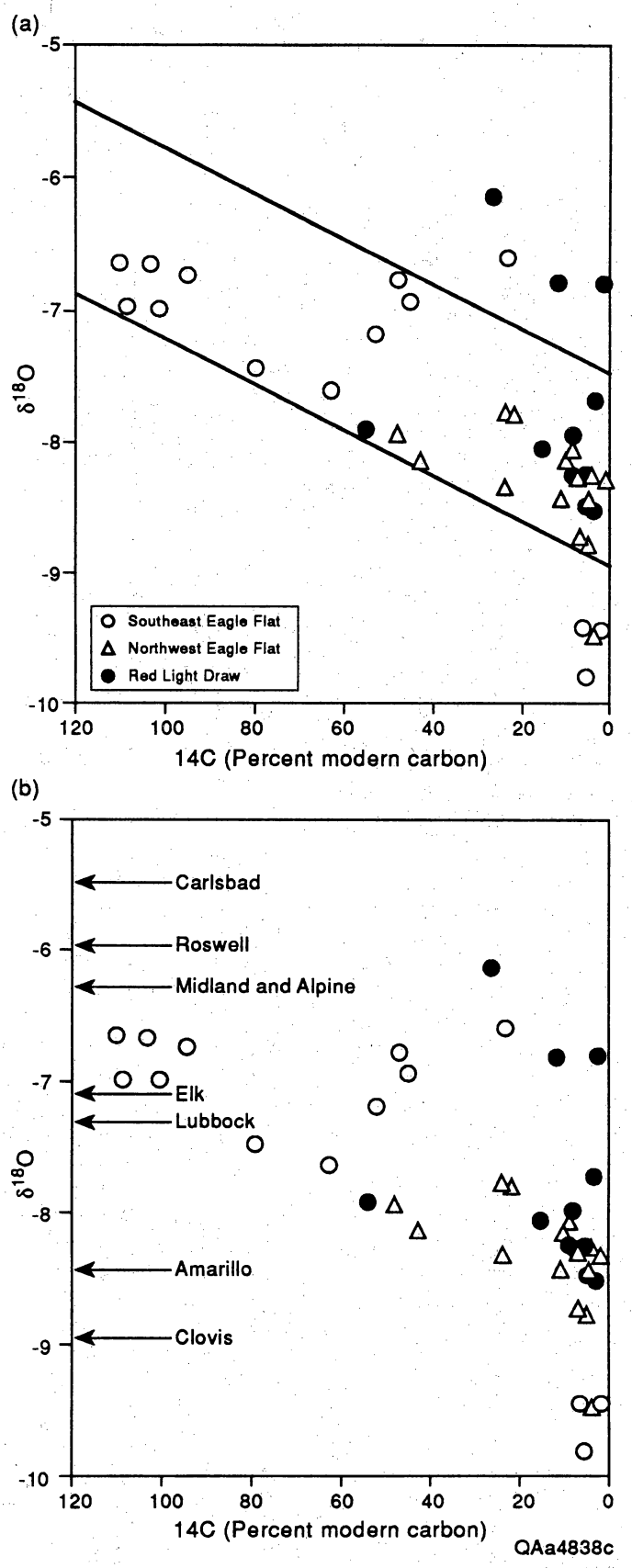

Figure 29. (a) Binary plot $\delta^{18}O$ versus pmc in southern Hudspeth County ground water. Downward-sloping lines mark decreasing trend of $\delta^{18}O$ values. (b) Binary plot of $\delta^{18}O$ versus pmc in southern Hudspeth County ground water. Weighted-average $\delta^{18}O$ values for precipitation from stations in West Texas and southeastern New Mexico are marked along the vertical axis. With few exceptions, ground-water d-values with less than 20 pmc are apparently lower than d-values from six of the eight locations.

San Augustin Plains of New Mexico (Markgraf and others, 1984), and to about 5,800 yr B.P. in Chaco Canyon (Hall, 1977).

The weighted-average $\delta^{18}O$ at Alpine (-6.28 ‰), Midland (-6.31 ‰), Carlsbad (-5.50 ‰), Roswell (-6.0 ‰), Elk (-7.10 ‰), and Lubbock (-7.32 ‰) are apparently heavier than $\delta^{18}O$ measurements of all southeast Eagle Flat, northwest Eagle Flat, and all but two Red Light Draw samples with less than 20 pmc (fig. 29B). Ground water with demonstrably modern δD and $\delta^{18}O$ signatures is found primarily in southeast Eagle Flat. These points are clustered near the weighted averages of Midland, Alpine, Elk, and Lubbock. The stable isotope values of the oldest waters appear to be more similar to the weighted averages of Amarillo (-8.48 ‰) and Clovis (-8.97 ‰). The downward drift of $\delta^{18}O$ with lower ^{14}C values indicates a time-dependent component that may be related to the climatic history outlined by Langford (1993).

Support for this hypothesis is offered by the $\delta^{18}O$ contour map (fig. 26). The occurrence of isotopically light $\delta^{18}O$ in the middle of northwest Eagle Flat and along the axis of Red Light Draw suggests dependence of stable isotope signatures on flowpaths and climatic conditions at the time of recharge. The decrease of hydraulic head from the topographically high boundaries of the study area toward the center of the basins enables one not only to trace ground-water flowpaths but also to identify areas where the oldest waters would be expected to occur (that is, along the axes of the basins and draws). Patterns of ^{14}C and ^{3}H suggest that the major recharge areas are in bedrock exposures in mountains and the uppermost areas of the mountain fans. Excluding the relatively depleted $\delta^{18}O$ values of modern ground water from the higher elevations of the Eagle Mountains (explained as a function of rainout over a topographically high area), the progression toward lower $\delta^{18}O$ with distance from the mountains toward the proposed repository site and the axis of Red Light Draw suggests that the isotopic signature of meteoric water falling over recharge areas might have been more negative in the past.

Recharge Areas

Recently recharged waters are Ca-HCO_3 to mixed-HCO_3 in type (fig. 13) and have ^3H greater than 1 TU and ^{14}C more than 50 pmc (fig. 22). Mixtures of older water and recently recharged water are indicated by the occurrence of ^3H values greater than 1 TU with moderate to low ^{14}C values.

In Northwest Eagle Flat Watershed, recharge appears to be centered around the northern Quitman Mountains, Sierra Blanca Peaks, and possibly Devil Ridge. Sufficient pathways for recharge may be provided by fractures that allow rapid percolation of meteoric water. The situation appears very different in the flats, as there is no substantial geochemical evidence that the aquifer is recharged through the basin floor.

One significant recharge area also is between the Bean Hills and Allamoore, the Streeruwitz Hills, and the Diablo Plateau, on the north side of the Southeast Eagle Flat Watershed. The Eagle Mountains constitute a second major recharge area. Within short distances of the mountain front, however, ^{14}C and ^3H activities decrease to low values, which suggest very slow rates of ground-water flow from the Eagle Mountains.

Ground-water flow in the Red Light Draw Watershed appears similar to that in the Northwest Eagle Flat Watershed. Recharge most likely occurs in the Quitman and Eagle Mountains, as indicated by tritium measurements ranging from 1.25 to 6.91 TU. Within a short distance basinward, tritium is typically below detection limits (fig. 22) and carbon-14 is less than 8 pmc (table 6).

Alluvial fans do not appear to constitute significant recharge areas for Red Light Draw. The ^{14}C activities in water samples from alluvial fans are consistently less than 8 pmc, and ^3H activities are essentially zero, which suggests very slow moving water. Langford (1993) documented the existence of well-developed Stage 4 calcic soil horizons in all fan areas of Red Light Draw. These impermeable soils may contribute to runoff by acting as barriers to the percolation of meteoric water (Gile and others, 1981).

Site Hydrogeology

Depth to ground water varies between 667 to 751 ft (203.5 to 229 m) below ground surface in Faskin Ranch wells. On top of the regional gradient in hydraulic head beneath the flats of Northwest Eagle Flat and Red Light Draw Watersheds, local trends are controlled by the location of recharge beneath the mountain ranges. This might be the case at the site. Locally, the gradient in the potentiometric surface suggests that ground water flows toward the northwest underneath the proposed site on Faskin Ranch and later merges with the southeasterly sloping regional hydraulic gradient (figs. 5 and 30). Using data from wells YM-18, YM-63, YM-19, YM-8, YM-7A, and 48-54-901, the local gradient in hydraulic head of ground water on the northern side of northwest Eagle Flat is directed toward the west or northwest. In such a picture, ground water enters Faskin Ranch from the northeast and east and then moves to the west or northwest before later merging with the regional flow direction toward the southwest. This curving flow path also is implied by the bend in the 3,600-ft equipotential line.

It is important to note that data from wells YM-18, YM-63, YM-19, YM-8, YM-7A, and 48-54-901 are not equal in quality nor measured at the same time. The water levels in the first five wells were measured during the course of the Bureau's site investigation. The water level at 48-54-901 is actually based on a "reported," not measured, depth to water as of March 1972. The well was since abandoned after partial collapse of the well bore, so water level could not be remeasured. It is possible that the water level at the location of 48-54-901 no longer is at an elevation of 3592 ft m.s.l. It also is possible that the reported 788-ft depth to water was inaccurate. These possibilities are important because the value from 48-54-901 alone accounts for most of the curvature of the 600-ft equipotential line.

If the water level from 48-54-901 is disregarded, then the inferred local direction of ground-water flow at the site might be toward to the west rather than northwest before flow merges with the regional flow direction toward the southwest. That 1972 water-level estimate cannot be

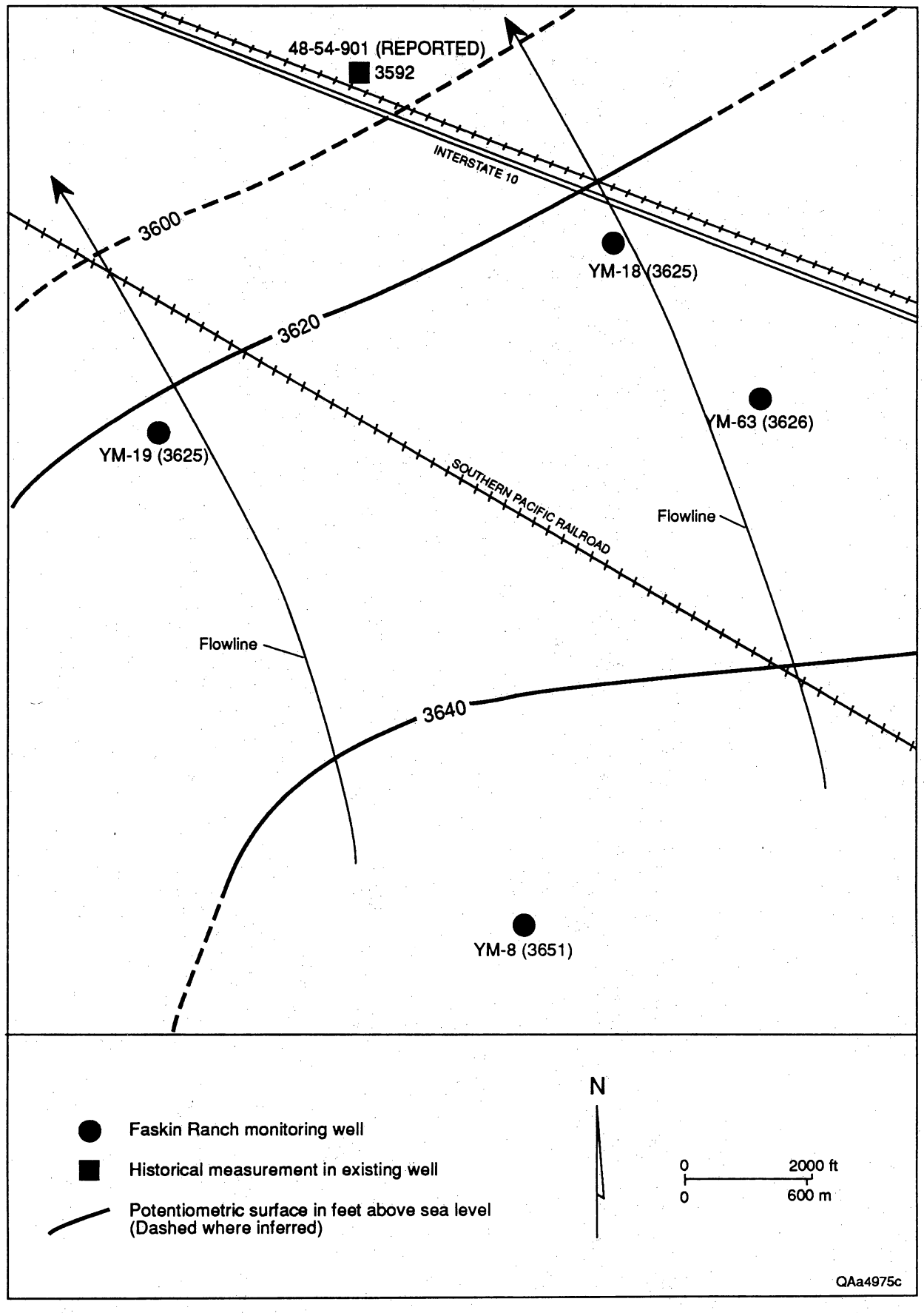

Figure 30. Map showing locations of monitoring wells and the potentiometric surface at Faskin Ranch.

disregarded, however, because to consistently eliminate all historic data would greatly limit the data set.

Curve matches with Hantush-Jacob (1955) type curves suggested a leaky confined aquifer beneath Faskin Ranch. Despite the match, the precise mechanism(s) of leakage could not be determined because many aquifer models emulate a leaky confined aquifer without storage in aquitards. For example, a diagrammatic representation of three different types of leaky confined aquifer systems is shown in figure 31. In systems one and two, each aquifer is composed of a semipermeable upper layer confining a main artesian aquifer. The distinction between models 1 and 2 is that an unconfined aquifer does not exist above the upper confining unit in model 2. In system three, a series of high-permeability and low-permeability strata form the main artesian aquifer, which emulates a leaky aquifer due to its partitioning into multiple confining and permeable water-bearing units. All of these leaky aquifer models can emulate a Hantush-Jacob (1955) type curve without storage in aquitards depending upon the hydraulic and elastic properties of the semipermeable confining units and permeable strata. The Hantush-Jacob (1955) and Hantush (1960) analytical solutions were derived under a simplified set of boundary conditions that have varying interpretations in field data.

For example, model 2 can emulate a leaky aquifer without storage in aquitards if the confining unit has storage *and* fracture permeability. In this instance, ground water can leak in substantial quantities through the confining unit matrix into confining unit fractures and replenish the leaky confined aquifer by vertical leakage as readily as could a water table above the confining unit. The slightly fractured confining unit acts as a confining layer because its overall permeability is less than the permeability of the aquifer, for example, by a factor of 10.

Models 1 and 3 can emulate a leaky aquifer without storage in aquitards depending on the physical properties of the confining unit(s). In the case of model 1, the confining layer transmits water from saturated units above or below the semipermeable layer but contains negligible water in storage. In model 3, the less permeable interbeds contain moderate amounts of available water in storage and are permeable enough to vertically convey water to adjacent, more permeable interbeds.

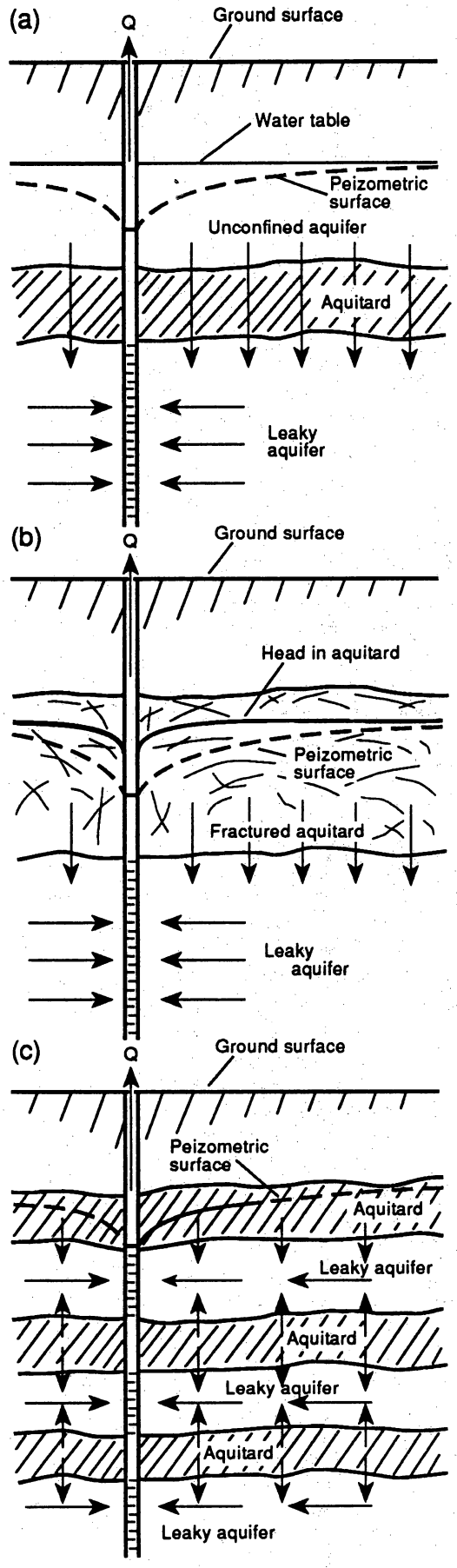

Figure 31. Various aquifer models (1, 2, and 3) that generate time-drawdown curves that emulate Hantush-Jacob (1955) type curves in leaky aquifers. Model 1 (a) has an unconfined aquifer above the semipervious unit; this model idealizes the Hantush-Jacob (1955) analytical model. Model 2 (b) has a semipervious unit with relatively high hydraulic conductivity and storage; in fact, this unit may almost be considered part of the aquifer. Model 3 (c) has a series of high- and low-permeability interbeds that emulate a leaky confined aquifer during a pump test. One cannot distinguish between these conceptual models with time-drawdown data only. Additional knowledge of the hydrogeology was needed to distinguish between these models in northwest Eagle Flat.

QAa4827c

In all of these models, leakage may come from underneath as well as above the aquifer if wells are partially penetrating.

Additional knowledge of the hydrogeology of the aquifer at Faskin Ranch was needed in order to discriminate between these conceptual models. To determine why the Hantush-Jacob (1955) method for leakage without storage in aquitards generally provided the best curve match, the upper hydrostratigraphic unit at YM-63 was hydraulically tested as the test hole was progressively deepened during drilling. At drilling depths of 735, 760, and 785 ft (224, 232, and 239 m), the estimated depth to either the confining unit(s) (if the aquifer emulates models 2 and 3) or water-table aquifer (if the aquifer emulates model 1), the borehole was evacuated of water three times, and water-level recovery rates in the borehole were monitored after final evacuation (fig. 32). Theis (1935) recovery analysis was used to provide a preliminary estimate of the transmissivity of the strata at these depths.

In addition to the monitoring of recovery rates, drilling mud was spiked with a rhodamine dye tracer, and water samples were collected for analyses of bromide, chloride, and rhodamine dye. These data were collected during testing for comparison with drilling mud samples before the well was completed and for comparison with water samples from the completed well.

Figure 33 compares recovery water for two penetration depths in the strata above 785 ft (239 m), the finished well, and a drilling mud sample. These data indicate that concentrations of conservative anions in recovery water are much higher than in drilling mud and are similar to ionic concentrations in the finished well. Moderately low concentrations of rhodamine dye also indicate that almost three-fourths of the recovery water is formation water for penetration depths of 760 and 785 ft (232 and 239 m) (fig. 33). No recovery water was collected at 735 ft (224 m) because the borehole was dry at that depth. Identical static water-level elevations at the 785-ft (239-m) test interval and in the completed water well (both 734 ft [224 m] below land surface) indicate hydraulic equilibrium between saturated strata above 785 ft (239 m) and in the aquifer.

Theis (1935) recovery analysis at the 785-ft (239-m) test interval provided a transmissivity estimate of 0.13 ft^2/day (0.012 m^2/day). Theis (1935) recovery analysis in the completed well

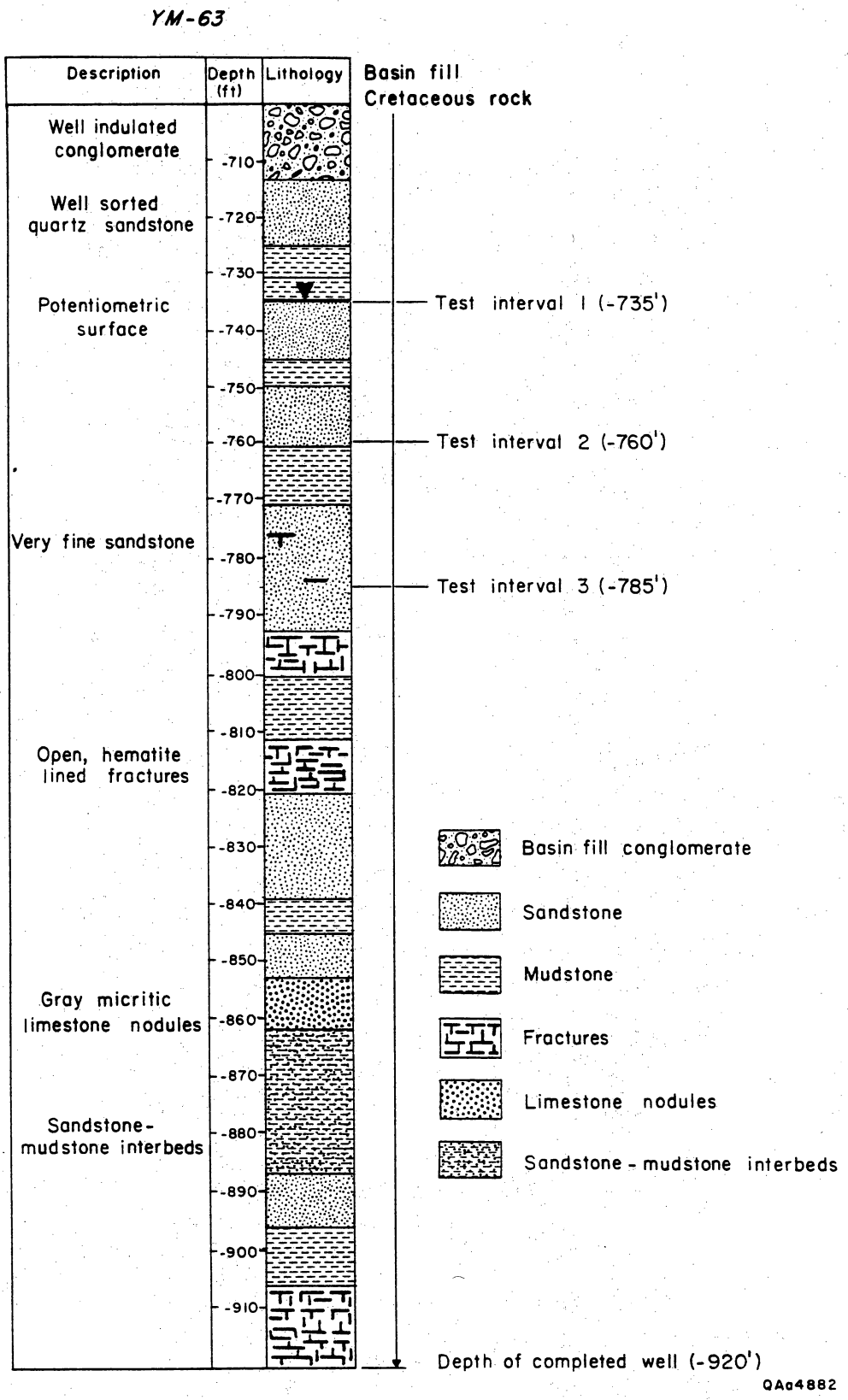

Figure 32. Schematic diagram that illustrates lithologies and depth intervals tested during coring operations at YM-63. At depths of 735, 760, and 785 ft below land surface, water samples were collected after the borehole was blown dry. Well recovery rates were analyzed and compared with recovery rates in the completed well (well depth = 920 ft). Water samples were collected during each recovery phase and compared with drilling mud and formation water from samples later collected at the completed well. Testing indicated confining strata at these test intervals. Testing of the confining layer at these core depths helped to distinguish between conceptual aquifer models 1 through 3 (see fig. 31).

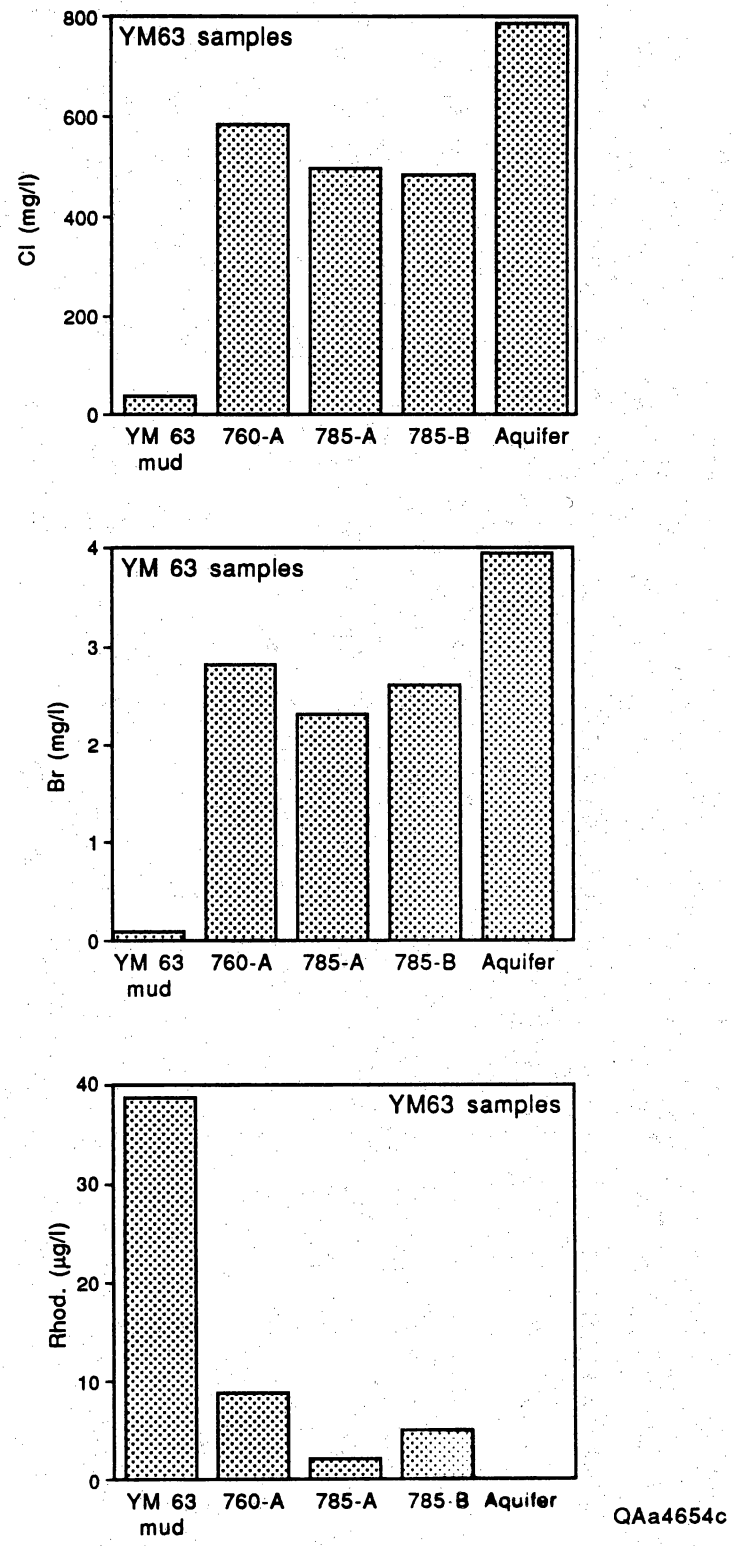

Figure 33. Comparison of conservative anions and rhodamine dye in drilling mud, recovery waters from well test intervals, and water collected from the completed well at YM-63. Two test samples collected at 785 ft (785-a and 785-b) and one test sample collected at 760 ft (760-a). Results of analysis of a drilling mud sample (YM-63 mud) and a sample from the completed well are shown. Comparisons between conservative anions and rhodamine dye indicate that almost three-fourths of recovery water is formation water at 760 and 785 ft. These results, along with recovery rates, indicate considerable storage and yield from the semiconfining unit or semiconfining interbeds at YM-63. These results imply conditions similar to conceptual models 2 or 3 (figure 31) at YM-63.

provided a transmissivity estimate of 2.45 ft^2/day (0.23 m^2/day). Such a transmissivity value in the upper strata suggests either fractured blocks and the release of water from storage in the matrix blocks (emulating model 2) or leakage from permeable interbeds above 785 ft (239 m) (emulating model 3). A water-table aquifer does not exist above 785 ft (239 m) because the relatively slow rate of recovery at the 785-ft (239-m) test interval is indicative of a confining layer, or layers above that test interval.

The core data (fig. 32) may indicate that model 3 depicts the aquifer in northwest Eagle Flat (at least at YM-63) because few fractures were found in the upper confining unit, and more and less permeable sandstone and mudstone interbeds were present above 785 ft (239 m). The data are not fully adequate to distinguish between model types 2 and 3, however, because wells may not fully penetrate the aquifer. One can only speculate on the hydraulic properties of the underlying strata that could leak small amounts of water vertically upward into strata adjacent to the pumping well. Even so, the data permit us to eliminate conceptual model 1 because a water table aquifer does not exist above 785 ft (239 m), where a confining unit was identified by Theis (1935) recovery analyses.

The leaky aquifers at Faskin Ranch showed a small range of transmissivity (2.4 to 10.2 ft^2/day [0.2 to 0.95 m^2/day] using the Hantush-Jacob [1955] method), but the transmissivity distribution between boreholes is unknown. Small variance of values at widely distributed test holes probably indicates fairly uniform transmissivities between boreholes.

Assuming that the aquifer transmissivity is uniform, the average linear ground-water velocity beneath Faskin Ranch can be computed simply:

$$v = K i / n = 1.6 \text{ ft/yr } (0.49 \text{ m/yr}), \quad (6)$$

where K is the hydraulic conductivity, i is the hydraulic gradient, and n is the effective porosity. Effective porosity was assumed to be 5 percent. The hydraulic conductivity of 0.11 ft/day (0.034 m/day) used for the calculation was the highest in situ estimate at Faskin Ranch (using Hantush-Jacob [1955], table 4). The local gradient in hydraulic head at Faskin Ranch varies from 0.002 to 0.009 (fig. 30). Using the higher gradient would give a velocity of 7 ft/yr (2.2 m/yr), or 0.7 mi/500 yr (1.1 km/500 yr). Gradients and hydraulic conductivities, of course, vary throughout

the study area, so choice of a given value for calculation of an apparent velocity should be conservative.

Ground water in the vicinity of Faskin Ranch, which is primarily Na-Cl to Na-SO_4-Cl in composition, is moderately saline (1,100 to 4,400 mg/L), with the highest salinities associated with the SO_4-dominated waters of wells 48-54-901, YM-18, and YM-63. Salinity increases significantly from Devil Ridge (figs. 13 and 14) toward YM-18 and YM-63. The high-Cl water can be traced southward, across Devil Ridge, and into the northeastern margin of Red Light Draw, where it is tapped by well 48-62-BOR. Average ^{14}C is less than 6.63 pmc at YM-7A, decreasing to less than 4 pmc at Faskin Ranch, the proposed disposal site. With few exceptions, tritium levels are among the lowest in the region (0.0 TU).

Regional Conceptual Flow Model

The regional ground-water flow system is more heterogeneous and complex than that at Faskin Ranch, having circuitous three-dimensional flow components, fracture and double-porosity flow, hydrochemically zoned water in alternating permeable and low-permeability rock and poorly consolidated strata, and areal transitions between unconfined, confined, and leaky confined aquifers.

A conceptual model of ground-water flow, presented in map view, is shown in figure 34. Lines identifying two-dimensional cross-sectional models are shown in figure 35, and the conceptual models are presented in figures 36 through 38. Local flow systems originate in recharge areas in mountains and along mountain fronts and replenish the aquifers in the low-lying draws and flats. Precipitation recharge is mostly absent in flats and draws, except where water is shallow (that is, 3 to 40 ft [0.9 to 12 m]) in terrace and alluvial deposits adjacent to the Rio Grande.

The extremely flat hydraulic gradients in northwest Eagle Flat, southeast Eagle Flat, and the northwestern part of Red Light Draw make it difficult to precisely delineate ground-water flowpaths in some low-lying areas (fig. 34), although the regional trends of flow paths are evident. With a reasonable degree of certainty, regional ground-water flow paths are interpreted to be oriented along

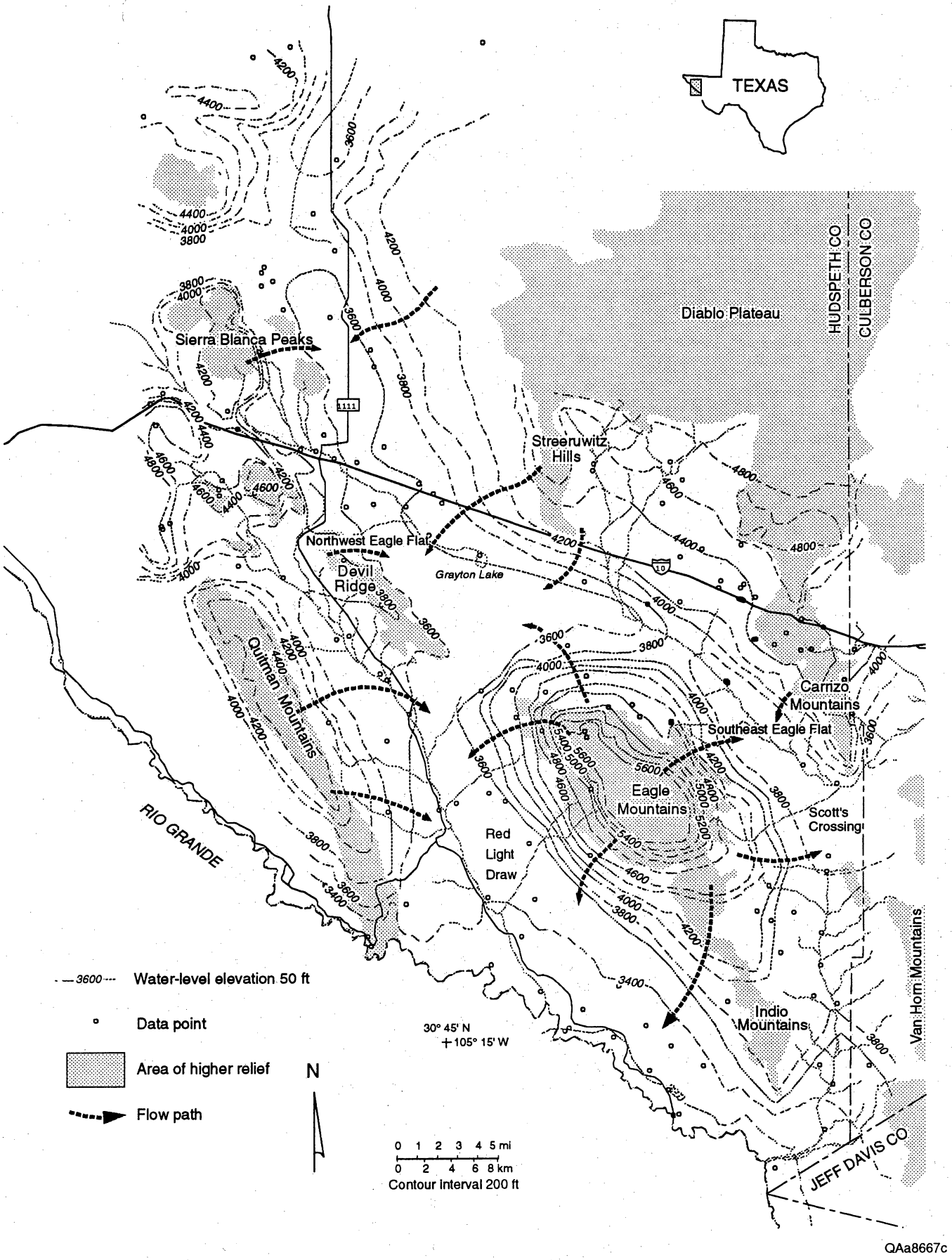

Figure 34. Planar conceptual model showing ground-water flow paths and potentiometric contours in map view.

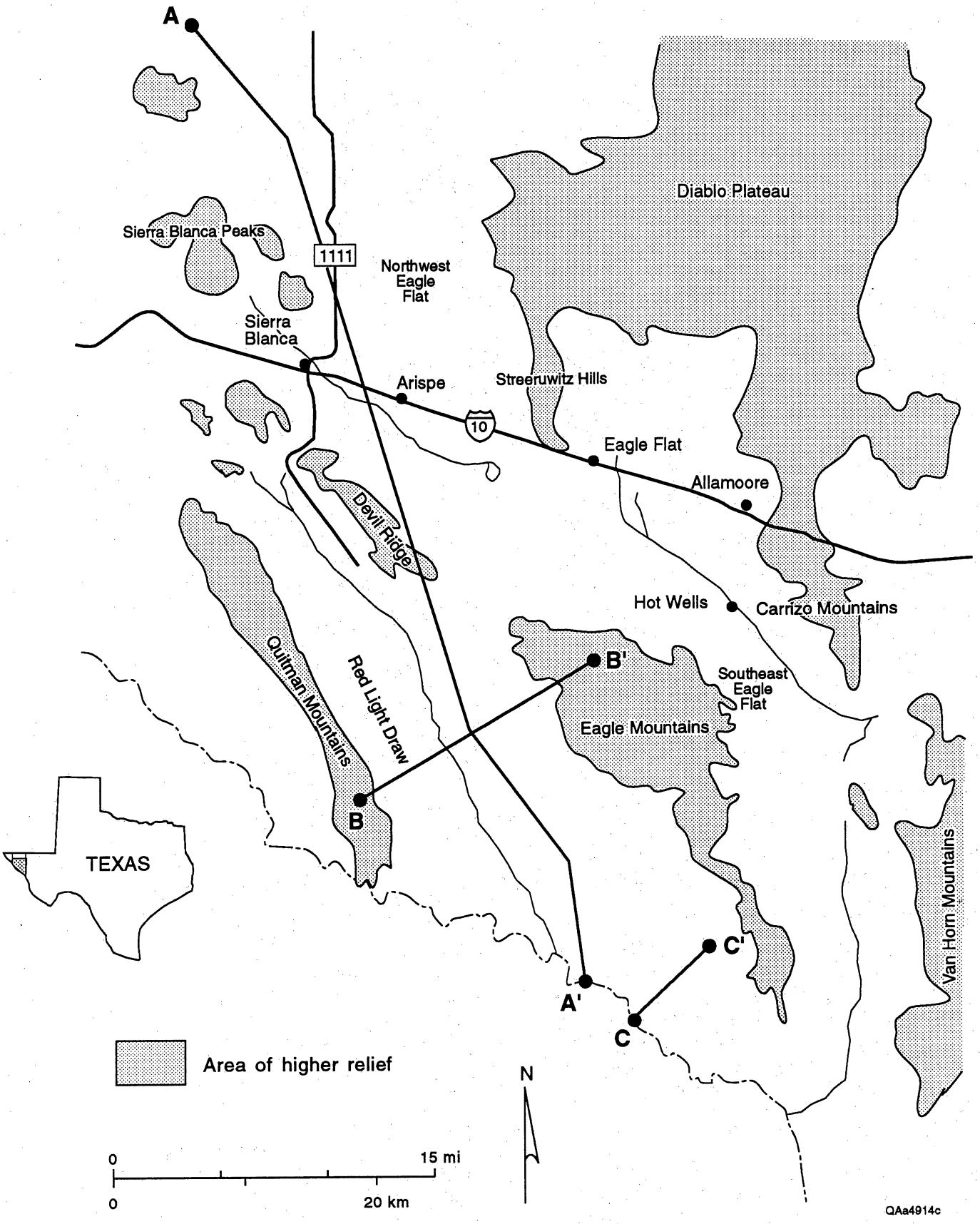

Figure 35. Location map showing orientation of conceptual hydrogeologic cross sections A–A′, B–B′, and C–C′.

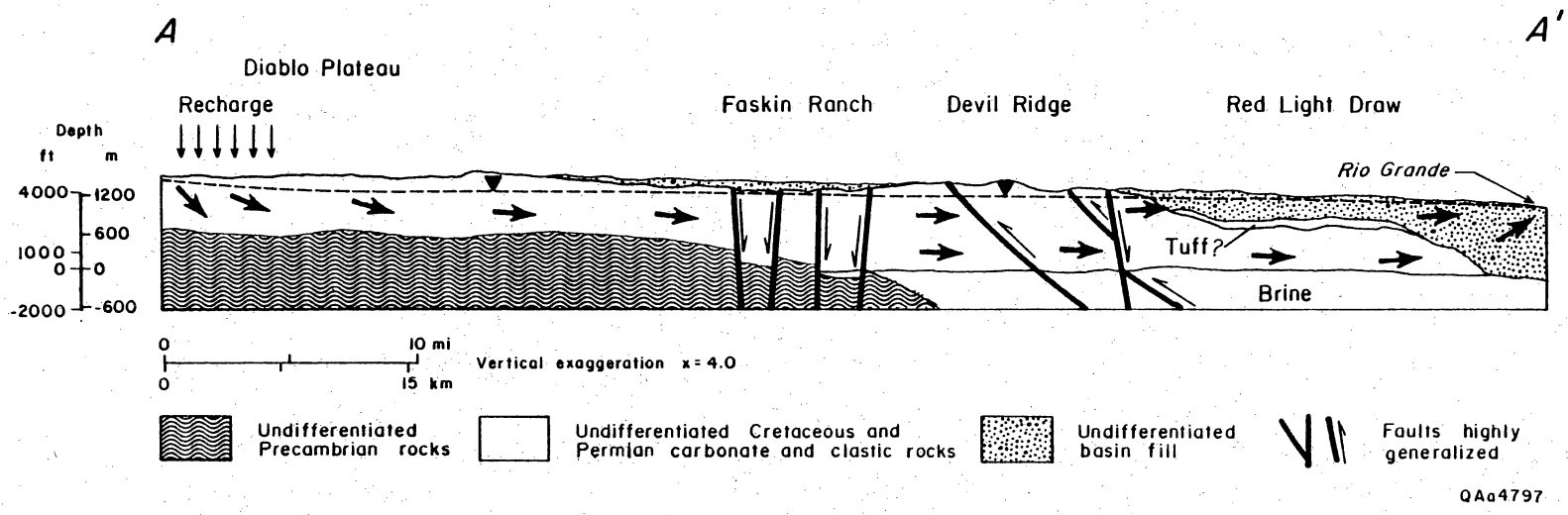

Figure 36. Conceptual hydrogeologic cross section A–A′.

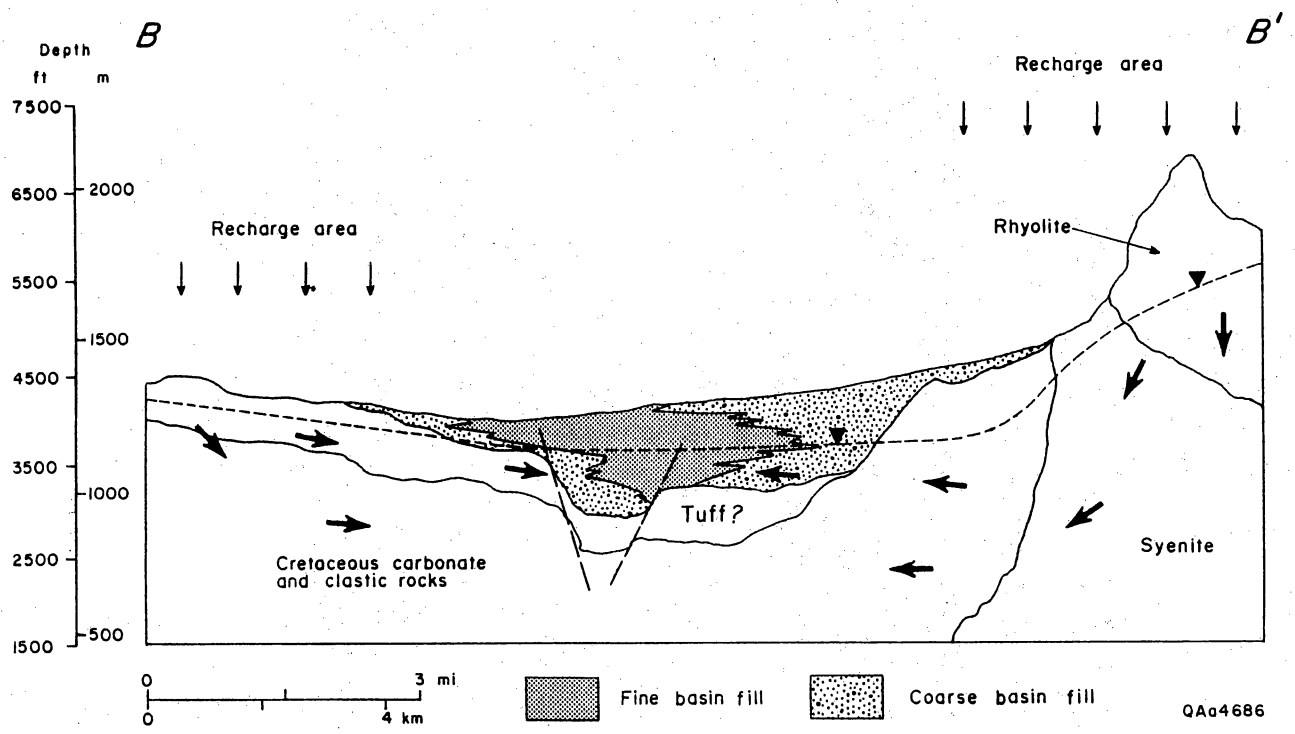

Figure 37. Conceptual hydrogeologic cross section B–B'.

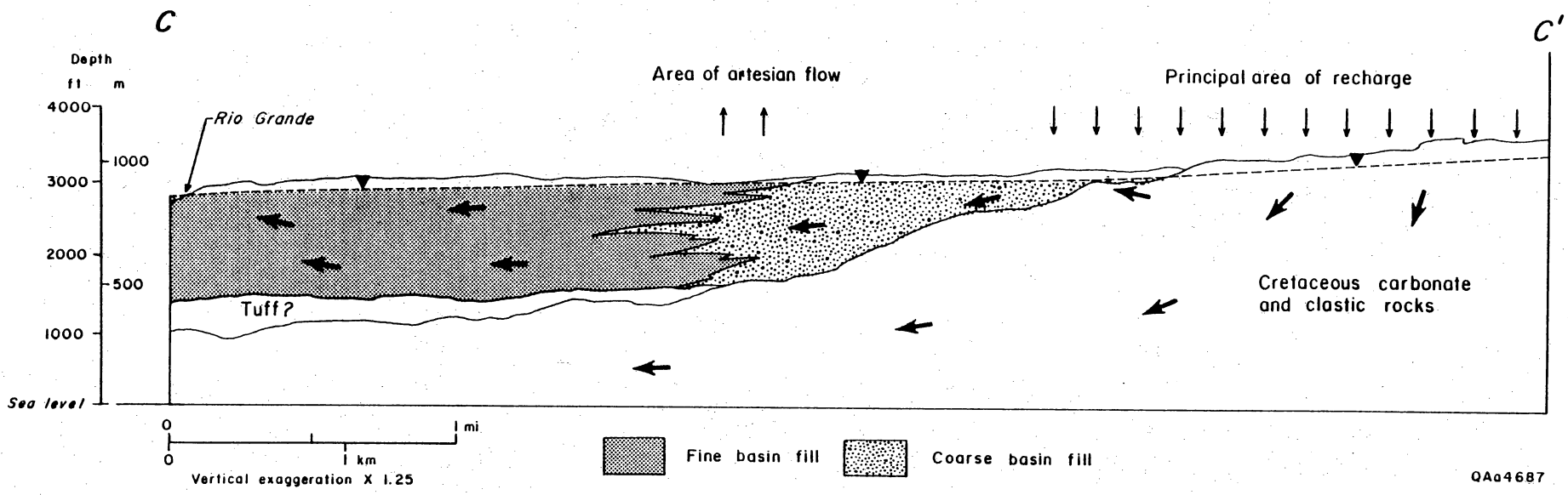

Figure 38. Conceptual hydrogeologic cross section C–C′.

a trough in the potentiometric surface, from the Diablo Plateau across northwest Eagle Flat and down Red Light Draw. As previously discussed, it is assumed that there is no hydrologic barrier between the Northwest Eagle Flat Watershed and Red Light Draw Watershed. Ground water probably ultimately discharges to low-lying areas along the Rio Grande, although discharge rates might be small (10 ft^3/s [0.3 m^3/s]), on the basis of limited stream gauging data. Because areas of high hydraulic head in mountainous terrains bound the trough in the potentiometric surface, it is the only hydrologically plausible pathway for regional ground-water flow.

Hydrochemical similarities between ground waters in northwest Eagle Flat and ground water to the south of Devil Ridge at well 48-62-BOR possibly establish a hydraulic connection between the basins and suggests flow, probably in very small quantities, via circuitous routing along pathways controlled by stratigraphy and fractures around Devil Ridge. Even though hydraulic gradients and potentiometric surface elevations are similar in northwest and southeast Eagle Flat, the hydrochemical differences and slightly higher hydraulic heads to the east preclude flow from northwest Eagle Flat toward Scott's Crossing.

The planar conceptual model (fig. 34) and geochemical data do not allow us to trace ground-water movement via the geochemical signature of waters from well 48-62-BOR in Red Light Draw to wells along the draw's southeast-trending axis. The lack of moderately saline waters along the trough may occur as a result of mixing of large quantities of much less saline water in the bolson aquifer of Red Light Draw or as a result of submergence of waters beneath the bolson aquifer and movement along the northwest-striking bedrock formations subparallel to the axis of Red Light Draw (fig. 34). Under the latter scenario, these saline waters eventually discharge to low-lying areas adjacent to the Rio Grande by upwelling at the lower (southeast) end of the basin.

Hydraulic segregation of saline waters may be enhanced by the presence of a semiconfining unit of pyroclastic flows and tuffs that locally rest on the valley floor in Red Light Draw, separating Cretaceous carbonate and sandstone formations from moderately to poorly indurated bolson fill (fig. 36). The low permeability of the volcanic rocks might keep the waters separate. Segregation may also be an artifact of sample depths, as many wells in Red Light Draw do not penetrate deeply

into the saturated bolson fill. These wells yield fresh waters that originally were derived from the Eagle and Quitman recharge areas and may be stratified atop the more saline waters that are not intercepted by small cones of depression associated with low production from livestock and domestic wells.

Unfortunately, our sampling plan cannot prove stratified waters because deep wells do not exist in Red Light Draw. There is only indirect geochemical evidence of submergence of saline waters beneath Red Light Draw (for example, Cl/Br ratios), along with the acknowledged view that "there commonly is a deep ground-water flow system that causes an upwelling of mineralized water at the lower end of the basins" along the Rio Grande (Kernodle, 1992). Numerical flow modeling and pathline simulations are the only means available at present to test flow hypotheses.

Numerical Flow Modeling

The numerical flow model tests hypotheses regarding segregation of slightly saline waters in Cretaceous bedrock aquifers beneath fresh water in Red Light Draw and eventual upwelling near the Rio Grande floodplain. The profile model, oriented northwest-southeast between the Diablo Plateau and the Rio Grande, corresponds to hydrogeologic cross section A–A′ (fig. 36). The model estimates ground-water flow velocities, horizontal and vertical pathlines, and residence times along the line of section.

The model mesh consists of 37 layers and 114 columns. Several model layers were constructed in order to simulate vertical flow components if and where they exist. Expected areas of vertical flow include recharge areas on the Diablo Plateau and discharge areas near the Rio Grande. The dimensions of the finite difference blocks are 125 by 2,500 ft (38 by 762 m), for a total of 4,218 nodes.

Boundary conditions were selected to correspond as closely as possible to actual hydrologic boundaries (fig. 39). A no-flow boundary was established at a depth of about 200 ft (61 m) below sea level at the brackish/brine water interface. The absolute depth to this transitional interface, though

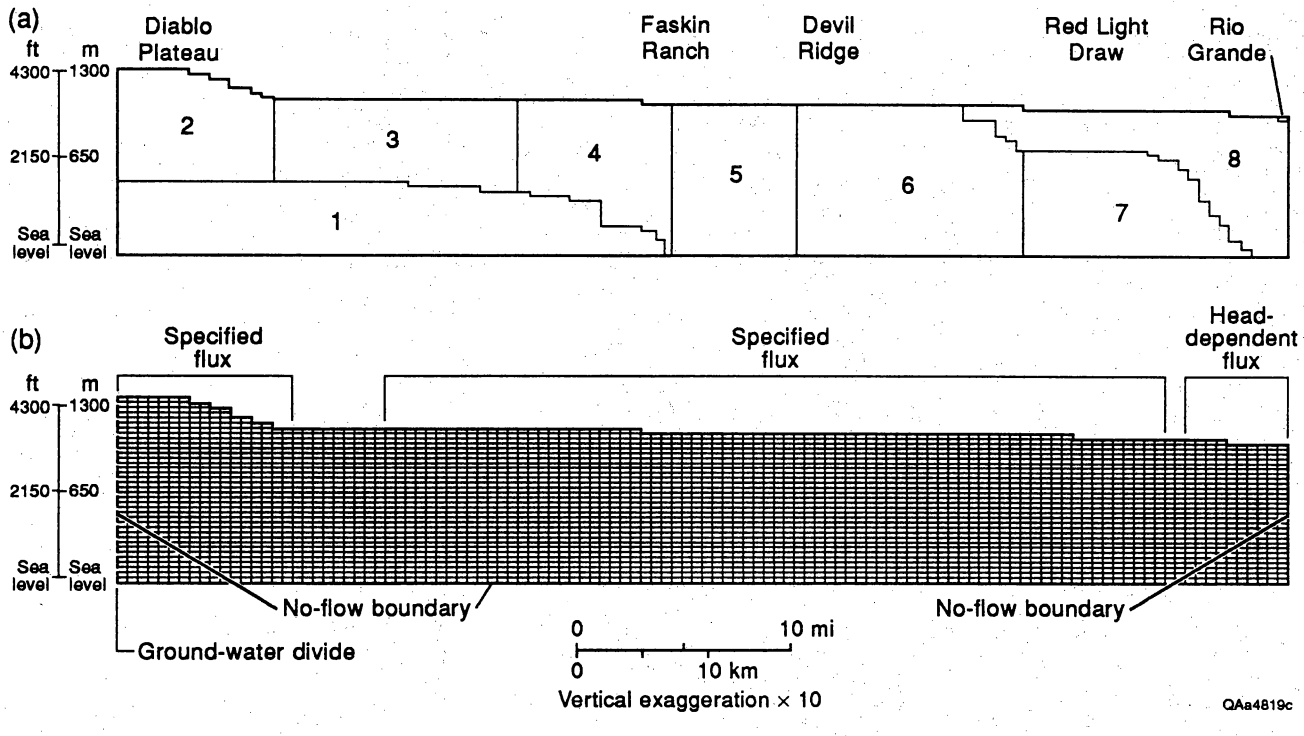

Figure 39. Diagram showing the gridding scheme, the aquifer zones, and the boundary conditions selected for the numerical profile model oriented between the Diablo Plateau and the Rio Grande.

uncertain, is selected to correspond to the elevation of the brine/brackish water interface identified at other Trans-Pecos aquifers near the Rio Grande (Alvarez and Buckner, 1980).

The northern boundary of the model is no flow, which corresponds to a ground-water divide on the Diablo Plateau (Kreitler and others, 1990; Mullican and Senger, 1992). A prescribed flux (Neumann) boundary replenishes the aquifer to the south of the divide. The southern boundary of the model corresponds to a head-dependent flux boundary at the Rio Grande, developed with the river package of MODFLOW. Head-dependent flux boundaries were also selected to correspond to low-lying areas close to the Rio Grande where discharge by evapotranspiration occurs.

The governing equations of the model are solved with the preconditioned conjugate gradient solver package of MODFLOW (Hill, 1990). The model includes a routine that allows cells to rewet during model iteration (McDonald and others, 1991). This routine is used because very large head changes during the first few model iterations resulted in the dewatering of an excessive number of cells. As the numerical model begins to converge to an acceptable solution, dry cells must rewet so that the cells are included in the final solution. Dry cells are not allowed to rewet in MODFLOW unless this routine is used.

Definition of Model Properties

Hydraulic conductivities assigned to the model grid (fig. 39) were selected to correspond to major rock units and sediment types on hydrogeologic cross section A–A′ (fig. 36). Where pump test and specific capacity data were available, rock types were separated into zones that correlated with spatial variations of transmissivity. These zones were refined after lithologic, structural, and geologic descriptions were summarized (for example, Underwood, 1962; Albritton and Smith, 1965; Jones and Reaser, 1970). Where well test data were not available, hydraulic conductivity values of rocks were selected from published values (Davis, 1969; Brace, 1980; Wolff, 1982; Bedinger and others, 1986; Kernodle, 1992; Mullican and Senger, 1992) and from lithologic descriptions of the rocks and sediments (King and Flawn, 1953; Underwood, 1962; Albritton and Smith, 1965; Jones and Reaser, 1970; Gates and others, 1976; Gates and others, 1980).

On the basis of published values (Brace, 1980; Bedinger and others, 1986) and lithologic descriptions (King and Flawn, 1953), the Precambrian basement rocks of zone 1 were assigned a low permeability value of 0.006 ft/day (0.002 m/day). Permian and Cretaceous carbonate and siliciclastic rocks were assigned permeabilities by zone. These zones were selected on the basis of field-estimated parameters, the structural characteristics of the rocks, and the potentiometric surface. Six zones (zones 2 through 7; fig. 39, table 8) were selected for Permian and Cretaceous rocks.

Zone 2 is in the Diablo Plateau recharge province, where steep hydraulic gradients probably indicate locally low transmissivity (for example, 10 to 50 ft^2/day [0.9 to 4.6 m^2/day]. An initial hydraulic conductivity value of 0.5 ft/day (0.15 m/day) was selected for this carbonate and siliciclastic zone. Zone 3 is enclosed by Blanca Draw, where steep hydraulic gradients characteristic of the margins of the Diablo Plateau become very flat (fig. 34). The flat hydraulic gradient may be associated with a considerable increase in permeability of the rocks. Specific capacity tests at wells 48-54-201 and 48-45-603 indicated relatively high transmissivity values (respectively, 20,499 ft^2/day and 891 ft^2/day [1,904 m^2/day and 83 m^2/day]) in this zone. High transmissivities may have resulted from fracturing and arching of these sedimentary rocks during emplacement of tertiary intrusives (for example, the Sierra Blanca laccolith). An initial hydraulic conductivity value of 2 ft/day (0.6 m/day) was selected for zone 3.

Hydraulic conductivity values of 0.17 and 0.09 ft/day (0.05 and 0.03 m/day) were selected, respectively, for zones 4 and 5. The permeability of these zones was selected from a specific capacity test on a 1,100-ft (335-m) deep well in Sierra Blanca (well 48-54-401; calibrated transmissivity = 56 ft^2/day [5 m^2/day]; table 4) and from well tests on Faskin Ranch (table 3), where the lowest transmissivity values were obtained. Zone 6 corresponds to the Red Hills and Devil Ridge thrust belt, where rocks are more highly jointed and fractured and are presumably quite permeable. A specific capacity test on well 48-62-TEX and calibrated test results of 2362 ft^2/day (219 m^2/day) confirmed a moderately high transmissivity in the zone. A hydraulic conductivity of 3.2 ft/day (1.0 m/day) was specified for rocks in zone 6.

Table 8. Initial hydraulic conductivities assigned to permeability zones in the model.

Permeability zone	Description	Initial hydraulic conductivity (ft/day)
1	Undifferentiated Precambrian Strata	0.006
2	Undifferentiated Cretaceous and Permian Strata (Diablo Plateau)	0.5
3	Undifferentiated Cretaceous and Permian Strata (Blanca Draw Area)	2
4	Undifferentiated Cretaceous and Permian Strata (Sierra Blanca Area)	0.17
5	Undifferentiated Cretaceous and Permian Strata (Faskin Ranch Area)	0.09
6	Undifferentiated Cretaceous and Permian Strata (Red Hills and Devil Ridge Thrust Belt)	3.2
7	Undifferentiated Cretaceous and Permian Strata (Beneath Red Light Draw)	0.9
8	Basin Fill (Red Light Draw)	0.25

Well test data were not available for carbonate and siliciclastic rocks beneath Red Light Draw (zone 7). The geologic and structural history of the draw would suggest that these rocks have moderate permeabilities (Underwood, 1962; Jones and Reaser, 1970). An initial hydraulic conductivity value of 0.9 ft/day (0.3 m/day) was selected for this zone.

Basin fill that comprises zone 8 was assigned a hydraulic conductivity value of 0.25 ft/day (0.08 m/day). This bulk value may overestimate hydraulic conductivity because geophysical information and test-hole data suggest that low-permeability volcanic tuffs and volcaniclastic materials may comprise most of the lower basin fill (Gates and others, 1976; Gates and others, 1980). Higher in the stratigraphic column, the bolson fill is predominantly mud-rich sediments that have characteristically low permeabilities (figs. 37 and 38). A somewhat high hydraulic conductivity value (0.25 ft/day [0.08 m/day]) is chosen for zone 8 because the bolson fill along the axis of Red Light Draw contains sand-and-gravel interbeds in the mud-dominated stratigraphic column.

Vertical flow within and between individual units was simulated by specifying vertical conductance between model layers. Vertical conductance is the thickness-weighted harmonic mean of the values of vertical hydraulic conductivity of each layer. Vertical conductance is computed with the following equation:

$$VCONT = \frac{1}{\frac{0.5 \times b_{i+1}}{K_{v_{i+1}}} + \frac{0.5 \times b_i}{K_{v_i}}}, \qquad (7)$$

where b_{i+1} is thickness of upper layer i+1, b_i is thickness of lower layer i, $K_{v(i+1)}$ is vertical hydraulic conductivity of upper layer i+1, and K_{vk} is vertical hydraulic conductivity of lower layer i. The values of vertical hydraulic conductivity for the cross-sectional model were based on measured values of horizontal conductivity and assumptions regarding unit anisotropy, as shown in table 7. In model scenario 1, vertical hydraulic conductivity was identical to mean horizontal hydraulic conductivity for each zone. In scenario 2, vertical hydraulic conductivity was 100 times less than horizontal hydraulic conductivity values. For model scenarios 3 and 4, hydraulic conductivity values were varied to test assumed hydrogeologic conditions.

Vertical hydraulic conductivity distribution in the model was not influenced by overburden pressure. Bedinger and others (1986) suggested that hydraulic conductivity is as much as an order of magnitude higher in the upper 100 to 500 ft (30.5 to 152 m) of bedrock because of weathering and expansion of fracture apertures that succeeds erosional unloading of overburden pressures. At depths greater than 100 to 500 ft (30.5 to 152 m), the hydraulic conductivity of the rocks is only slightly influenced by additional overburden pressures. Overburden pressures, therefore, probably do not cause a systematic decrease in hydraulic conductivity at depths greater than 100 to 500 ft (30.5 to 152 m) beneath the bedrock surface (Bedinger and others, 1986).

In most areas, the profile model simulates flow in water-bearing strata at depths greater than 500 ft (152 m) beneath the top of bedrock. No data exist on the hydraulic conductivity of water-bearing strata beneath the uppermost saturated units. Therefore, a systematic decrease (or increase) in hydraulic conductivity with depth cannot be simulated in the model. Horizontal and vertical hydraulic conductivity values are assumed constant with depth in any particular zone.

Porosity values for particle-tracking simulations were assumed as follows: Precambrian rocks (0.02), Permian and Cretaceous carbonate and siliciclastic rocks (0.05), and bolson fill (0.18). These values were compiled from literature values (Wolff, 1982; Bedinger and others, 1986) and from lithologic descriptions of the rocks and sediments (King and Flawn, 1953; Jones and Reaser, 1970; Gates and others, 1980).

Steady-State Simulation

Inflows occur along the flanks of the profile where areas of high head bound the trough in the potentiometric surface (fig. 40a). These inflows influence hydraulic gradients and account for added water mass to the system. These additions of water mass are represented as prescribed fluxes at the upper model boundary (fig. 40b). The model was developed by matching the simulated hydraulic gradient with the measured hydraulic gradient between the Diablo Plateau and the Rio Grande. This was accomplished in four separate model scenarios (table 9) with varying prescribed flux inputs in areas where water mass is added along the trough flanks (zones 4, 5, 6, and 8).

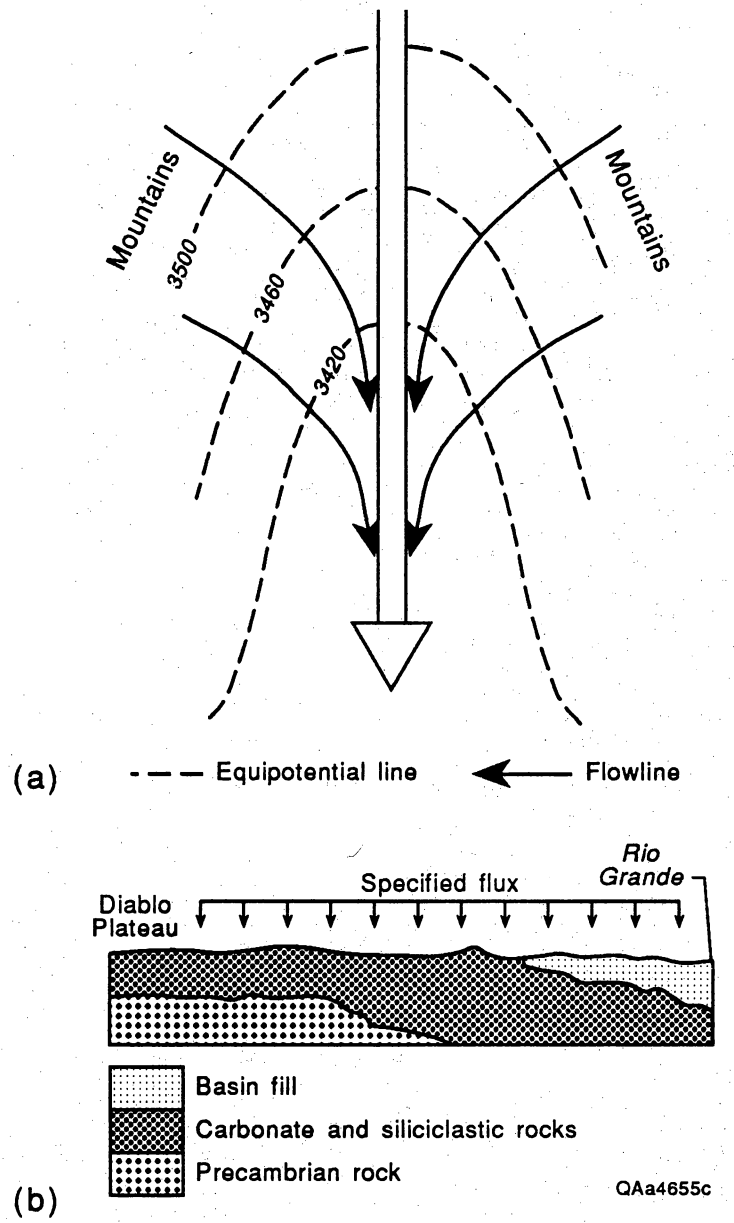

Figure 40. Conceptual diagram indicating how inflows of water from adjacent highlands (a) add water mass to regional flowpath A–A'. This is evident in figure 34. These inflows must be accounted for in the profile model and are treated as specified flux rates to the upper model grid (b). These rates are adjusted during model development to match the simulated hydraulic gradient along the regional flowpath with the measured hydraulic gradient.

Table 9. Summary of hydraulic conductivity and horizontal to vertical anisotropy ratios specified in four model scenarios.

Model scenario	Hydraulic conductivity	Horizontal to vertical anisotropy ratio
1	Initial input values from table 8 modified slightly to match the simulated and measured hydraulic gradient.	1
2	Final values used in model scenario 1.	100
3	Final values used in model scenario 1, except for zone 7, which is decreased by one order of magnitude.	1
4	Final values used in model scenario 1 increased by one order of magnitude in every zone.	1

In the first model scenario the agreement between the measured and simulated potentiometric surface is good (fig. 41). Where prescribed flux inputs were maintained at constant rates at zones 2 and 3, the hydraulic conductivity values were adjusted from initial values of 0.5 and 2 ft/day (0.2 and 0.6 m/day) to final values of 0.0091 and 0.97 ft/day (0.0028 and 0.30 m/day) (table 10). Through repeated trials, the match between the measured and simulated heads was obtained with only very small fluxes at zones 4 to 8 (table 11). The recharge rate in the Diablo Plateau that established the fit is 0.123 inch/yr (0.312 cm/yr or 1.02 percent of mean annual precipitation).

Pathline modeling illustrates vertical flow between northwest Eagle Flat and Red Light Draw, downward beneath Devil Ridge in the thrust belt zone (zone 6). Waters move laterally underneath Red Light Draw and then discharge by vertical upwelling beneath the Rio Grande discharge boundary in the model (fig. 42). Each particle path is flagged by time markers at 4,000-yr intervals. These results estimate a total travel time of 60,178 yr between the Diablo Plateau recharge area and the Rio Grande (table 12). Travel times along intermediate pathways are shown in the diagram. A travel time of 19,134 yr, for example, is estimated between Faskin Ranch and the Rio Grande.

Horizontal to vertical anisotropies may vary between 10 and 1000 in basin fill (Hearne and Dewey, 1988; Frenzel and Kaehler, 1992; Kernodle, 1992). These ratios also may vary in rock aquifers depending upon the orientation and interconnectedness of fractures and the strike and dip of the strata and bedding planes. The effect of horizontal to vertical anisotropy was tested in the second model scenario.

The vertical conductance is decreased by a factor of 100 at all model nodes to simulate a horizontal to vertical anisotropy ratio of 100 (table 10). A slightly lower recharge rate of 0.0876 inch/yr (0.223 cm/yr or 0.73 percent mean annual precipitation) in the Diablo Plateau provided a match between the measured and simulated gradient (table 11, fig. 43). Vertical pathlines are slightly more subdued in this simulation despite longer residence times (fig. 44). Particles of water require additional time to "leak" through the less permeable interfaces between adjacent model layers. A total travel time of 97,789 yr is shown for particles tracked from the Diablo

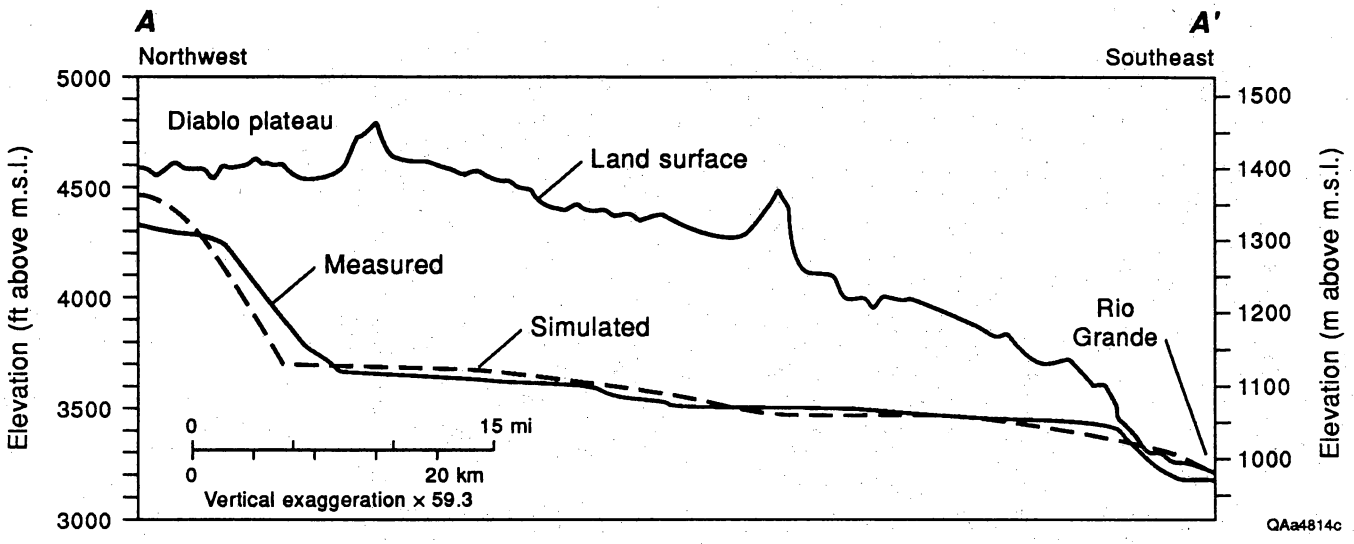

Figure 41. Comparison of measured and simulated potentiometric surface shown in cross section for model scenario 1. Simulated potentiometric surface obtained by using the simulated head value in the uppermost saturated cell in each column of the model.

Table 10. Comparison of initial and final model hydraulic conductivities.

INITIAL AND FINAL MODEL PARAMETERS IN 4 MODEL SCENARIOS					
Model scenario	**Zone and rock or sediment unit**	**Initial hydraulic conductivity (ft/day)**	**Final hydraulic conductivity (ft/day)**	**Effective porosity**	**Horizontal to vertical anisotropy ratio**
1	#1: Precambrian Rocks	0.006	0.006	0.02	1
1	#2: Carbonate & clastic	0.5	0.0091	0.05	1
1	#3: Carbonate & clastic	2	0.97	0.05	1
1	#4: Carbonate & clastic	0.17	0.17	0.05	1
1	#5: Carbonate & clastic	0.09	0.09	0.05	1
1	#6: Carbonate & clastic	3.2	3.2	0.05	1
1	#7: Carbonate & clastic	0.9	0.9	0.05	1
1	#8: Basin fill	0.25	0.25	0.18	1
2	#1: Precambrian Rocks	-	0.006	0.02	100
2	#2: Carbonate & clastic	-	0.0091	0.05	100
2	#3: Carbonate & clastic	-	0.97	0.05	100
2	#4: Carbonate & clastic	-	0.17	0.05	100
2	#5: Carbonate & clastic	-	0.09	0.05	100
2	#6: Carbonate & clastic	-	3.2	0.05	100
2	#7: Carbonate & clastic	-	0.9	0.05	100
2	#8: Basin fill	-	0.25	0.18	100
3	#1: Precambrian Rocks	-	0.006	0.02	1
3	#2: Carbonate & clastic	-	0.0091	0.05	1
3	#3: Carbonate & clastic	-	0.97	0.05	1
3	#4: Carbonate & clastic	-	0.17	0.05	1
3	#5: Carbonate & clastic	-	0.09	0.05	1
3	#6: Carbonate & clastic	-	3.2	0.05	1
3	#7: Carbonate & clastic	-	0.09	0.05	1
3	#8: Basin fill	-	0.25	0.18	1
4	#1: Precambrian Rocks	-	0.06	0.02	1
4	#2: Carbonate & clastic	-	0.091	0.05	1
4	#3: Carbonate & clastic	-	9.7	0.05	1
4	#4: Carbonate & clastic	-	1.7	0.05	1
4	#5: Carbonate & clastic	-	0.9	0.05	1
4	#6: Carbonate & clastic	-	32	0.05	1
4	#7: Carbonate & clastic	-	0.9	0.05	1
4	#8: Basin fill	-	2.5	0.18	1

Table 11. Model recharge rates specified in the Diablo Plateau and inflow rates specified in zones 4, 5, 6, and 8.

FINAL RECHARGE AND INFLOW RATES FOR MODEL SCENARIOS 1 TO 4			
Model scenario	**Recharge area or inflow zone**	**Average recharge or inflow (in/year)**	**Percentage of annual precipitation (%)**
1	Diablo Plateau	0.123	1.02
1	Inflow to zones 4,5,6,8	0.131	1.10
2	Diablo Plateau	0.0876	0.73
2	Inflow to zones 4,5,6,8	0.0569	0.47
3	Diablo Plateau	0.0788	0.66
3	Inflow to zones 4,5,6,8	0.0394	0.33
4	Diablo Plateau	1.231	10.26
4	Inflow to zones 4,5,6,8	1.73	14.42

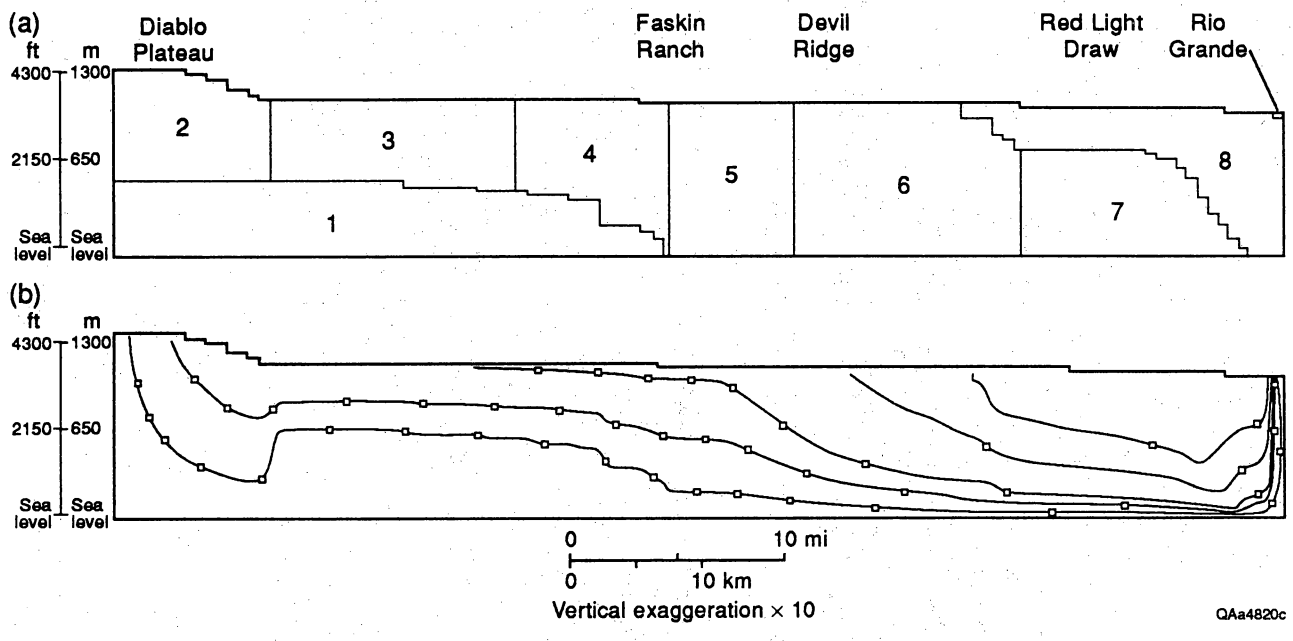

Figure 42. Particle tracking simulations showing pathlines moving underneath the Red Light Draw bolson; model scenario 1; heterogeneous, isotropic units. Each pathline marker indicates a travel time of 4,000 yr. Pathlines originating at the top of the model profile (zones 3 through 8) are representative of inflows from adjacent highlands (see fig. 41).

Table 12. Summary of ground-water travel times between the Diablo Plateau and the Rio Grande and between Faskin Ranch and the Rio Grande in four model scenarios.

MODEL ESTIMATED TRAVEL TIMES IN YEARS			
Model	**Scenario**	**Diablo Plateau - Rio Grande**	**Faskin Ranch - Rio Grande**
1		60,178	19,134
2		97,789	29,775
3		101,820	43,619
4		8,054	2,995

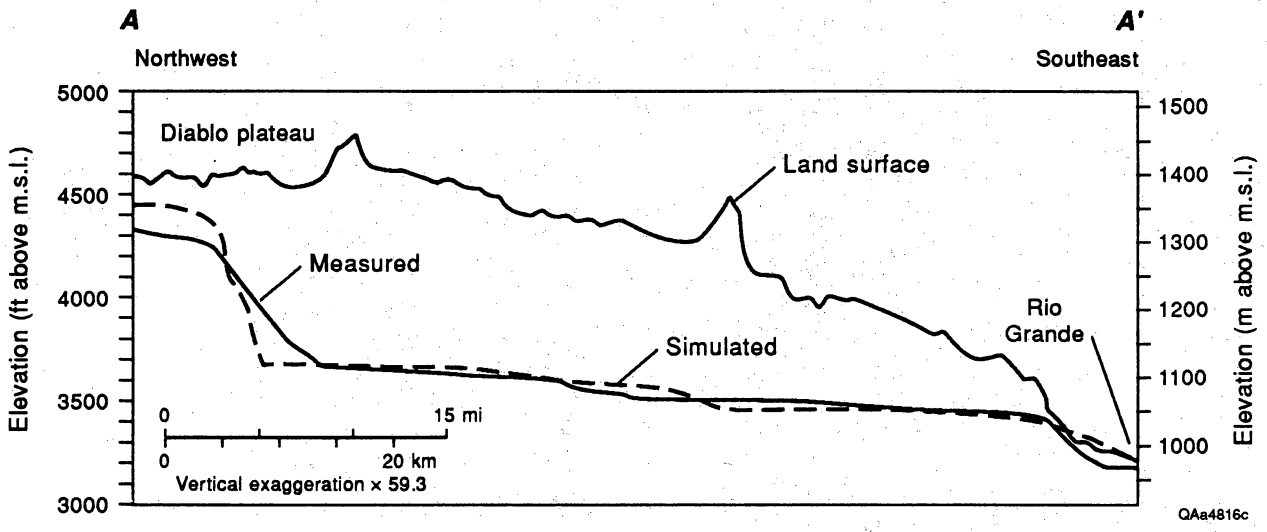

Figure 43. Comparison of measured and simulated potentiometric surface shown in cross section for model scenario 2 (horizontal to vertical anisotropy = 100:1). Simulated potentiometric surface obtained by using the simulated head value in the uppermost saturated cell in each column of the model.

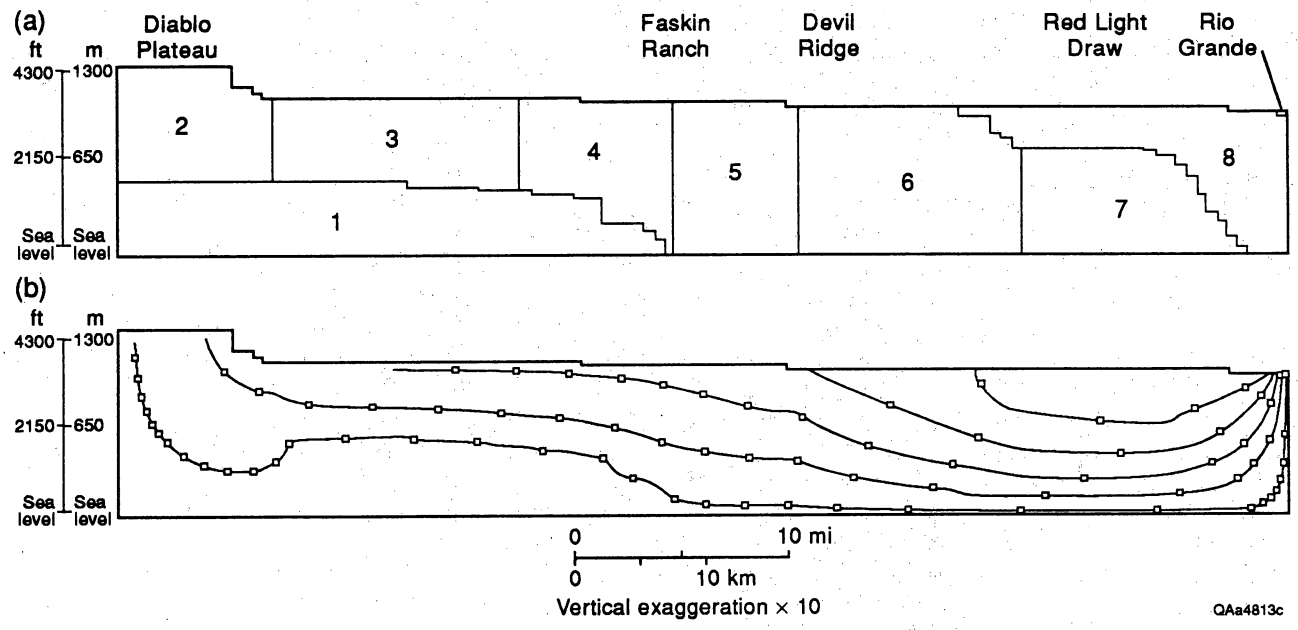

Figure 44. Particle tracking simulations showing pathlines moving underneath the Red Light Draw bolson; model scenario 2; heterogeneous, anisotropic units (horizontal to vertical anisotropy = 100:1). Each pathline marker indicates a travel time of 4,000 yr.

Plateau to the Rio Grande (table 12). The simulated travel time between Faskin Ranch and the Rio Grande is 29,775 yr.

In the third model scenario, the sensitivity of model pathlines to lower bedrock permeabilities beneath Red Light Draw was tested. The hydraulic conductivity of zone 7 was decreased to 0.09 ft/day (0.03 m/day) from an initial value of 0.9 ft/day (0.3 m/day) (table 10). This hydraulic conductivity value is about 2.5 times less than the simulated hydraulic conductivity of Red Light Draw bolson (zone 8).

A recharge rate of approximately 0.08 inch/yr (0.2 cm/yr or 0.7 percent of mean annual precipitation) in the Diablo Plateau provided a match between the measured and simulated gradient in model scenario 3 (table 11, fig. 45). Vertical pathlines move beneath Red Light Draw, although the effect of higher relative permeability in zone 8 is evident on pathlines beneath the bolson fills (fig. 46). A total travel time of more than 101,000 yr is shown for particles tracked from the Diablo Plateau to the Rio Grande (table 12). The simulated travel time between Faskin Ranch and the Rio Grande is approximately 43,600 yr in the third model scenario.

In order to demonstrate that hydraulic conductivities selected for model scenarios 1 through 3 are reasonable, a fourth model scenario was developed to test the extent to which ground-water velocities increase with uniformly higher hydraulic conductivities. These higher velocities are compared with ground-water ages inferred by ground-water isotopes. Horizontal and vertical hydraulic conductivities used in model scenario 1 were increased by one order of magnitude in the final simulation (table 10).

The recharge rate in the Diablo Plateau was approximately 1.2 inch/yr (3.1 cm/yr or 10.3 percent of mean annual precipitation) to provide the match between the simulated and measured hydraulic gradient (table 11 and fig. 47). The total travel time for particles tracked from the Diablo Plateau to the Rio Grande is 8,054 yr (table 12, fig. 48). The simulated travel time between Faskin Ranch and the Rio Grande is 2,995 yr. Ground water beneath northwest Eagle Flat is simulated to pass under the Red Light Draw Watershed and to discharge by vertical upwelling beneath the Rio Grande discharge boundary.

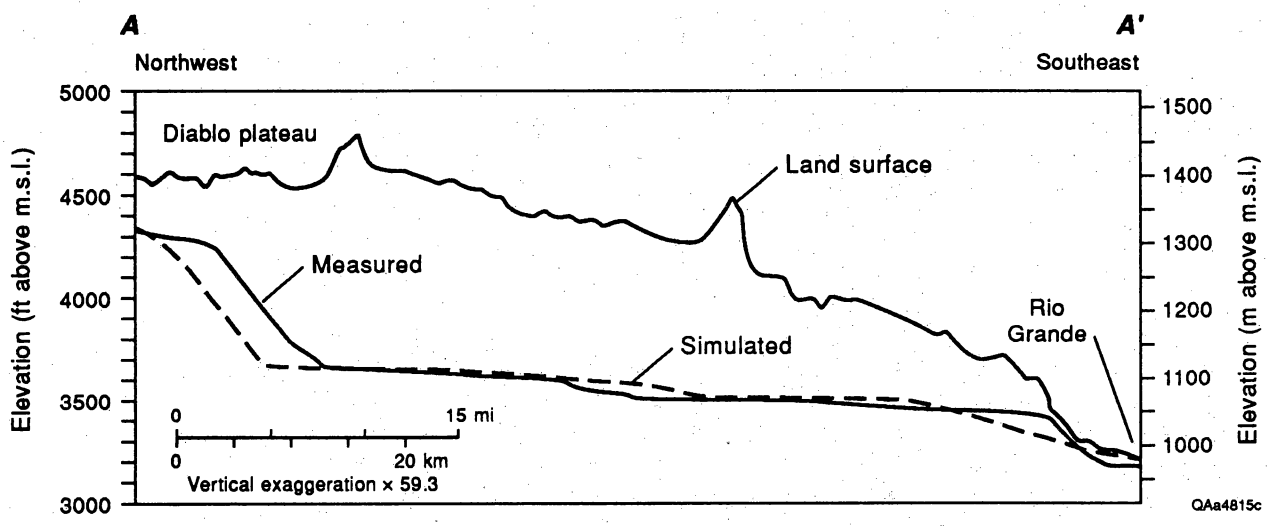

Figure 45. Comparison of measured and simulated potentiometric surface shown in cross section for model scenario 3. Simulated potentiometric surface obtained by using the simulated head value in the uppermost saturated cell in each column of the model.

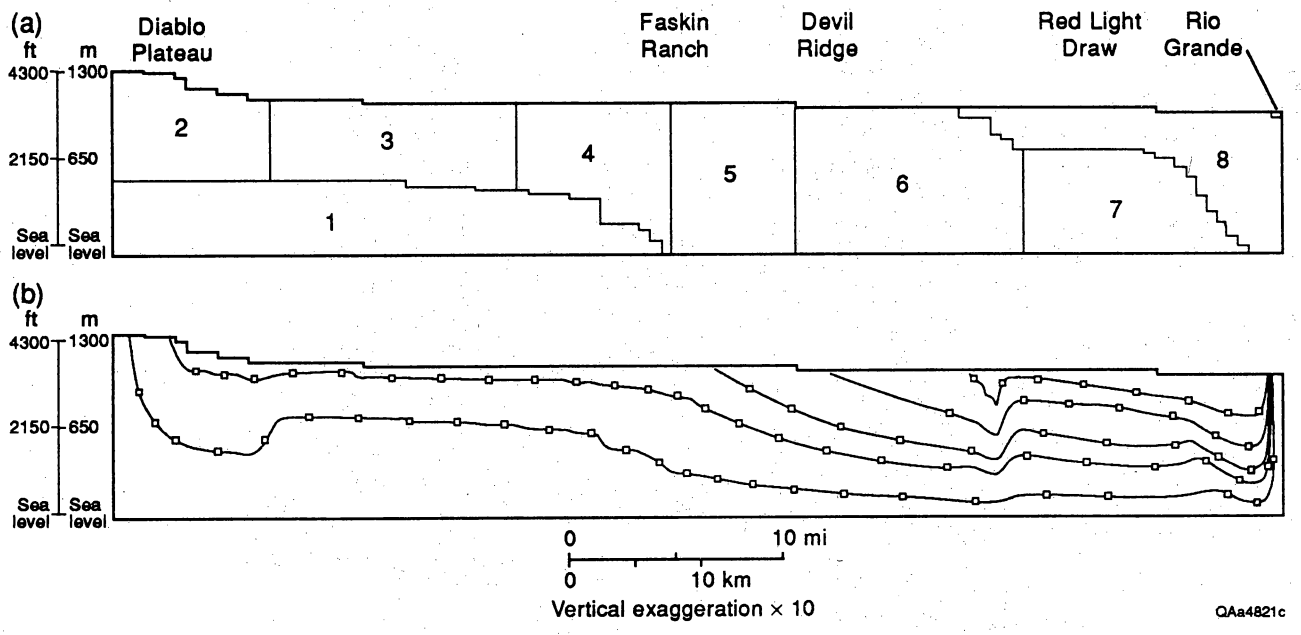

Figure 46. Particle tracking simulations showing selected pathlines moving underneath Red Light Draw; model scenario 3; heterogeneous, isotropic units. Hydraulic conductivity was decreased one order of magnitude in zone 7 for this simulation. Each pathline marker indicates a travel time of 4,000 yr.

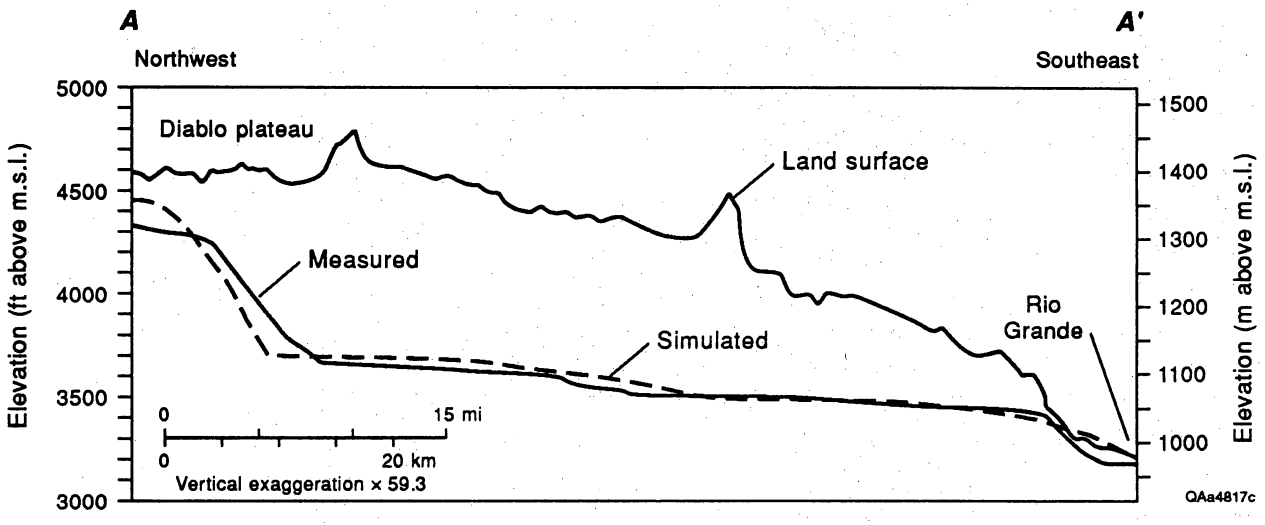

Figure 47. Comparison of measured and simulated potentiometric surface shown in cross section for model scenario 4. Simulated potentiometric surface obtained by using the simulated head value in the uppermost saturated cell in each column of the model.

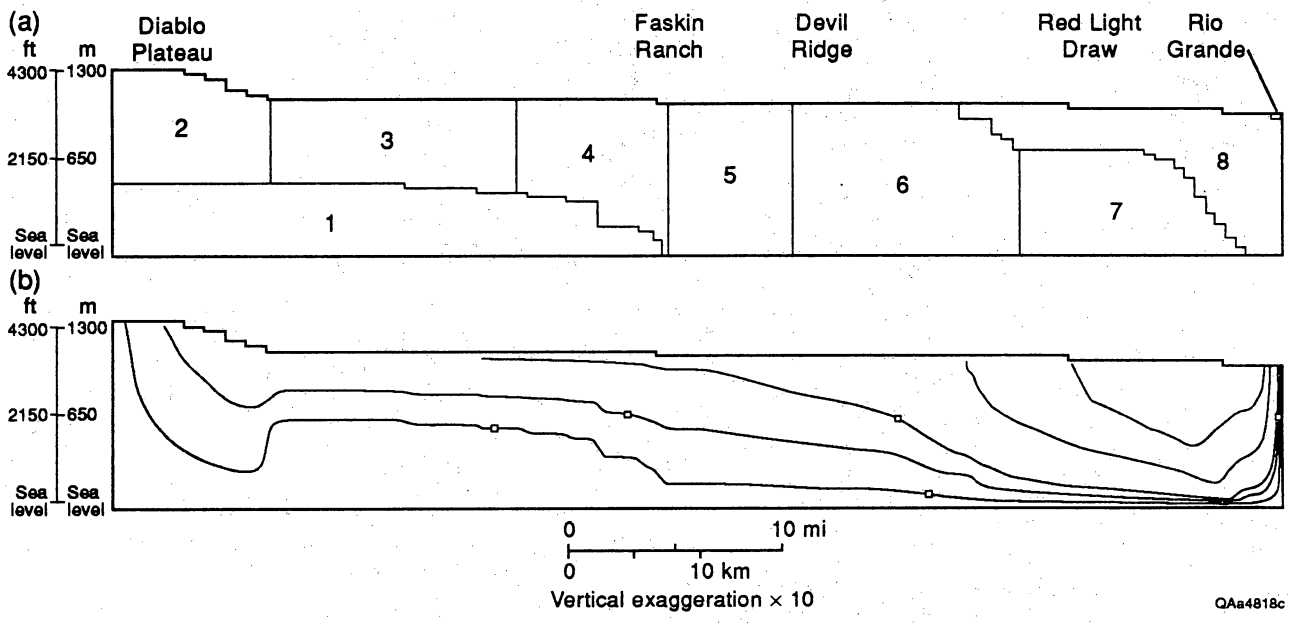

Figure 48. Particle tracking simulations showing selected pathlines moving underneath Red Light Draw; model scenario 4; heterogeneous, isotropic units. Horizontal and vertical hydraulic conductivity was increased one order of magnitude in all zones for this simulation. Each pathline marker indicates a travel time of 4,000 yr.

Discussion and Model Limitations

Recharge rates to the Diablo Plateau in model scenarios 1, 2, and 3 vary between 0.66 and 1.02 percent mean annual precipitation (table 11) and are consistent with estimated recharge rates of between 0.5 and 3 percent of the available precipitation falling on mountain drainage areas in Trans-Pecos Texas (Kelly and Hearne, 1976; Orr and Risser, 1992). The recharge rate of 10.26 percent mean annual precipitation in model scenario 4 (table 10) is considerably higher than recharge rates estimated in other Trans-Pecos investigations. The higher recharge rate needed to match the measured and simulated hydraulic gradient is a direct consequence of higher hydraulic conductivity values specified in the model. The short residence times estimated in model scenario 4 are inconsistent with ground-water ages determined by ground-water isotopes. These results probably imply that hydraulic conductivities are too high in model scenario 4. True hydraulic conductivities and ground-water velocities are probably much closer to hydraulic conductivities specified in model scenarios 1 through 3.

Overall, the model results agree with the hydrochemical segregation hypothesis formulated earlier. These results are a simple consequence of the tendency of the flowpaths to refract and move downward when a zone of higher permeability is encountered as waters move from zone 6 to zone 7. This is a realistic scenario because extensive fracturing and jointing in thrust belts tend to increase rock permeability. The geochemical data and model results provide reasonable evidence for segregation of waters.

A semiconfining layer of tuffs and pyroclastic flows that probably underlies sediment fills in Red Light Draw (Gates and White, 1976; Gates and others, 1980) was not simulated in the present version of the model. These types of rocks usually are low permeability, even when slightly to moderately fractured (for example, 0.001 ft/day [0.0003 m/day]) (Bedinger and others, 1986). Volcanic tuffs and pyroclastic flows usually have hydraulic conductivities that are lower than slightly to moderately fractured carbonate rocks (Bedinger and others, 1986). A low-permeability

layer of tuffs and pyroclastic flows simulated between zones 7 and 8 would accentuate model results.

The paucity of data along the model profile limits the use of the model beyond that of an interpretive tool for estimating specific ground-water flowpaths and velocities. The model presents a simplified picture of the hydrostratigraphy of the area, as defined by major structural and geologic features such as the Red Hills and Devils Ridge thrust belt (zone 6). The simulated hydraulic gradient was fairly well matched with the measured hydraulic gradient in every model scenario, but the model's reliability is limited by the lack of information on vertical and horizontal hydraulic conductivity, effective porosity, and hydrostratigraphy. The limiting factors that are most pertinent to this modeling effort include the assumptions that

- fractured rock, at large scales, is equivalent to a porous medium;
- ground-water flow is restricted to the plane of the profile model; and
- each of the zones has a constant vertical and horizontal hydraulic conductivity and effective porosity.

Of these, the most limiting is the last assumption. It is certain that rock units in any particular zone are laterally and vertically heterogeneous. These zones, in most cases, were defined by the boundaries between rock and sediment types. Within Permian and Cretaceous rocks for example, a few aquifer tests along with structural attributes and transitions in the potentiometric surface were used to separate the water-bearing unit into zones. The simplistic definition of zones that have uniform hydrogeologic properties is required because borehole and aquifer test data are unavailable at most depths simulated in the model.

CONCLUSIONS

This report presents the results of local hydrogeologic and hydrochemical investigations at Faskin Ranch and vicinity and regional ground-water studies in a 1,200 mi^2 (3,110 km^2) area of southern Hudspeth County, Texas. Faskin Ranch is a proposed repository site for storage of low-level radioactive waste. The regional study area is bounded to the south and southwest by the Rio

Grande and Quitman Mountains, to the east by the Van Horn and Carrizo Mountains, and to the north by the Diablo Plateau.

Aquifer tests results from five well tests in northwest Eagle Flat indicate a leaky confined aquifer with transmissivity values that vary from 2.4 to 68 ft^2/day (0.2 to 6.3 m^2/day). At Faskin Ranch transmissivity values are between 2.4 and 10.2 ft^2/day (0.2 to 0.95 m^2/day). Depths to water typically vary between 667 and 920 ft (203.5 and 280.5 m) in northwest Eagle Flat and between 667 and 751 ft (203.5 and 229 m) at Faskin Ranch. Ground water beneath Faskin Ranch is primarily Na-Cl to Na-SO_4-Cl in composition, with total dissolved solids between 1,500 to 4,000 mg/L. The slightly to moderately saline ground-water moves to the west to northwest beneath Faskin Ranch at an estimated flow rate of about 1.6 ft/yr (0.5 m/yr), where it merges with ground water that flows along the southeasterly sloping regional hydraulic gradient.

In the regional flow system, recharge is limited to areas with exposures of bedrock or where bedrock is covered by thin basin fill. Recharge waters have low total dissolved solids, ^{14}C signatures between 60 to 100 pmc, and tritium ranging from 1 to 8 TU. The most significant recharge zone is in the Streeruwitz, Bean, and Millican Hills, south of the Diablo Plateau escarpment. The Eagle Mountains constitute a second major area of recharge.

Southeast Eagle Flat is separated from ground water in the northwest Eagle Flat area by a hydrologic divide approximately 11 mi (17.7 km) east of Grayton Lake. The approximate location of the divide was based on water-level measurements (table 1) and on observed changes in ground-water facies between northwest and southeast Eagle Flat (fig. 13). The ground-water divide lies nearly 5 mi (8.05 km) east of, and subparallel to, the divide that separates surface flow in Eagle Flat into northwestern and southeastern components.

Ground water in southeast Eagle Flat drains toward the south-southeast, mixing with other, more dilute water from the Eagle Mountains to the south and the Carrizo Mountains to the east. In northwest Eagle Flat, west of the Eagle Flat ground-water divide, regional ground-water flow paths are oriented along a ground-water trough, northwest-southeast from the Diablo Plateau, across northwest Eagle Flat and Red Light Draw where ground water probably discharges in very small

amounts to low-lying areas along the Rio Grande. Carbon-14 values less than 8 pmc and numerical modeling indicate that ground-water flow rates along this regional flow path are extremely low (for example, 1 to 3 ft/yr).

Along the regional hydraulic gradient, slightly saline water flows southeast across northwest Eagle Flat and Red Light Draw via circuitous routing along pathways controlled by stratigraphy and fractures adjacent to Devil Ridge. The slightly saline waters later disappear in the Red Light Draw bolson, probably as a result of either mixing with dilute waters in the bolson or by movement underneath the Red Light Draw bolson along northwest-striking bedrock formations. In the latter hypothesis, the slightly saline waters eventually discharge to the Rio Grande by vertical upwelling.

Higher salinities and elevated Cl/Br ratios in lower Red Light Draw, a geochemical signature that could not develop by evaporation of bolson water in upgradient areas, support the second hypothesis. Numerical simulations in several model scenarios suggest that ground water in northwest Eagle Flat moves underneath the Red Light Draw bolson and discharges by vertical upwelling near the Rio Grande, providing some support for hypothesis two. Ground-water travel times between Faskin Ranch and the Rio Grande estimated by numerical simulations vary between 19,134 and 43,619 yr in what are considered to be the most plausible model scenarios.

ACKNOWLEDGMENTS

This report was prepared for the Texas Low-Level Radioactive Waste Disposal Authority under Interagency Contract No. (92-93)-0910. The conclusions of the authors are neither approved nor endorsed by the Authority. Jay Raney was the Principal Investigator. Illustrations were drafted by Richard L. Dillon, Michele Bailey, William Bergquist, Randy Hitt, Susan Krepps, Joel Lardon, and Maria Saenz. Word processing was by Susan Lloyd, editing was by Amanda R. Masterson and Jeannette Miether, and layout was by Margaret L. Evans and Jamie H. Coggin. We also thank T. Warren, I. Jones, and R. Boghici for their technical assistance. Finally, we are grateful to the landowners of southern Hudspeth County for granting us access to their property.

REFERENCES

Albritton, C. C., Jr., and Smith, J. F., Jr., 1965, Geology of the Sierra Blanca area, Hudspeth County, Texas: U.S. Geological Survey Professional Paper 479, 131 p.

Alvarez, H. J., and Buckner, A. W., 1980, Ground-water development in the El Paso region with emphasis on the resources of the lower El Paso Valley, Texas: Texas Department of Water Resources, Report 246, 350 p.

Axelrod, D. I., and Bailey, H. D., 1976, Tertiary vegetation, climate and altitude of the Rio Grande depression, New Mexico-Colorado: Paleobiology, v. 2, p. 235–254.

Banner, J. L., and Hanson, G. N., 1990, Calculation of simultaneous isotopic and trace element variations during water-rock interaction with applications to carbonate diagenesis: Geochimica et Cosmochimica Acta, v. 54, p. 3123–3137.

Bedinger, M. S., Langer, W. H., and Reed, J. E., 1986, Synthesis of hydraulic properties of rocks with reference to the basin and range province, southwestern United States, in Selected papers in the hydrologic sciences: U.S. Geological Survey Water-Supply Paper 2310, 142 p.

Bedinger, M. S., Sargent, K. A., and Langer, W. H., 1989, Studies of geology and hydrology in the Basin and Range Province, southwestern United States, for isolation of high-level radioactive waste—characterization of the Trans-Pecos region, Texas: U.S. Geological Survey Professional Paper 1370-B, 43 p., 7 pl.

Brace, W. F., 1980, Permeability of crystalline and argillaceous rocks: International Journal of Rock Mechanics and Mining Sciences and Geomechanics Abstracts, v. 17, no. 5, p. 241–251.

Bureau of Economic Geology, 1989, Collection, determination of unstable properties, and field treatment of water samples for isotopic and ionic analyses: Technical Program Manual, Specific Work Instruction 3.1, 13 p.

Chapman, J. B., 1986, Stable isotopes in southeastern New Mexico groundwater: implications for dating recharge in the WIPP area: New Mexico Environmental Evaluation Group, EEG-35, 76 p.

Chapman, J. B., Ingraham, N. L., and Hess, J. W., 1992, Isotopic investigation of infiltration and unsaturated zone flow processes at Carlsbad Cavern, New Mexico: Journal of Hydrology, v. 133, p. 343–363.

Collins, E. W., and Raney, J. A., 1993, Late Cenozoic faults of the region surrounding the Eagle Flat study area, northwestern Trans-Pecos Texas: The University of Texas at Austin, Bureau of Economic Geology final contract report, prepared for Texas Low-Level Radioactive Waste Disposal Authority under Interagency Contract IAC(92-93)-0910, 74 p.

Cooper, H. H., and Jacob, C. E., 1946, A generalized graphical method for evaluating formation constants and summarizing well field history: American Geophysical Union Transactions, v. 27, p. 526–534.

Craig, H., 1961, Isotopic variations in meteoric waters: Science, v. 133, p. 1701–1703.

Dansgaard, W., 1964, Stable isotopes in precipitation: Tellus, v. 16, p. 436–469.

Davis, S. N., 1969, Porosity and permeability of natural materials, in DeWiest, R. J. M., ed., Flow through porous media: New York, Academic Press, p. 54–89.

DeFord, R. K., and Haenggi, W. T., 1970, Stratigraphic nomenclature of Cretaceous rocks in northeastern Chihuahua, *in* The geologic framework of the Chihuahua tectonic belt: West Texas Geological Society, p. 175–196.

Dorfman, M., and Kehle, R. O., 1974, Potential geothermal resources of Texas: The University of Texas at Austin, Bureau of Economic Geology Geological Circular 74-4, 33 p.

Duffield, G. M., and Rumbaugh, J. O., III, 1989, Geraghty & Miller's AQTESOLV Aquifer Test Solver, Version 1.00, 135 p.

Dutton, A. R., 1993, Sources and ages of ground water in unconfined and confined aquifers beneath the U.S. High Plains: The University of Texas at Austin, Bureau of Economic Geology Technical Report, draft prepared for U.S. Geological Survey under award 14-08-0001-G-1885.

Dutton, A. R., and Simpkins, W. W., 1989, Isotopic evidence for paleohydrologic evolution of ground-water flow paths, southern Great Plains, U.S.A.: Geology, v. 17, no. 7, p. 653–656.

Elliot, R. D., 1949, Forecasting the weather—the weather types of North America: Weatherwise, v. 2, p. 15–18.

Evans, G. V., Otlet, R. L., Downing, R. A., Monkhouse, R. A., and Rae, G., 1979, Some problems in the interpretation of isotope measurements in United Kingdom aquifers, *in* Proceedings of the International Symposium of Isotope Hydrology, v. 2: International Atomic Energy Agency, p. 679–706.

Faure, G., 1986, Principles of isotope geology: New York, John Wiley & Sons, 589 p.

_____ 1991, Principles and applications of inorganic geochemistry: New York, MacMillan, 626 p.

Fisher, R. S., and Mullican, W. F. III, 1990, Integration of ground-water and vadose-zone geochemistry to investigate hydrochemical evolution: a case study in arid lands of the northern Chihuahuan Desert, Trans-Pecos Texas: The University of Texas at Austin Bureau of Economic Geology Geological Circular 90-5, 36 p.

Fontes, J.-Ch., and Garnier, J.-M., 1979, Determination of the initial ^{14}C activity of the total dissolved carbon: a review of existing models and a new approach: Water Resources Research, v. 15, no. 2, p. 399–413.

Freeze, R. A., and Cherry, J. A., 1979, Groundwater: Englewood Cliffs, NJ, Prentice-Hall, Inc., 604 p.

Frenzel and Kaehler, 1992, Geohydrology and simulation of ground-water flow in the Mesilla Basin, Dona Ana County, New Mexico, and El Paso County, Texas: U.S. Geological Survey Professional Paper 1407-C, 105 p.

Gates, J. S., and White, D. E., 1976, Test drilling for ground water in Hudspeth, Culberson and Presidio Counties in westernmost Texas : U.S. Geological Survey Open-File Report 76-338, 76 p.

Gates, J. S., White, D. E., Stanley, W. D., and Ackermann, H. D., 1980, Availability of fresh and slightly saline ground water in the basins of westernmost Texas : Texas Department of Water Resources Report 256, 108 p.

Gile, L. H., Hawley, J. W., and Grossman, R. B., 1981, Soils and geomorphology in the Basin and Range area of Southern New Mexico—Guidebook to the Desert Project: New Mexico Bureau of Mines and Mineral Resources, Memoir 39, 222 p.

Gonfiantini, R., Dincer, T., and Derekoy, A. M., 1974, Environmental isotope hydrology in the Hodna region, Algeria, *in* Isotope techniques in groundwater hydrology 1974: International Atomic Energy Agency, v. 1, p. 293–316.

Groat, C. G., 1972, Presidio Bolson, Trans-Pecos Texas and adjacent Mexico, geology of a desert basin aquifer system: The University of Texas at Austin, Bureau of Economic Geology Report of Investigations No. 76, 46 p.

Gustavson, T. C., 1991, Arid basin depositional systems and paleosols: Fort Hancock and Camp Rice Formations (Pliocene-Pleistocene), Hueco Bolson, west Texas and adjacent Mexico: The University of Texas at Austin, Bureau of Economic Geology Report of Investigations No. 198, 49 p.

HACH, 1989, Water analysis handbook: Loveland, Colorado, Hach Company, 691 p.

Hall, S. A., 1977, Late Quaternary sedimentation and paleoecological history of Chaco Canyon, New Mexico: Geological Society of America Bulletin, v. 88, p. 1593–1618.

_____ 1985, Quaternary pollen analysis and vegetational history of the southwest, *in* Pollen records of Lake-Quaternary North America: Bryant, V.M., Jr., and Holloway, R.G., eds., Dallas, Texas, American Association of Stratigraphic Palynologists, p. 95–123.

Hantush, M. S., 1960, Modification of the theory of leaky aquifers: Journal of Geophysical Research, v. 65, no. 11, p. 3713–3725.

Hantush, M. S., and Jacob, C. E., 1955, Non-steady radial flow in an infinite leaky aquifer: American Geophysical Union Transactions, v.36, p. 95–100.

Hassan, A., 1982, Methodologies for extraction of dissolved inorganic carbon for stable carbon isotope studies: evaluation and alternatives: U.S. Geological Survey, Water Resources Investigations 82-6, 51 p.

Hearne, G. A., and Dewey, J. D., 1988, Hydrologic analysis of the Rio Grande basin north of Embudo, New Mexico, Colorado and New Mexico: U.S. Geological Survey Water-Resources Investigations Report 86-4113, 244 p.

Hem, J. D., 1985, Study and interpretation of the chemical characteristics of natural water: U.S. Geological Survey Water-Supply Paper 2254, 263 p.

Henry, C. D., 1979, Geologic setting and geochemistry of thermal water and geothermal assessment, Trans-Pecos Texas: The University of Texas at Austin, Bureau of Economic Geology Report of Investigations No. 96, 48 p.

Henry, C. D., Price, J. G., and Hutchins, M. F., 1983, Mineral resources areas of the Basin and Range Province of Texas : U.S. Geological Survey Open-File Report 83-709, 7 p.

Hill, M. C., 1990, Preconditioned conjugate-gradient 2 (PCG2), a computer program for solving ground-water flow equations: U.S. Geological Survey Water-Resources Investigations Report 87-4091, 34 p.

Hoffer, J. M., 1978, Thermal water occurrences in Trans-Pecos Texas: The Texas Journal of Science, v. 30, no. 4, p. 309–319.

Holser, W. T., 1979, Trace elements and isotopes in evaporites, *in* Marine Minerals: Mineral Society of America, p. 295–346.

Horowitz, A., Gerald, R. E., and Chaiffetz, M. S., 1981, Preliminary paleoenvironmental implications of pollen analyzed from Archaid, Formative and Historic sites near El Paso, Texas: The Texas Journal of Science, v. 33, no. 1, p. 61–72.

Hoy, R. N., and Gross, G. W., 1982, A baseline study of oxygen-18 and deuterium in the Roswell, New Mexico groundwater basin: New Mexico Water Resources Research Institute Report 44, 95 p.

Jackson, M. L. W., Langford, R. P., and Whitlaw, M., 1993, Quaternary history, basin-fill stratigraphy, and paleomagnetics, fissures, and pseudofissures of the Eagle Flat study area: The University of Texas at Austin, Bureau of Economic Geology final contract report prepared for Texas Low-Level Radioactive Waste Disposal Authority under Interagency Contract IAC(92-93)-0910.

Jones, B. R., and Reaser, D. F., 1970, Geology of southern Quitman Mountains, Hudspeth County, Texas: The University of Texas at Austin, Bureau of Economic Geology Geologic Quadrangle Map No. 39, scale 1:48,000, 24-p. text.

Kelly, T. E., and Hearne, G. A., 1976, The effects of ground-water development on the water supply in the Post Headquarters area, White Sands Missile Range, New Mexico: U.S. Geological Survey Open-File Report 76-277, 97 p.

Kernodle, J. M., 1992, Summary of U.S. Geological Survey ground-water flow models of basin-fill aquifers in the southwestern alluvial basins region, Colorado, New Mexico, and Texas: U.S. Geological Survey Open-File Report 90-361, 81 p.

King, P. B., and Flawn, P. T., 1953, Geology and mineral deposits of Precambrian rocks of the Van Horn area, Texas: The University of Texas at Austin, Bureau of Economic Geology Publication 5301, 218 p.

Kreitler, C. W., Mullican, W. F., III, and Nativ, R., 1990, Hydrogeology of the Diablo Plateau, Trans-Pecos Texas, *in* Kreitler, C. W., and Sharp, J. M., Jr., eds., The University of Texas at Austin, Bureau of Economic Geology Guidebook 25, p. 49-58.

Kreitler, C. W., Raney, J. A., Nativ, R., Collins, E. W., Mullican, W. F., III, Gustavson, T. C., and Henry, C. D., 1986, Preliminary geologic and hydrologic studies of selected areas in Culberson and Hudspeth counties, Texas, final report for the Texas Low-Level Radioactive Waste Disposal Authority under contract no. IAC(86-87)0818, 184 p.

Kruseman, G. P., and De Ridder, N. A., 1979, Analysis and evaluation of pumping test data: Bulletin 11, International institute for Land Reclamation and Improvements, Wageningen, Netherlands, 200 p.

Lambert, S. J., 1987, Feasibility study: applicability of geochronologic methods involving radiocarbon and other nuclides to the groundwater hydrology of the Rustler Formation, southeastern New Mexico: Sandia National Laboratories, 72 p.

Lambert, S. J., and Harvey, D. M., 1987, Stable-isotope geochemistry of groundwaters in the Delaware Basin of southeastern New Mexico: Sandia National Laboratories, Albuquerque, New Mexico, prepared for U.S. Department of Energy under contract DE-ACO4-76DP00789, 218 p.

Langford, R. P., 1993, Landscape evolution of Eagle Flat and Red Light basins, Chihuahuan Desert, South-Central Trans-Pecos Texas: The University of Texas at Austin, Bureau of Economic Geology contract report, prepared for Texas Low-Level Radioactive Waste Disposal Authority under Interagency Contract IAC(92-93)-0910.

Larkin, T. J., and Bomar, G.W., 1983, Climatic atlas of Texas : Texas Dept. of Water Resources Publication LP-192, 151 p.

Markgraf, V., Bradbury, J. P., Forrester, R. M., Singh, G., and Sternberg, R. S., 1984, San Augustin Plains, New Mexico: age and environmental potential reassessed: Quaternary Research, v. 22, p. 336–343.

Mazor, E., 1991, Applied chemical and isotopic groundwater hydrology: Halsted Press, 274 p.

Mazor, E., Drever, J. I., Finley, J., Huntoon, P. W., and Lundy, D. A., 1993, Hydrochemical implications of groundwater mixing: an example from the southern Laramie Basin, Wyoming: Water Resources Research, v. 29, no. 1, p. 193–205.

McDonald, M. G., and Harbaugh, A. W., 1988, A modular three-dimensional finite difference ground-water flow model: U.S. Geological Survey Techniques of Water-Resources Investigations, Book 6, Chapter A1, 586 p.

McDonald, M. G., Harbaugh, A. W., Orr, B. R., and Ackerman, D. J., 1991, A method of converting no-flow cells to variable-head cells for the U.S. Geological Survey modular finite-difference ground-water flow model: U.S. Geological Survey Open-File Report 91-536, 99 p.

Mook, W. G., 1980, Carbon-14 in hydrogeological studies, *in* Fritz, P. and Fontes, J.-Ch., eds., Handbook of environmental isotope geochemistry: Elsevier, v. 1, p. 49–74.

Motts, W. S., 1965, Hydrologic types of playas and closed valleys and some relations of hydrology to playa geology, *in* Neal, J. T., ed., Geology, mineralogy, and hydrology of U.S. playas: Air Force Cambridge Research Laboratory, Environmental Research Paper 96, p. 73–104.

Muller, A. B., and Mayo, A. L., 1986, ^{13}C variation in limestone on an aquifer-wide scale and its effects on groundwater ^{14}C dating models: Radiocarbon, v. 28, no. 3, p. 1041–1054.

Mullican, W. F. III, and Senger, R. K., 1992, Hydrogeologic investigations of deep ground-water flow in the Chihuahuan Desert, Texas: The University of Texas at Austin, Bureau of Economic Geology, Report of Investigations No. 205, 60 p.

Musgrove, M., 1993, Origin, evolution, and mixing of saline and dilute groundwaters in three regional flow systems, midcontinent, U.S.A.: The University of Texas at Austin, Master's thesis, 225 p.

Nativ, R., and Gutierrez, R. N., 1988, Hydrogeology and hydrochemistry of Cretaceous aquifers, Texas panhandle and eastern New Mexico: The University of Texas at Austin, Bureau of Economic Geology Geological Circular 88-3, 32 p.

Nativ, R., and Riggio, R., 1990, Precipitation in the southern High Plains: Meteorologic and Isotopic Features: Journal Geophysical Research, v. 95, D13, p. 22,559–22,564.

Nativ, Ronit, and Smith, D. A., 1987, Hydrogeology and geochemistry of the Ogallala aquifer, Southern High Plains: Journal of Hydrology, v. 91, p. 217–253.

Orr, B. R., and Risser, D. W., 1992, Geohydrology and potential effects of development of freshwater resources in the northern part of the Hueco Bolson, Dona Ana and Otero Counties, New

Mexico, and El Paso County, Texas: U.S. Geological Survey Water Resources Investigations Report 91-4082, 92 p.

Payne, B. R., and Yurtsever, Y., 1974, Environmental isotopes as a hydrogeological tool in Nicaragua, in Isotopes in groundwater hydrology 1974: International Atomic Energy Agency, v. 1, p. 193–202.

Plummer, L. N., Prestemon, E. C., and Parkhurst, D. L., 1991, An interactive code (NETPATH) for modeling net geochemical reactions along a flow path: U.S. Geol. Survey Water-Resources Investigations Report 91-4078, 227 p.

Pollock, D. W., 1989a, Documentation of computer programs to compute and display pathlines using results from the U.S. Geological Survey modular three-dimensional finite-difference ground-water flow model: U.S. Geological Survey Open-File Report 89-381, various pagination.

Raney, J. A., and Collins, E., 1993, Regional geologic setting of the Eagle Flat study area, Hudspeth County, Texas: The University of Texas at Austin, Bureau of Economic Geology contract report, prepared for Texas Low-Level Radioactive Waste Disposal Authority under Interagency Contract IAC(92-93)-0910, 53 p.

Richardson, G. B., 1904, Report of a reconnaissance in Trans-Pecos Texas north of the Texas and Pacific Railway: The University of Texas Mineral Survey, 119 p.

Sami, K., 1992, Recharge mechanisms and geochemical processes in a semi-arid sedimentary basin, Eastern Cape, South Africa: Journal of Hydrology, v. 139, p. 27–48.

Scanlon, B. R., Wang, F. P., and Richter, B. C., 1991, Field studies and numerical modeling of unsaturated flow in the Chihuahuan Desert, Texas: The University of Texas at Austin, Bureau of Economic Geology Report of Investigations No. 199, 56 p.

Schoch-Fischer, H., Rozanki, K., Jacob, H. J., Sonntag, C., Jouzel, I., Oustlund, G., and Geyh, M. A., 1983, Hydrometerological factors controlling the time variation of D, ^{18}O and ^{3}H in atmospheric water vapor and precipitation in the northern westwind belt, *in* Isotope Hydrology 1983: International Atomic Energy Agency, p. 3–30.

Siegel, D. I., 1991, Evidence for dilution of deep, confined ground water by vertical recharge of isotopically heavy Pleistocene water: Geology v. 19, p. 433-436.

Siegenthaler, U., and Oeschger, H., 1980, Correlation of ^{18}O in precipitation with temperature and altitude: Nature, p. 314–317.

Sofer, Z., and Gat, J. R., 1972, Activities and concentrations of oxygen-18 in concentrated aqueous salt solutions: analytical and geophysical implications: Earth and Planetary Science Letters, v. 15, p. 232–238.

Sonntag, C., Klitzsch, E., Lohnert, E. P., Ee-Shazly, E. M., Munich, K. O., Junghans, Ch., Thorweihe, U., Weistroffer, K., and Swailem, F. M., 1979, Paleoclimatic information from deuterium and oxygen-18 in carbon-14 dated north Saharan groundwaters, *in* Isotope hydrology 1978: International Atomic Energy Agency, v. 2, p. 569–581.

Theis, C. V., 1935, The relation between the lowering of the piezometric surface and the rate and duration of discharge of a well using groundwater storage: American Geophysical Union Transactions, v. 16, p. 519–524.

Underwood, J. R., Jr., 1962, Geology of the Eagle Mountains and vicinity, Trans-Pecos, Texas: The University of Texas at Austin, Ph.D. dissertation, 560 p.

Van Devender, T. R., and Spaulding, W. G., 1979, Development of vegetation and climate in the southwestern United States: Science, v. 204, p. 701–710.

Walton, W. C., 1962, Selected analytical methods for well and aquifer evaluation: Illinois State Water Survey Bulletin 49, 81 p.

Wells, S. G., Bullard, T. F., and Smith, L. N., 1982, Origin and evolution of deserts in the Basin and Range and Colorado Plateau Provinces of western North America, *in* The geological story of the world's deserts: Stria, v. 17, p. 101–111.

White, D. E., Gates, J. S., Smith, J. T., and Fry, B. J., 1980, Ground-water data for the Salt Basin, Eagle Flat, Red Light Draw, Green River Valley, and Presidio Bolson in westernmost Texas: Texas Department of Water Resources Report 259, 97 p.

Wolff, R. C., 1982, Physical properties of rocks—porosity, permeability, distribution coefficients, and dispersivity: U.S. Geological Survey Open-File Report 82-166, 118 p.

Wood, W. W., 1976, Guidelines for collection and field analysis of ground-water samples for selected unstable constituents: U.S. Geological Survey Water-Resources Investigations, Chapter D2, 24 p.